Generation of Thermotropic Liquid Crystalline Polymer (TLCP)-Thermoplastic Composite Filaments and Their Processing in Fused Filament Fabrication (FFF)

Mubashir Q. Ansari

Dissertation submitted to the faculty of the Virginia Polytechnic Institute and State University in partial fulfillment of the requirements for the degree of

Doctor of Philosophy
In
Chemical Engineering

Donald G. Baird, Chair
Richey M. Davis
Christopher B. Williams
Michael J. Bortner

2/7/2019
Blacksburg, Virginia

Keywords: Additive Manufacturing, 3D Printing, Fused Filament Fabrication, Dual Extrusion Technology, Thermotropic Liquid Crystalline Polymers, *In-situ* Composites

Generation of Thermotropic Liquid Crystalline Polymer (TLCP)-Thermoplastic Composite Filaments and Their Processing in Fused Filament Fabrication (FFF)

Mubashir Q. Ansari

ABSTRACT (academic)

One of the major limitations in Fused Filament Fabrication (FFF), a form of additive manufacturing, is the lack of composites with superior mechanical properties. Traditionally, carbon and glass fibers are widely used to improve the physical properties of polymeric matrices. However, the blending methods lead to fiber breakage, preventing generation of long fiber reinforced filaments essential for printing load-bearing components. Our approach to improve tensile properties of the printed parts was to use *in-situ* composites to avoid fiber breakage during filament generation. In the filaments generated, we used thermotropic liquid crystalline polymers (TLCPs) to reinforce acrylonitrile butadiene styrene (ABS) and a high performance thermoplastic, polyphenylene sulfide (PPS). The TLCPs are composed of rod-like monomers which are highly aligned under extensional kinematics imparting excellent one-dimensional tensile properties. The tensile strength and modulus of the 40 wt.% TLCP/ABS filaments was improved by 7 and 20 times, respectively. On the other hand, the 67 wt.% TLCP/PPS filament tensile strength and modulus were improved by 2 and 12 times, respectively.

The filaments were generated using dual extrusion technology to produce nearly continuously reinforced filaments and to avoid matrix degradation. Rheological tests were taken advantage of to determine the processing conditions. Dual extrusion technology allowed plasticating the matrix and the reinforcing polymer separately in different extruders. Then continuous streams of TLCP were injected below the TLCP melting temperature into the matrix polymer to avoid matrix degradation. The blend was then passed through a series of static mixers,

subdividing the layers into finer streams, eventually leading to nearly continuous fibrils which were an order of magnitude lower in diameter than those of the carbon and glass fibers.

The composite filaments were printed below the melting temperature of the TLCPs, and the conditions were determined to avoid the relaxation of the order in the TLCPs. On printing, a matrix-like printing performance was obtained, such that the printer was able to take sharp turns in comparison with the traditionally used fibers. Moreover, the filaments led to a significant improvement in the tensile properties on using in FFF and other conventional technologies such as injection and compression molding.

Generation of Thermotropic Liquid Crystalline Polymer (TLCP)-Thermoplastic Composite Filaments and Their Processing in Fused Filament Fabrication (FFF)

Mubashir Q. Ansari

General Audience Abstract

In this work two thermoplastic matrices, acrylonitrile butadiene styrene (ABS) and polyphenylene sulfide (PPS), were reinforced with higher melting thermoplastics of superior properties called thermotropic liquid crystalline polymers (TLCPs). This was done so that the resulting filaments could be 3D-printed without melting the TLCPs. The goal of this work was to generate nearly continuous reinforcement in the filaments and to avoid matrix degradation, and, hence, a technology called dual extrusion technology was used for the filament generation. The temperatures required for filament generation were determined using rheology, which involves the study of flow behavior of complex fluids.

Dual extrusion technology allows processing of the constituent polymers separately at different temperatures, followed by a continuous injection of multiple TLCP-streams into the matrix polymers. In addition, the use of static mixers (metallic components kept in the path of flow to striate incoming streams) leads to further divisions of the TLCP-streams which are eventually drawn by pulling to orient the TLCP phase. The resulting filaments exhibited specific properties (normalized tensile properties) higher than aluminum and contained fibers that were nearly continuous, highly oriented, and an order in magnitude lower in diameter than those of carbon and glass fiber, which are commonly used reinforcements. High alignment and lower fiber diameter are essential for printing smoother printed parts.

The filaments were intended to be printed without melting the TLCPs. However, previous studies involving the use of TLCP reinforced composites in conventional technologies have reported the occurrence of orientation relaxation on postprocessing, which decreases their tensile

properties. Therefore, temperatures required for 3D printing were determined using compression molding to retain filament properties on printing to the maximum extent. On printing using an unmodified 3D printer, parts were printed by taking 180º turns during material deposition. Contrarily, the use of continuous carbon fibers required a modified 3D printer to allow impregnation during 3D printing. Moreover, the performance comparison showed that the continuous carbon fibers could not be deposited in tighter loops. The properties of the printed parts were higher than those obtained on using short fibers and approaching those of the continuous fiber composites.

Dedicated to my dad, Qamarul Hassan Ansari and mom, Rashida Qamar

Acknowledgements

It gives me an immense pleasure to thank everyone whose support made this dissertation possible. Most importantly, my adviser, Dr. Donald Baird, for his continuous support, motivation and flexibility which not only allowed me to conduct this research, but also gave me the liberty to pursue extracurricular activities at Virginia Tech. These technical and personal development opportunities led me to build confidence and meet many interesting people. I would also like to acknowledge my committee members, Dr. Richey Davis, Dr. Christopher Williams and Dr. Michael Bortner, for their constructive criticisms and efforts in aligning me with the required resources.

Other faculty members whom I would like to acknowledge include Dr. Stephen Martin for the access to his laboratory equipment and Dr. Gary Whiting for mentoring me in various entrepreneurial projects. I am also sincerely thankful to Cailean Pritchard, Joseph Kubalak, Wenhui Li, and Ethan Smith for training me on the equipment critical for conducting the research. The gratitude also extends to Mac McCord from the BEAM department for the tensile testing data. The office staff of the chemical engineering department, especially Dianne Cannaday, Tina Russel, Andrea Linkous, Michael Vought and Kevin Holshouser deserve gratitude for their support.

I have been privileged to have colleagues who made it very enjoyable to conduct this research. I am especially grateful to Craig Mansfield for the help received in the experiments, entrepreneurial projects, and for his patience to sit through most of my practice talks. I would also like to thank other current and former members of my group: Greg Lambert, Juan Pretelt, Jianger Yu, Tianran Chen and Jeongin Gug. The time spent in

Blacksburg was made worth cherishing by my roommate, Asad Khan. I want to thank him for the constant feedback on the professional front and many interesting conversations.

In my personal life, many people have shaped me into the person I am today. Of all, my parents and brothers, Mufakir and Mudabir, have provided me support and motivation in all walks of my life and deserve my utmost respect and gratitude. Their unending belief in me and continual encouragement has always motivated me to do my best. I am immensely grateful to my wife, Dr. Zaira Zahir, whose love and support made this dissertation possible. Lastly, I am grateful to the Late Professor Abdul Hamid Dar who motivated me to be an engineer.

Original Contributions

The following are the original contributions of this research:

1. The work carried out to generate thermotropic liquid crystalline polymer (TLCP) reinforced composites differs from the work done previously in terms of the application of the rheological tests to select TLCPs and to identify the processing temperatures. The results obtained led to successfully generating nearly continuously reinforced *in-situ* composites using the dual extrusion technology. The rheological tests conducted include shear step strain tests for identifying the minimum processing temperatures of the TLCPs to eliminate residual crystallites, small amplitude oscillatory tests (SAOS) in the cooling mode to identify the extent of supercooling for TLCP selection, and SAOS tests under isothermal conditions to identify stable blending temperatures. Although the shear step strain test has been used to study the TLCPs previously, its application for the identification of the processing condition is novel.
2. The use of nearly continuously reinforced and wholly thermoplastic filaments in FFF was successfully demonstrated by using acrylonitrile butadiene styrene (ABS) and polyphenylene sulfide (PPS) reinforced with TLCPs. Previously, in the only attempt at using TLCP reinforced filaments in FFF by Gray et al. [1], the continuity of the reinforcement was disrupted before processing the filaments, such that the TLCP reinforcement was similar to short fiber reinforced composites. In the current work, the filaments generated using dual extrusion technology, were directly used in a desktop 3D printer without requiring any modification. Additionally, the performance was also compared against the commercially available printers that

enable continuous reinforcement using continuous carbon fiber, glass fiber, and Kevlar. It was found that the TLCP reinforced composites performed similarly to pure matrices, unlike continuous carbon fiber reinforcement, when tighter turns during material deposition were desired.

3. A rigorous postprocessing temperature selection of the TLCP reinforced filaments was demonstrated, which was not attempted previously, to enable sharp turns during the material deposition and to retain the tensile properties of the filaments to the maximum extent on printing. The methods include the use of compression molding to study the effect of temperature on the tensile properties of the compression molded plaques and a novel dynamic mechanical analysis (DMA) method to study the effect of postprocessing conditions on the dynamic properties of the pure TLCP.

Reference:

[1] R.W. Gray IV, D.G. Baird, J. H. Bøhn, Effects of processing conditions on short TLCP fiber reinforced FDM parts, 4(1) (1998) 14-25.

Format of Dissertation

This dissertation follows the manuscript format. Chapter 1 discusses the overall motivation, objectives and a summary of the research work. Chapter 2 provides a detailed discussion of the concepts and technologies associated with the work. Further details of the research have been discussed in Chapter 3, Chapter 4 and Chapter 5, which contain independent motivations, objectives, results, conclusions and references. The overall conclusions and recommendation of the work are presented in Chapter 6. Lastly, the appendix contains a conference paper presented at the Society of plastics Engineers' (SPE) 18th Annual Automotive Composites Conference & Exhibition (ACCE), Detroit. This paper covers the recyclability aspects of the materials generated in this research.

Table of Contents

List of Figures

List of Tables

1 Introduction

Chapter 1: Introduction

Additive manufacturing (AM) is the "process of joining materials to make objects from 3D model data, usually layer upon layer, as opposed to subtractive manufacturing methodologies" [1]. AM has recently attracted immense attention, both in industry as well as academia. With its advent in 1980's, the technology has evolved significantly and differentiated into multiple variants to an extent that it no longer solely serves its original purpose of prototyping [2, 3]. AM has the potential to directly fabricate objects that can be used in a variety of applications, including the fabrication of load bearing components [4]. The automobile and the aerospace industries have also shown interest in fabricating components using AM, to benefit from the advantages that AM brings, i.e. lighter parts due to innovative designs, less waste generation, cost reduction and the ease of changing designs [2, 5, 6]. The push to adopt AM by the automotive and aerospace industries comes from the intense pressure on these industries to improve fuel efficiency which significantly reduces not only the cost per mile of transportation but also helps in reducing greenhouse gas emissions [4, 5]. Some of these goals of the automotive and aerospace industries can be realized by using AM to make the components lighter using complex and lighter designs.

Metals have always outperformed composites in traditional manufacturing whenever load-bearing components are to be fabricated. Similarly, metals have fared significantly well in AM due to their inherent properties. However, the composites have an edge over metals due to lower densities, which has prompted escalating replacement of metals in the automobile industry [7]. Therefore, the use of metals in AM is not a desired solution to print stronger components.

Because the scope of this work did not extend to improve AM technologies, the effort was confined to improve the material properties of the feedstock used in one of the types of AM

technologies, called as Fused Filament Fabrication (FFF). In FFF, polymer-based filaments are used as feedstock for printing objects [8, 9]. The commonly used polymer matrices lack inherent physical properties required for printing stronger parts. Therefore, to overcome such issues composites of the commonly used matrices is preferred when stronger parts are desired. However, the potential use of the composites in FFF has not been fully explored, primarily due to lesser availability of compatible composites and its incompetency to process traditionally used composites [10]. Researchers have demonstrated that the need to print stronger parts can be fulfilled by reinforcing matrices with carbon fiber [11-19], glass fiber [20], ceramic and metallic fillers [8, 21], carbon nanotubes [22] and graphene nanoplatelets [23]. In addition, the matrices used in material extrusion AM has also been broadened to include high performance matrices to enable printing of stronger parts [24-26].

Recently, continuous fiber reinforcements have gained attention for their use in printing components with superior tensile properties [15, 16, 18, 19, 27]. However, these attempts required modification of the printers. Contrarily, our effort was to generate nearly continuously reinforced filaments and to process those without modifying the printers. This was achieved by reinforcing a commonly used thermoplastic, acrylonitrile butadiene styrene (ABS), with a thermotropic liquid crystalline polymer (TLCP). The work was extended to reinforce a high performance polymer, polyphenylene sulfide (PPS) with another TLCP.

To overcome the processing challenges on blending ABS and PPS with TLCPs, the rheology of the matrices and available TLCPs was studied to enable the selection of desired TLCPs and processing conditions, discussed in detail in Chapter 3, Chapter 4 and Chapter 5. It was desired to generate nearly continuous reinforcement and to avoid exceeding temperatures at which ABS

and PPS do not exhibit a stable melt, therefore dual extrusion technology was used to generate filaments [28, 29].

The remainder of this chapter briefly introduces the concepts and technologies associated with the generation of filaments reinforced with TLCPs for application in FFF. In addition, a brief summary of the work discussed in Chapter 3, Chapter 4 and Chapter 5 has also been provided wherever required. These concepts will be discussed in detail in Chapter 2. The section 1.1 gives an overview of FFF and the section 1.2 summarizes filament reinforcement work. In section 1.3, dual extrusion technology has been introduced, which was used to generate the composite filaments. The section 1.4 deals with the significance of rheology associated with filament generation and the section 1.5 covers postprocessing temperature of the TLCP-reinforced composites. Finally, section 1.6 presents the research objectives of the work discussed in this dissertation.

1.1 Fused Filament Fabrication (FFF)

Fused Filament Fabrication (FFF) and Fused Deposition Modeling (FDM) are the terms used interchangeably to describe material extrusion additive manufacturing (MEAM) systems that use filaments as feedstock. FFF was coined to avoid using FDM, a term coined by Stratasys Inc. to trademark its product. In FFF, as shown by the schematic in Fig. 1, polymeric filaments are fed into a chamber, known as the hot end, using a screw feeding mechanism, or a pinch roller mechanism. In the hot end, the matrix component of the filament melts and the extrudate is pushed out from the nozzle by the piston action of the solid portion of the filament. The extruded material is deposited layer upon layer until the object is created [8, 17, 20-23, 30-33]. The tool path is generated using a software that drives the scanning mechanism. Initially only a limited material

selection was available for use in FFF such as acrylonitrile butadiene styrene (ABS), polylactic acid (PLA), and polycarbonate (PC). These matrices lack the tensile properties desired for printing load bearing components. Moreover, the tensile properties of the printed parts are found to be lower than those of the filaments due to the introduction of multiple weld lines during the printing process [11, 30]. Researchers have directed their attention to increase the tensile properties of the printed parts by improving the weld strength [34] and by improving the filament properties by using reinforcements [8, 17, 20-23, 33]. Because the scope of this work is to improve the tensile properties of the filaments to print stronger parts, efforts made to print stronger parts by using composites will now be summarized in section 1.2.

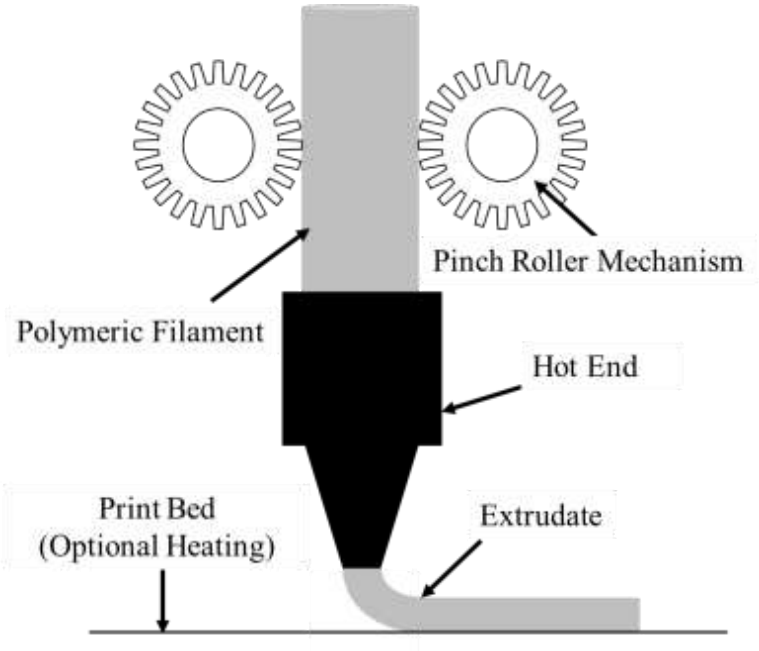

Figure 1-1: Schematic of Fused Filament Fabrication.

1.2 The use of Composites in FFF

Numerous efforts have been made to improve the tensile properties of the printed parts using a wide range of additives, such as metallic and ceramic fillers, carbon and glass fiber, Kevlar, and carbon nanotubes. The use of metallic and ceramic fillers is to print metallic and ceramic parts by burning off the polymeric component (green part), which does not fall within the scope of this work [8, 21]. However, the use of fibers is a very common method to generate composite filaments for printing stronger parts using FFF.

Fiber reinforcements used by the researchers can be broadly categorized into short and continuous fibers. The short fibers such as carbon and glass fibers have been reported to improve the tensile properties of the filaments and hence those of the printed parts [8, 17, 20-23]. The processing method utilized to reinforce the filaments using the extruders leads to a drop in the length of the fibers, thereby diminishing the reinforcing potential of the fibers [11]. This challenge of fiber breakage in extruders does not allow generating continuously reinforced filaments. This problem has been recently overcome by modifying the FFF machines to allow impregnation of the continuous fibers during the printing process [15, 16, 18, 19]. Several other researchers have chosen to sandwich layers of carbon fibers to produce stronger parts [18, 35].

Fiber breakage problems that arises in reinforcing filaments during fabrication process in the extruders was avoided to generate continuously reinforced filaments by using thermotropic liquid crystalline polymers (TLCPs) as reinforcing fibers [32, 36]. This was realized using dual extrusion technology, invented by Baird and Sukhadia [28], that allows formation of the reinforcing fibrils during filament generation. TLCPs are composed of rigid rod-like monomers which are aligned under extensional flow kinematics yielding excellent tensile properties [37].

TLCPs being thermoplastic, possess low density and on blending with the matrices generate wholly thermoplastic composites.

The use of TLCP reinforced composites in FFF has been attempted before by Gray IV et. al [33, 36]. However, the nearly continuously reinforced filaments that were generated using the dual extrusion technology were chopped into pellets, thereby reducing the length of the fibers. The length of the fibers has a strong influence on the tensile properties of the composites [11, 12, 15, 16, 18, 19]. Therefore, the work carried out by Gray IV and coworkers [36] did not fully utilize the reinforcing potential of the TLCPs as the composite filaments were like short fiber reinforced composites. The work presented in this document explored the performance of nearly continuous reinforcement by processing TLCP/ABS and TLCP/PPS filaments in FFF. A method of selection of TLCPs and processing conditions were rigorously devised using rheological tests to result in the generation of filaments that contained higher melting TLCP fibrils in a lower melting matrix. Following filament generation, postprocessing temperature selection of the filaments for processing in FFF was carried out, which resulted in the postprocessing of the filaments like carbon and glass fiber composites.

1.3 Dual Extrusion Technology

TLCPs possess excellent tensile properties that were taken advantage of, to reinforce one of the commonly used thermoplastics in FFF, ABS, and a high performance thermoplastic, PPS. TLCPs are composed of rigid rod-like monomers, which under extensional flow conditions are highly aligned and form long fibrils leading to significantly improved tensile properties [33, 36, 38-42]. Also, the low viscosity of the TLCP-thermoplastic blends makes their blending less energy intensive compared to the solid fiber containing melts [31, 36]. Another major advantage of TLCPs

is that the process of fibril generation takes place during the composite generation which avoids fiber breakage problems that are very common on using solid reinforcements such a carbon and glass fibers [9, 11]. Moreover, the TLCPs cause minimal wear on the processing equipment [42]. Another advantage arises by selecting TLCPs of higher melting temperature for blending with polymer matrices which enables postprocessing of the resulting composites like carbon and glass fiber reinforced composites.

Taking advantage of the above-mentioned properties of the TLCPs becomes a challenge if TLCPs and the matrix polymers are blended in a single extruder. This is because TLCPs have been reported to exhibit processing temperatures above that of the matrix polymer [36, 37]. Therefore, blending is preferred using dual extrusion technology, invented by Baird and coworkers [28, 29], that enables taking advantage of the supercooling behavior of the TLCPs to match the processing conditions of the TLCPs with those of the matrices. The supercooling behavior allows solidification of the TLCPs below their melting temperatures once higher melting crystallites are removed by heating [33, 36, 38-43]. Moreover, dual extrusion technology allows a continuous injection of TLCPs into the matrices, thereby generating nearly continuous reinforcement, as will be discussed in Chapter 4 and Chapter 5.

In dual extrusion technology, shown by the schematic in Figure 2, the TLCP and the matrix resins are plasticated in two different extruders at different temperatures and then multiple TLCP-streams are injected into the matrix-stream. The blend is then passed through a series of static mixers which subdivide the TLCP streams into finer streams, and then the extrudate is drawn to impart molecular orientation in the TLCP phase to generate composite filaments on cooling in a water bath.

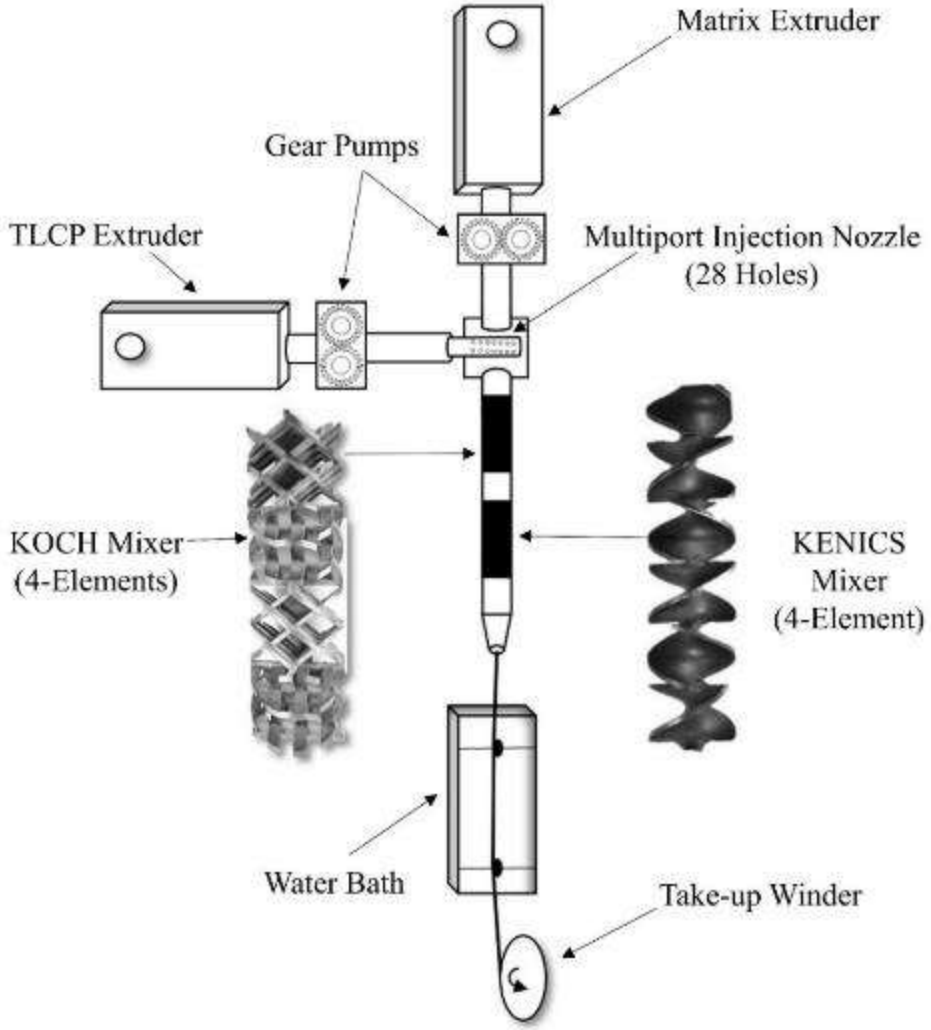

Figure 1-2: Schematic of Dual Extrusion Technology.

1.4 Rheology

The rheological information required to fabricate TLCP-thermoplastic composite filaments in the dual extrusion technology is to select appropriate TLCPs and the processing conditions. The TLCP-selection is crucial and was carried out to avoid matrix degradation and to enable postprocessing of the filaments as a solid-filled system. Small amplitude oscillatory shear (SAOS)

measurements have been extensively used to study the viscoelastic behavior of the polymers. In these measurements, the material is subjected to sinusoidal strain (or stress) and the resulting stress (or strain) is monitored [44, 45]. The matrix polymers and TLCPs were studied using SAOS tests.

The TLCPs need to be heated to temperatures above their melting temperatures to melt all high melting crystallites, which is important to obtain wider supercooling window to match the processing temperatures of the matrix polymer with that of the TLCP. Therefore, identification of such temperatures has been discussed in Chapter 5 using shear step strain experiments. The extent of supercooling of the TLCPs was determined using SAOS tests in the cooling mode. However, the melt stability of the TLCPs below their melting temperature has been reported to be dependent on the temperatures in supercooled regime [37, 46]. SAOS tests in isothermal mode allowed determination of such temperatures. Following injection of the TLCPs into the matrix polymer, the temperature needs to be kept above this temperature to avoid premature solidification of the blend.

1.5 Postprocessing of the TLCP/ABS and TLCP/PPS Composites

The TLCP reinforcement differs from the traditionally used reinforcements such as carbon and glass fiber due to its thermoplastic nature. This demands selection of the post processing temperatures to keep the TLCP-fibrils generated during filament fabrication in solid state. Therefore, the postprocessing temperatures need to be below TLCP melting temperature. It has been reported that the orientation of the TLCPs relax on postprocessing, leading to a drop in the tensile properties of the composite filaments [33, 42]. Therefore, the goal was to minimize drop in the properties on postprocessing the filaments in FFF. The postprocessing temperatures were determined using compression molding, discussed in detail in Chapter 3, Chapter 4 and Chapter

5. In addition, a dynamic mechanical analysis test was also used to study the effect of temperature and residence time on a dynamic property of a TLCP, discussed in Chapter 3. The composite filaments were postprocessed in FFF and the performance has been discussed in Chapter 4 and Chapter 5. The advantage of the TLCP-fibril flexibility at the elevated temperatures was taken in FFF to print rectangular specimens by depositing the composites in tighter loops. The performance was also compared with that of the continuous carbon fiber, discussed in Chapter 4.

1.6 Research Objectives

Objective 1: Establish a method of selection of TLCP's and processing conditions for reinforcing acrylonitrile butadiene styrene (ABS) and polyphenylene sulfide (PPS) using the dual extrusion technology for use in Fused Filament Fabrication (FFF).

Objective 2: Identify a procedure for the selection of the printing temperatures of the TLCP-reinforced filaments to retain their optimum tensile properties.

Objective 3: Using the conditions determined in Objective 2, determine the performance (printing characteristics and tensile properties) of the printed specimens using TLCP/ABS and TLCP/PPS filaments.

References

[1] A. Standard, F2792-12a.(2012).", Standard Terminology for Additive Manufacturing Technologies," ASTM International, West Conshohocken, Pa.

[2] I. Gibson, D. Rosen, B. Stucker, Additive manufacturing technologies: 3D printing, rapid prototyping, and direct digital manufacturing, Springer2014.

[3] T. Wohler, Wohler's 2012 Report on Additive Manufacturing and 3D printing, Wohler Associate, Inc., Fort Collins, CO, USA (2012).

[4] B.P. Conner, G.P. Manogharan, A.N. Martof, L.M. Rodomsky, C.M. Rodomsky, D.C. Jordan, J.W. Limperos, Making sense of 3-D printing: Creating a map of additive manufacturing products and services, Additive Manufacturing 1 (2014) 64-76.

[5] B. Lyons, Additive manufacturing in aerospace: Examples and research outlook, The Bridge 44(3) (2014).

[6] S.H. Huang, P. Liu, A. Mokasdar, L. Hou, Additive manufacturing and its societal impact: a literature review, The International Journal of Advanced Manufacturing Technology (2013) 1-13.

[7] G. Cole, A. Sherman, Light weight materials for automotive applications, Materials characterization 35(1) (1995) 3-9.

[8] M. Nikzad, S. Masood, I. Sbarski, Thermo-mechanical properties of a highly filled polymeric composites for fused deposition modeling, Materials & Design 32(6) (2011) 3448-3456.

[9] S.-Y. Fu, B. Lauke, E. Mäder, C.-Y. Yue, X. Hu, Tensile properties of short-glass-fiber-and short-carbon-fiber-reinforced polypropylene composites, Composites Part A: Applied Science and Manufacturing 31(10) (2000) 1117-1125.

[10] I.J. Petrick, T.W. Simpson, 3D printing disrupts manufacturing: how economies of one create new rules of competition, Research-Technology Management 56(6) (2013) 12-16.

[11] H.L. Tekinalp, V. Kunc, G.M. Velez-Garcia, C.E. Duty, L.J. Love, A.K. Naskar, C.A. Blue, S. Ozcan, Highly oriented carbon fiber–polymer composites via additive manufacturing, Composites Science and Technology 105 (2014) 144-150.

[12] X. Tian, T. Liu, C. Yang, Q. Wang, D. Li, Interface and performance of 3D printed continuous carbon fiber reinforced PLA composites, Composites Part A: Applied Science and Manufacturing 88 (2016) 198-205.

[13] M. Chapiro, Current achievements and future outlook for composites in 3D printing, Reinforced Plastics 60(6) (2016) 372-375.

[14] R.T.L. Ferreira, I.C. Amatte, T.A. Dutra, D. Bürger, Experimental characterization and micrography of 3D printed PLA and PLA reinforced with short carbon fibers, Composites Part B: Engineering 124 (2017) 88-100.

[15] G.W. Melenka, B.K. Cheung, J.S. Schofield, M.R. Dawson, J.P. Carey, Evaluation and prediction of the tensile properties of continuous fiber-reinforced 3D printed structures, Composite Structures 153 (2016) 866-875.

[16] N. Li, Y. Li, S. Liu, Rapid prototyping of continuous carbon fiber reinforced polylactic acid composites by 3D printing, Journal of Materials Processing Technology 238 (2016) 218-225.

[17] F. Ning, W. Cong, J. Qiu, J. Wei, S. Wang, Additive manufacturing of carbon fiber reinforced thermoplastic composites using fused deposition modeling, Composites Part B: Engineering 80 (2015) 369-378.

[18] F. Van Der Klift, Y. Koga, A. Todoroki, M. Ueda, Y. Hirano, R. Matsuzaki, 3D printing of continuous carbon fibre reinforced thermo-plastic (CFRTP) tensile test specimens, Open Journal of Composite Materials 6(01) (2015) 18.

[19] R. Matsuzaki, M. Ueda, M. Namiki, T.-K. Jeong, H. Asahara, K. Horiguchi, T. Nakamura, A. Todoroki, Y. Hirano, Three-dimensional printing of continuous-fiber composites by in-nozzle impregnation, Scientific reports 6 (2016) 23058.

[20] W. Zhong, F. Li, Z. Zhang, L. Song, Z. Li, Short fiber reinforced composites for fused deposition modeling, Materials Science and Engineering: A 301(2) (2001) 125-130.

[21] M. Allahverdi, S. Danforth, M. Jafari, A. Safari, Processing of advanced electroceramic components by fused deposition technique, Journal of the European Ceramic Society 21(10) (2001) 1485-1490.

[22] J. Zhu, B. Wang, Effects of Multi-Walled Carbon Nanotubes on the Properties of Acrylonitrile Butadiene Styrene Nanocomposites Potentially Used for Fused Deposition Modeling, Materials Science Forum, Trans Tech Publ, 2017, pp. 2384-2391.

[23] D. Zhu, Y. Ren, G. Liao, S. Jiang, F. Liu, J. Guo, G. Xu, Thermal and mechanical properties of polyamide 12/graphene nanoplatelets nanocomposites and parts fabricated by fused deposition modeling, Journal of Applied Polymer Science (2017).

[24] P. Geng, J. Zhao, W. Wu, Y. Wang, B. Wang, S. Wang, G. Li, Effect of Thermal Processing and Heat Treatment Condition on 3D Printing PPS Properties, Polymers 10(8) (2018) 875.

[25] A.A. Hassen, J. Lindahl, X. Chen, B. Post, L. Love, V. Kunc, Additive manufacturing of composite tooling using high temperature thermoplastic materials, SAMPE Conference Proceedings, Long Beach, CA, May, 2016, pp. 23-26.

[26] V. Kunc, R.B. Dinwiddie, B.K. Post, L.J. Love, C. Duty, M. Matlack, R. Fahey Jr, A.A. Hassen, Investigation of In-autoclave Additive Manufacturing Composite Tooling.

[27] A.N. Dickson, J.N. Barry, K.A. McDonnell, D.P. Dowling, Fabrication of continuous carbon, glass and Kevlar fibre reinforced polymer composites using additive manufacturing, Additive Manufacturing 16 (2017) 146-152.

[28] D.G. Baird, A. Sukhadia, Mixing process for generating in-situ reinforced thermoplastics, U.S. Patent, 5225488, 1991.

[29] A. Handlos, D. Baird, Processing and associated properties of in situ composites based on thermotropic liquid crystalline polymers and thermoplastics, Journal of Macromolecular Science, Part C: Polymer Reviews 35(2) (1995) 183-238.

[30] S.-H. Ahn, M. Montero, D. Odell, S. Roundy, P.K. Wright, Anisotropic material properties of fused deposition modeling ABS, Rapid prototyping journal 8(4) (2002) 248-257.

[31] A. Datta, H. Chen, D.G. Baird, The effect of compatibilization on blends of polypropylene with a liquid-crystalline polymer, Polymer 34(4) (1993) 759-766.

[32] D. Baird, Effects of Processing Conditions on Prototypes Reinforced with TLCPs for Fused Deposition Modeling.

[33] R. Gray, D.G. Baird, J.H. Bøhn, Thermoplastic composites reinforced with long fiber thermotropic liquid crystalline polymers for fused deposition modeling, Polymer composites 19(4) (1998) 383-394.

[34] N.P. Levenhagen, M.D. Dadmun, Bimodal molecular weight samples improve the isotropy of 3D printed polymeric samples, Polymer 122 (2017) 232-241.

[35] X. Yao, C. Luan, D. Zhang, L. Lan, J. Fu, Evaluation of carbon fiber-embedded 3D printed structures for strengthening and structural-health monitoring, Materials & Design 114 (2017) 424-432.

[36] R.W. Gray IV, D.G. Baird, J. Helge Bøhn, Effects of processing conditions on short TLCP fiber reinforced FDM parts, Rapid Prototyping Journal 4(1) (1998) 14-25.

[37] R.K. Krishnaswamy, D.G. Baird, Wholly thermoplastic composites from woven preforms based on nylon-11 fibers reinforced in situ with a hydroquinone-based liquid crystalline polyester, Polymer composites 18(4) (1997) 526-538.

[38] M. McLeod, D. Baird, The crystallization behavior of blends of thermotropic liquid crystalline polymers, Polymer 40(13) (1999) 3743-3752.

[39] M. Mcleod, D. Baird, Coinjection molded pregenerated microcomposites, Journal of Elastomers & Plastics 31(2) (1999) 143-161.

[40] M. McLeod, D. Baird, Modification of the processing window of a thermotropic liquid crystalline polymer by blending with another thermotropic liquid crystalline polymer, Journal of applied polymer science 73(11) (1999) 2209-2218.

[41] M. McLeod, D. Baird, Injection molding of poly (ethylene terephthalate) reinforced with pregenerated thermotropic liquid crystalline polymer microfibrils, Polymer composites 20(1) (1999) 3-18.

[42] M.A. McLeod, D.G. Baird, The influence of processing variables on the mechanical properties of injection molded pregenerated microcomposites, Composites Part B: Engineering 30(3) (1999) 297-308.

[43] C. Qian, D.G. Baird, The transient shear rheology of a thermotropic liquid crystalline polymer in the super-cooled state, Polymer 102 (2016) 63-72.

[44] K. Hyun, M. Wilhelm, C.O. Klein, K.S. Cho, J.G. Nam, K.H. Ahn, S.J. Lee, R.H. Ewoldt, G.H. McKinley, A review of nonlinear oscillatory shear tests: Analysis and application of large amplitude oscillatory shear (LAOS), Progress in Polymer Science 36(12) (2011) 1697-1753.

[45] R. Subramanian, S. Gunasekaran, Small amplitude oscillatory shear studies on Mozzarella cheese Part I. Region of linear viscoelasticity, Journal of Texture Studies 28(6) (1997) 633-642.

[46] C. Qian, G. Wan, C.E. Frazier, D.G. Baird, Isothermal crystallization of blends containing two thermotropic liquid crystalline polymers, Materials Today Communications 9 (2016) 16-21.

2 Literature Review

Chapter 2: Literature Review

This chapter aims at providing a discussion of the technologies, processes, and concepts relevant to the research discussed in chapters 3-5. The relevance of the topics to the research serves as a guiding factor to decide on the extent of discussion. Section 2.1 gives an overview of additive manufacturing (AM). In section 2.2, the technology relevant to the research, called Fused Filament Fabrication (FFF), is discussed at length as a subtype of the material extrusion additive manufacturing (MEAM). The reinforcing techniques used in FFF have also been reviewed in section 2.3. Section 2.4 is pertinent to a non-conventional type of reinforcement used in FFF called thermotropic liquid crystalline polymers (TLCPs), which is relevant to this research. TLCPs have been discussed as a subclassification of liquid crystalline polymers (LCPs). Section 2.5 is concerned with dual extrusion technology, the method used to generate TLCP-reinforced filaments. A review of the work involving the use of TLCPs as a reinforcement in FFF has also been carried out in section 2.5. Moreover, additional motivation and background have been provided in chapters 3-5, which is relevant to the work.

2.1 Additive Manufacturing (AM)

Additive Manufacturing (AM), as defined by the American Society for Testing and Materials (ASTM), is a "process of joining materials to make objects from 3D model data, usually layer upon layer, as opposed to subtractive manufacturing and formative manufacturing methodologies" [1]. AM translates digital models into physical objects using layer-wise deposition of materials. The advent of AM began with one of its types called stereolithography in 1987, discussed in detail in subsection 2.1.4 [2]. As time progressed, more AM technologies were invented. Presently, AM is a group of seven technologies that allow layer wise fabrication of objects. These technologies include material extrusion, binder jetting, material jetting, vat

photopolymerization, powder bed fusion, directed energy deposition and sheet lamination [2, 3]. With the diversification, the range of materials that can be processed using AM technologies also increased to include polymers, composites, glass, ceramics, metals, food, and biomaterials [4]. AM was initially used for prototyping applications to create scale models of the parts for visualization and assembly testing before actual fabrication and commercialization [5]. However, due to the technological advancements of both AM machines and the materials, objects intended for end-use are also realized [5, 6]. One of the leading market analysts of the AM industry, Wohler associates Inc, in their latest report published in 2018 reported around 30% of AM usage is employed to manufacture end-use products. In its current state AM is used for prototyping, fabrication of tooling components such as molds for injection molding, and the production of end-use products. The increased adoption of AM as a tool for manufacturing or to assist manufacturing has led to an impressive growth of the AM industry. The Wohler report 2018 pegged the growth rate of the industry at 21% to over $7 billion in 2017 [7]. The subsection 2.1.1 describes steps involved in the fabrication of objects using AM, which is followed by the coverage of the major advantages of adopting AM as a manufacturing tool in the subsection 2.1.2 and the major challenges of AM in the subsection 2.1.3. Finally, the types of AM technologies are covered in the subsection 2.1.4, which covers the mechanisms involved and the types of materials processed by those technologies.

2.1.1 Steps involved in the Fabrication of Objects using AM

To fully understand the advantages of AM, it is of immense importance to understand the mechanism of fabrication of objects using AM. Of particular importance is to understand how AM differs from traditional manufacturing technologies, such as injection molding. Because the major objective of this dissertation is to enable processing of the novel composites using one of the types

of AM technologies, a comparison with traditional polymer composite processing technologies, such as injection molding, is merely a method to highlight the differences. The steps involved in the fabrication of objects using AM are listed below [4, 8-10]:

i) A digital model of the object is created

ii) The model is used to generate toolpaths for the 3D printer

iii) Fabrication of the object is executed using layer-by-layer material deposition

The steps listed above are basic steps involved in fabricating objects of any complexity. The digital models can be obtained using CAD software or 3D scanning. In the medical and the dental industry, due to patient-specific customization, images can also be obtained using other imaging techniques such as X-ray scanning and CT-scanning. The decisions taken at the model generation stage to design for AM differs from the decisions made for the conventional manufacturing technologies [4]. The models are generated without considering manufacturing constraints because objects of any complexity can be fabricated without the requirement of part-specific tooling such as the use of dies and molds. Therefore, design freedom is fully utilized to obtain models that can lead to lightweight and performance-targeted printed parts [8, 11, 12]. Comparatively, in traditional manufacturing technologies only those designs are permitted which minimize manufacturing hurdles and lower the manufacturing and assembly cost [4, 8]. For example, in injection molding, the complexity of the mold dictates the complexity of the final part.

During the design stage, the advantage of optimization tools, such as topology optimization may also be taken on using AM to further improve the performance of the printed parts. For instance, Atzeni and Salmi [8] studied the reduction in weight that is possible on using AM to

fabricate a landing gear model and showed that the optimized model was 2.7 times lighter than the model meant for fabrication using conventionally used high-pressure die-cast process.

Once the model is generated, it is sliced into numerous layers to generate the tool path for material deposition. The decisions taken at this stage affects the properties of the printed parts and the parameters that can be controlled depend on the type of AM technology. For example, in the type of AM technology that uses filaments as feedstock (relevant to this work), these factors constitute print speed, layer height, layer width, print temperature, and bed temperature [13]. Additionally, the parameters may be chosen to strike a fine balance between the desired properties of the printed parts and the fabrication time. For instance, smaller layer height leads to better surface finish, at the cost of longer fabrication times. The parts generated may also be affected by introducing porosity at this stage, which is done to achieve desired properties such as lighter parts. The porosity of the printed parts is controlled by incorporating gaps between the roads of the materials that are deposited.

Finally, on executing part fabrication, minimal monitoring is required. The parts fabrication depends on the type of AM technology and eventually on the feedstock such as filaments, pellets, and powders that are composed of polymers, composites, metals, and ceramics [6, 14]. Due to the complexity of the fabrication techniques, flaws introduced during printing lead to quality control issues, therefore monitoring is recommended to obtain consistent parts.

2.1.2 Advantages of adopting AM as a Manufacturing Tool

The advantages of AM arise due to layer-by-layer fabrication technique and no part specific tooling requirement. The ability of AM to fabricate complex shapes leads to lightweight and efficient parts, which reduces raw material usage [4, 6, 15]. Because the material that is required

in the part is only used during fabrication, raw material wastage is minimized compared to the conventional subtractive manufacturing technologies. Additionally, due to minimal manufacturing constraint number of spare parts can be minimized which reduced the assembly cost [4]. For example, GE successfully tested a plane powered by a turboprop engine that was manufactured by deploying AM in conjugation with other manufacturing technologies [16]. It was reported that the number of spare parts were minimized from 855 to just 12. Additionally, a reduction of 100 pounds in the weight of the engine was achieved that improved the fuel efficiency by 20%.

On using AM, part specific tools such as dies and molds can be avoided, which leads to a significant reduction in the lead times for the product development [17]. This benefits industries that require fast design changes, such as the apparel, footwear, and the sports industries [18, 19].

2.1.3 Major Challenges faced by AM

Although tessellation of layers in AM leads to many advantages as discussed in the previous subsection, but this mode of fabrication also gives rise to many disadvantages. Due to layer-wise material deposition, the tensile properties of the parts are generally lower in the direction perpendicular to the layer due to poor inter-layer adhesion [20]. In addition, the appearance of the printed parts is rougher, and the time required to fabricate objects is longer as the objects require layer wise material deposition [6]. Moreover, flaws introduced during fabrication in any layer is propagated to subsequent layers.

Apart from the problems that arise due to the mode of fabrication, limited material selection also leads to inferior properties of the printed parts in comparison with those fabricated using conventional technologies. Traditionally, automotive and aerospace industry have replaced metals with composites in the pursuits of light weighting to achieve high fuel economy. Due to material

limitation, AM has only served to reverse the trend by promoting metals over the composites because of the poor printed properties that arises on using polymers and polymer derived feedstock. Although the use of metals is recent in comparison with the use of polymeric materials in AM. Wohler report 2018 reported the growth of around 80% for the metal AM in 2017 [7]. These numbers demonstrate higher interest in metallic AM, over the other technologies. Therefore, the requirement of high performance materials is quite essential to avoid going back to metals for superior properties.

2.1.4 Types of AM Technologies

The remainder of this section gives an overview of the major AM technologies by discussing their working principles. However, the type of AM technology relevant to this research, called Fused Filament Fabrication (FFF), will be discussed at length in section 2.2 and has not been covered in this section.

2.1.4.1 Powder bed fusion (PBF)

Powder bed fusion (PBF) involves the fabrication of parts by inducing fusion between powdered raw materials using an energy source comprising of either lasers or electronic beams [3, 4]. The PBF systems have a mechanism to prepare a layer of a powder bed and a mechanism to deliver energy to a specified location on the bed. The energy source fuses the powder by either partially melting (a process called sintering) or completely melting to cure a layer. Upon the completion of each layer, next layer is prepared by spreading the powder. The primitive PBF, invented by Dechard and Beaman, processed polymers and, hence, was narrow in its scope [21, 22]. Modern PBF is capable of processing metals, polymers, composites, and ceramics [3, 4]. Polymer PBF's use polyamide, epoxy or a combination of polyamide and epoxy based raw

materials for processing [4]. The examples of metal powders that are processed in PBF are Titanium, stainless steel, aluminum, cobalt-chrome [23].

2.1.4.2 Stereolithography

In this technology, radiation curable resins are used to form 3D printed parts. The radiation, most commonly ultraviolet light, scans a layer of resin in a vat to cure a layer [4]. Once the layer is completed, fresh resin is applied on the previously formed layer to cure using the radiation. This process is repeated multiple times until the part is formed. The resins commonly used are acrylate and epoxy-based monomers [4, 24].

2.1.4.3 Laminated Object Manufacturing

In this technology, sheets of materials such as those of metals and papers are successively laminated to form different layers of the object that is printed [4]. The individual sheets are bonded together by adhesive bonding, thermal bonding, clamping or ultrasonic welding. The sheets are cut as per the geometry of each layer and, the unused portion of the sheet is removed, which generates waste similar to subtractive manufacturing technologies [3].

2.1.4.4 Material Jetting

In material jetting, material that forms the part is dispensed from the print head like inkjet printing. The dispensed material upon impacting the surface, forms the layer after either heating or photocuring. Once a layer is complete, the process is repeated after lowering the print bed by a layer [4].

2.1.4.5 Binder Jetting

Binder jetting process operates as a combination of material jetting and PBF. In this technology, binder is dispensed from the print head on to a powder bed that forms the structural component of the object being printed [4]. Once the binder is spread on a layer, the print bed is lowered down by a layer and a fresh powder layer is coated [25]. This process is repeated multiple times until the object is printed.

2.2 Material Extrusion Additive Manufacturing (MEAM)

As discussed, several AM technologies are available to fabricate objects. However, the most common and comparatively less expensive is a type called Fused Filament Fabrication (FFF). As per the Wohler report published in 2018, the number of desktop printers sold in 2017, consisting of most commonly FFF systems was more than 500,000, almost double than that sold in 2016 [7]. The revenue generated from these desktop printers constitutes more than 30% of that generated from all AM. Despite high share of the revenue, revenue from the filament feedstock constitutes only 20% [7]. This is due to higher attention given to the metallic AM due to superior properties that, generally, leads to end-use parts. Therefore, a detailed discussion of FFF is highly required to determine the scope of improvement of the printed parts, which is the overall motivation of the research.

MEAM constitutes the most common form of AM technology in which the material that forms various layers of the part under fabrication is extruded through a nozzle [13, 20]. MEAM can broadly be categorized into two parts. The most pervasive form uses filaments as feedstock and is called Fused Filament Fabrication (FFF) [26, 27]. These systems are smaller in scale and mostly desktop sized. The other form is industrially more pertinent, called Large Format Additive

Manufacturing (LFAM) or Big Area Additive Manufacturing (BAAM), which use pellets as feedstock [28-32]. In these systems extruders are mounted on a gantry that is capable of scanning in 3-dimensions to deposit the extruded material. Although a detailed discussion of LFAM/BAAM is beyond the scope of this effort, the terms LFAM and BAAM will be used interchangeably throughout this. In the remainder of this section FFF is discussed in detail due to its relevancy to the research.

2.2.1 Fused Filament Fabrication (FFF)

In FFF, a filament feeding mechanism comprised of a pinch roller mechanism delivers filaments into a liquefier called a hot end. As shown in Figure 2-1, the polymer-based filament is heated in the hot end, where it melts and is then pushed out from a nozzle by the piston action of the solid portion of the filament. The parts are fabricated on a print bed with optional heating. In certain cases, the whole assembly is enclosed in chambers to control the temperature. The combination of the print bed and the print head movements enable scanning of the enclosed space to deposit the extrudate. Once a layer is fabricated, either the print bed or the print head moves by a layer in the height direction to print the next layer. The motion of the pinch rollers, hot-end temperature, and the motion of the print head is computer-controlled.

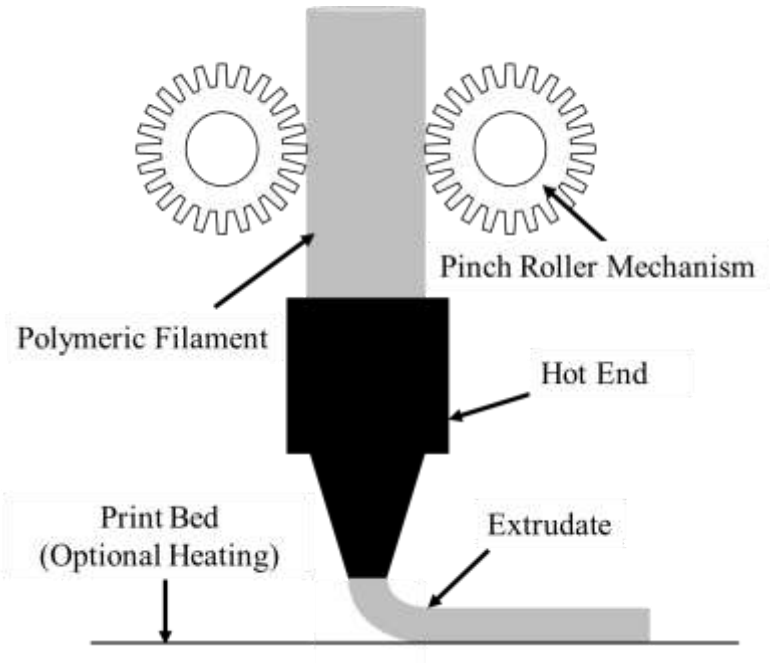

Figure 2-1: A schematic of FFF.

The mechanisms used to feed material in MEAM systems can widely vary from machine to machine. Pinch rollers are widely used in FFF and the screw feeding mechanisms are common in other MEAM systems [4, 13, 28-34]. The advantage of the screw feeding mechanism, more commonly used in LFAM/BAAM systems, is that higher flow rates can be achieved [28, 29, 31, 32]. To compare, the volumetric flow rate of BAAM has been reported to be more than 16387 cm^3/hr., around 1000 times that of FFF [29]. Moreover, the screw feeding mechanism have been reported to avoid problems associated with the processing of high viscosity matrices such as polyether-ether-ketone [35]. Another advantage is that inexpensive pellets can be processed in BAAM, instead of filaments, which eliminates an additional filament generation step. To compare the raw material cost, acrylonitrile butadiene styrene (ABS) pellets can be purchased for $2-3/lb., whereas the filaments of ABS are sold for $20-30/lb. [28, 29, 31, 32].

The pinch roller mechanism is ubiquitous due to its ease of operation and comparatively inexpensive installation and is used to process low viscosity matrices in FFF to avoid flow instabilities such as that arising due to buckling [35]. It uses filaments, which requires tight filament diameter tolerance to avoid inconsistencies in the extrudate flow rate. The inconsistent flow rate leads to uneven deposition of the extrudate which affects the quality of the printed parts. Recently, continuous fibers have been used to print functional components. Several researchers have demonstrated the use of continuous carbon, glass and Kevlar fiber to attain superior tensile properties [36-41]. These solutions demand the use of the pinch roller mechanism because the screw feeding mechanism leads to fiber breakage, thereby disrupting the continuity of the reinforcement. The major disadvantage of the pinch roller mechanism is that the flow rate is limited by buckling, slippage of the filaments between the rollers, and backflow of the polymeric melt [35, 42]. Because the scope of this dissertation is to emphasize the methods of improvement of the filament properties, these inefficiencies will not be discussed. The discussion in the next subsection covers the properties of the pure matrices used in FFF. Section 2.3 emphasizes the methods of improvement of the tensile properties of the printed parts.

2.2.2 Matrices used in FFF

Acrylonitrile butadiene styrene (ABS), polycarbonate (PC) and polylactic acid (PLA) are the most common polymeric matrices used to fabricate filaments for applications in FFF [4, 13]. As can be seen in Table 2-1, which shows the tensile properties of the matrices used in FFF, the tensile properties of pure ABS, PC and PLA are inadequate to print end-use objects [43-46]. It is important to understand that the tensile properties of the printed specimens are lower than those of the filament due to the defects that are introduced during printing, such as poor inter-layer adhesion due to high cooling rates [20]. Researchers have extensively reported introduction of voids and

poor inter layer bonding in the specimens fabricated using FFF which leads to a drop in the physical properties of the printed parts. Duty and coworkers [28] reported the presence of triangular defects that were introduced due to poor bonding between the beads. Moreover, the presence of bubbles, believed to be due to outgassing of the volatiles at elevated temperatures, was also reported in the printed specimens. Dawoud et al. [47] did a comparative study of the tensile properties obtained on processing ABS using FDM and injection molding. It was found that the tensile strength of the printed specimens was lower compared to that obtained for the injection molded specimens. Injection molded specimens were 37.7 MPa in tensile strength, whereas the printed specimens were 34.3 MPa in tensile strength. Higher properties obtained on injection molding were explained by higher densities of the parts. Thus, FDM parts were reported to possess a lower compaction leading to lower tensile strength. Recently, attention has shifted to high performance polymers to harness the advantages of superior tensile properties in realizing stronger printed objects. These matrices can maintain properties even in harsh chemical and thermal conditions [48]. Table 2-1 also lists the tensile properties of the high performance polymers used in FFF. Comparatively, the tensile properties are higher than those of ABS, PC and PLA. Although not listed in the table, polyphenylsulfone (PPSU) and polyaryletherketone (PAEK) have also been used as matrices in FFF [48].

Table 2-1: Tensile properties of matrices used in FFF.

Matrix	Manufacturer	Specimen	Tensile strength MPa	Tensile modulus GPa	Reference
ABS	Stratasys	Filament	26.0	2.2	[49]
PC	N/A	Printed	44.3	1.6	[50]
PLA	3DXTech	Printed	3.4	59.3	[51]
Nylon-6	Markforged	Printed	61.0	0.5	[36]
PEEK	Victrex	Bulk Property	98.0	3.2	[35]
PEI	Stratasys	Filament	33.0	2.3	[49]
PPS	N/A	Printed	61.1	2.2	[20]

ABS=Acrylonitrile Butadiene Styrene, PLA=polylactic acid, PC=polycarbonate, PEI= polyetherimide, PEEK= polyaryletherketone, PPS= polyphenylene sulfide.

2.2.3 Print Patterns used in FFF

FFF, like other AM technologies, allows deposition of the material that forms different layers of the objects wherever specified. The control over the location of the material deposition allows achieving desirable performance of the printed parts. Any object can be printed using three basic print patterns, contour, raster and a combination of the two, as shown in the Figure 2-2. To achieve smoother surfaces, a contour pattern may be chosen to print exterior regions of the objects

because the tool path generated allows deposition of the extrudate parallel to the surface of the object. In the contour pattern, the print head starts from a point and ends adjacent to the starting point. This requires detachment of the nozzle from the print surface, a process called severing. For pure matrices, severing does not require any additional mechanism as the extrudate is soft enough to be detached by the motion of the print head. The interior regions of the objects are generally printed using raster pattern. This pattern doesn't require severing and allows variation of the gap between the roads to minimize filament consumption, which leads to lighter parts. Additionally, the roads can be varied between layer to layer to achieve desirable tensile properties.

Objects are printed by using a combination of the contour and the raster pattern, as shown in Figure 2-2. The contour may be chosen to form the outer surface while the raster may form the inner roads. It is important to understand that the tensile properties of the parts are highly dependent on the orientation of the roads, as has been reported by several researchers [47]. If all roads are aligned in the loading direction, the tensile properties are maximum. Any change in the angle of the roads with respect to the loading direction leads to a drop in the tensile properties.

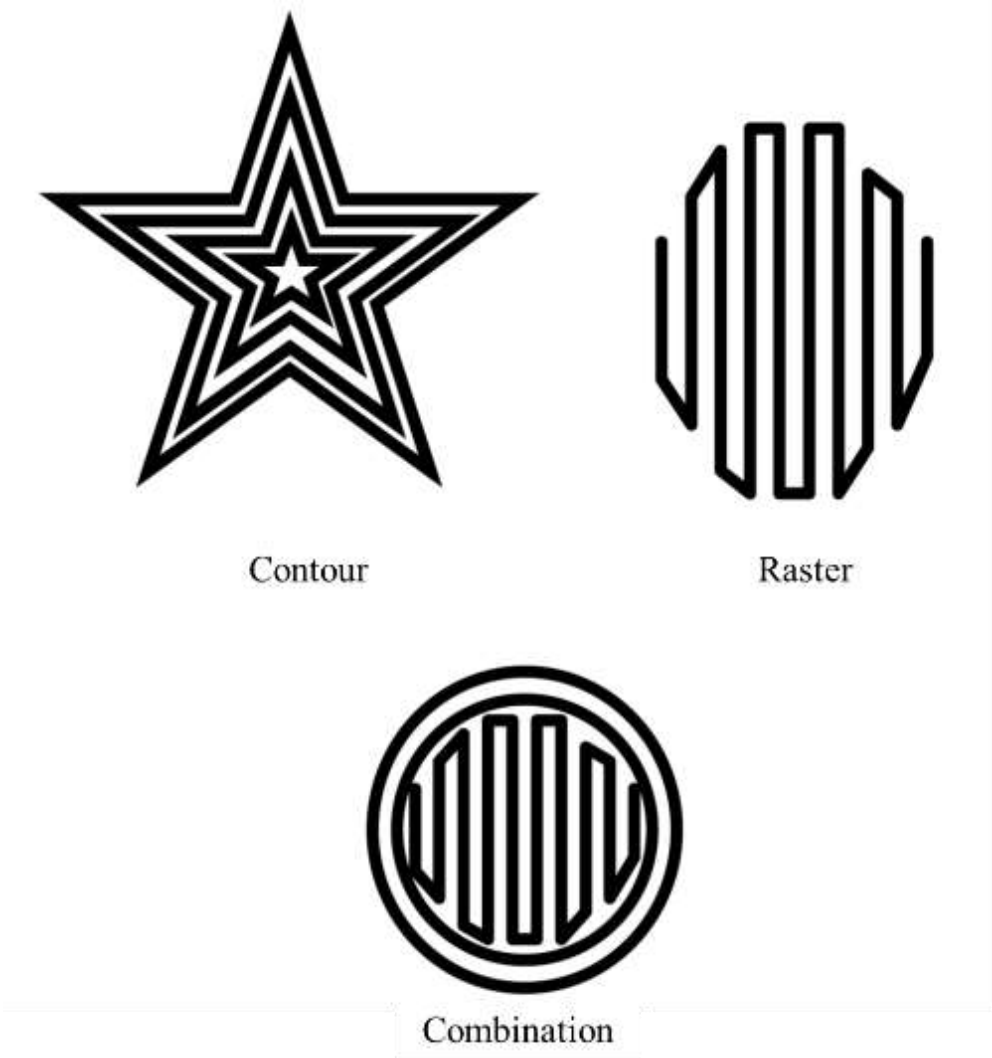

Figure 2-2: Commonly used print patterns in FFF [52].

2.3 Printing Composite Parts using FFF

The tensile properties of the commonly used matrices in FFF, such as ABS, PLA and PC, lack the tensile properties required to print stronger parts as shown in the previous section. Therefore, the superior properties of the fillers such as metallic and ceramic fillers, carbon nanotube, carbon fiber, glass fiber, Kevlar, and jute fiber are taken advantage of to form

composites [8, 26, 34, 36]. These composites exhibit improved properties in comparison with those of the pure matrices. Additionally, further improvement in the tensile properties of the high performance matrices is also carried out using fibers [29, 32-34]. The metallic and ceramic fillers have been used in the matrices to fabricate filaments for application in FFF. Nikzad et al. [53] used metallic fillers in ABS and studied the thermal and mechanical properties of the filaments produced. The fillers used were copper and iron, 45 μm in diameter. Concentrations up to 40 wt.% filler were used in the filament fabrication, following which the improvement in the properties of the printed specimens were reported. Most of the work carried out by the researchers using metallic and ceramic fillers was to fabricate metallic and ceramic parts for the end use [54]. The polymer matrix only forms the binder and is referred to as the green part [26]. The composite parts printed using the filaments are then subjected to postprocessing by removing the green part to sinter the filler which leads to the metallic and ceramic final parts. In such applications, researchers have used iron, copper, steel, alumina, silicon nitride [26, 27, 53, 55]. Because this form of FFF is beyond the scope of this research, further discussion will not follow. However, a detailed review of the work carried out using short and long fiber reinforcement is provided due to the relevance to the work discussed in this research. Subsection 2.3.1 gives an overview of the short fiber reinforcement work, which is followed by the overview of continuous fiber reinforcement work in subsection 2.3.2.

2.3.1 Short Fiber Reinforcement

Short fibers have been traditionally used to achieve improvement in the tensile properties of composites. Similarly in FFF the use of short fibers is also a common technique to enable printing stronger components than that is possible with pure matrices. In this method, the composite filaments are generated by blending the reinforcement with the matrices in an extruder

[34]. The composite filaments are then postprocessed in FFF to print stronger parts. Few researchers have reported abrasion of the hot end on processing short fiber reinforced composites and recommended the use of abrasion resistant hot ends [56]. Barring minor inexpensive modifications, the use of short fibers in FFF is the most economical method to print stronger parts. Contrarily, the use of continuous fibers, as is discussed section 2.3.2, require costly modifications of the printer. A wide range of polymers such as ABS, PLA, PC and Nylon 6 have been reinforced using short fibers [4, 43, 53, 57].

Researchers have extensively used carbon fiber (CF) to fabricate reinforced parts using FFF to take the advantage of its superior tensile properties and low density (1.8 g/cm^3) [32, 58, 59]. The tensile modulus and strength of the neat carbon fiber can be as high as 4.9 GPa and 230 GPa, respectively [58]. Another important advantages of using carbon fiber as reinforcement is that it increases the thermal conductivity of the matrix-fiber blend. The thermal conductivity of pure ABS was reported to be 0.18 W/m K, lower than that of 13 wt.% carbon fiber/ABS (thermal conductivity: of 0.4 W/m K). It was reported that higher thermal conductivity of the blend led to reduction of the thermal gradient during printing, which enabled printing parts of larger dimension with minimal warpage [32]. A comparison of the warpage in a 1.8 m long curl bars was performed by Love et al. [32]. It was found that the part containing carbon fiber was resistant to warpage compared to the bars fabricated using pure ABS. Additionally, Love et al. [32] reported an increase in the tensile properties on using 13 wt.% carbon fiber/ABS. The print direction tensile strength and modulus were 70.7±4.0 MPa and 8.9±1.0 GPa, respectively, whereas those in the transverse direction were found to be 7.0±2.6 MPa and 1.5±0.1 GPa, respectively.

Tekinalp et al. [34] used carbon fiber 0.2-0.4 mm in length to reinforce ABS and obtained around 115% increase in the tensile strength and around 700% increase in the tensile modulus of

the printed parts. The effect of the carbon fiber concentration was also studied. It was found that nozzle clogging was prominent at higher loading. Moreover, the original length of the carbon fibers was 3.2 mm, which on blending led to a drop in the fiber length to 0.2-0.4 mm due to fiber breakage. Fiber breakage arising due to fiber-fiber, fiber-matrix, and fiber-equipment interactions is the biggest disadvantage that arises on using traditionally used fibers [60]. Because the tensile properties of the composites are highly dependent on the aspect ratio of the fibers, the reinforcing potential of the short fibers are not fully utilized.

PLA has also been reinforced with carbon fiber for postprocessing in FFF [40, 43]. Ferreira et al. [43] reinforced PLA with 15 wt.% carbon fiber of length 60 μm and reported improvement in the tensile properties. The maximum tensile modulus obtained in the fiber alignment direction was 7.5±0.1 GPa in comparison with 3.4±0.2 GPa for pure PLA. The maximum tensile strength obtained for the same configuration was 53.4±0.2 MPa compared to 54.7±1.9 MPa for pure PLA. The insignificant improvement in strength was attributed to poor adhesion between carbon fiber and PLA and to the shorter length of the fibers.

Glass fiber (GF) is another common reinforcement used to print stronger parts due to its high tensile strength (~2.0 GPa) and modulus (~78.5 GPa). However, the density of the glass fiber (~2.6 g/cm^3) is higher compared to that of the carbon fiber (~1.8 g/cm^3), which lowers the specific properties (tensile properties divided by the density) of the glass fiber composites [44]. Zhong et al. [46] used short glass fibers to reinforce ABS using different concentrations, up to 18 wt.% of glass fiber, and reported a maximum tensile strength of 58.6±11.15 MPa.

Anwer et al. [61] used carbon nanofibers (CNF's) to reinforce PLA for application in FFF. CNF's possess high stiffness (240 GPa), high strength (2.9 GPa) and are cheaper compared to

carbon nanotubes [61]. The composites of concentrations up to 15 wt.% CNF were fabricated using a twin screw extruder. The average diameter of the CNF's was 150 nm. Although a significant increase in the tensile modulus was reported, the increase in the tensile strength was less.

In conclusion, the use of short fibers leads to improvement in the tensile properties of the printed parts. Additionally, their use does not require major modifications of the printer and leads to increment in the tensile properties. However, the major disadvantage is the extensive fiber breakage that arises during filament fabrication that prevents taking optimum advantage of the reinforcing potential of the fibers. Moreover, the random fiber orientation leads to a further drop in the tensile properties in comparison with those of the highly aligned fiber composites. In addition, nozzle clogging, and poor fiber wetting is also a concern at higher fiber loading. It is required to have a stronger adhesion between the matrix and fiber to transfer the load from the matrix to the fiber [44]. These problems have shifted the attention of the researchers to the continuous fibers, which is discussed in detail in the next subsection.

2.3.2 Continuous Fiber Reinforcement

Longer fibers lead to higher tensile strength and modulus in comparison with shorter fibers due to higher aspect ratio of the fibers [43]. In addition, short fibers reduce the mechanical properties as the composites contain more fiber ends which have been reported to act as stress concentrators [62]. The aspect ratio of the fiber is further reduced during the compounding step due to fiber breakage [34]. As discussed in subsection 2.3.1, Tekinalp [34] used carbon fiber, 3.5 mm in length, to reinforce ABS and found that the length dropped to 0.2-0.3 mm after extruding. Similarly, Bigg and coworkers [62] reported a drop in fiber length from 6.0 mm to 0.5 mm on using the extrusion process. To achieve the maximum reinforcing capability of the fibers, the

aspect ratio of the fiber should be above a critical value, which depends on the ratio of fiber strength and fiber-matrix bond strength [63, 64]. Bigg [63] showed that the fibers require aspect ratio at least 10 times higher than the critical value to obtain 95% tensile strength of the fiber [62]. Thus, the use of long fibers is highly recommended to print stronger parts.

To take advantage of using long fibers, researchers have attempted two different approaches. The first approach is to sandwich carbon fiber between the layers of matrices and the second approach is to impregnate fibers separately into the parts during the fabrication process [15, 37, 38, 40, 65]. The first approach is not very common in comparison with the later approach. The later approach leads to a continuous reinforcement and is also commercially available. Mori et al. [65] embedded 70 mm carbon fibers between the layers of ABS using the sandwiching technique. Although, improvement in the tensile properties was reported, the sandwiching process was not continuous as the bottom and the top layers were first printed and then carbon fibers are introduced, followed by the thermal consolidation of the layers.

In the nozzle impregnation method, as shown in Figure 2-3, the filament and the continuous fiber reinforcement are separately fed into the hot end of the FFF machine [36-41, 66]. The parts printed have a continuous fiber reinforcement, thereby improving the mechanical properties significantly. Researchers have used carbon fiber, glass fiber, jute fiber and Kevlar to impregnate the parts during printing. Matsuzaki et al. [38] reinforced PLA using carbon fiber and jute fiber using the nozzle impregnation technique. The tensile modulus and strength of the carbon fiber reinforced parts were 19.5±2.1 GPa and 185.2±24.6 MPa, respectively, an increase of 599% and 435% compared to the tensile strength and modulus of pure PLA specimens [67]. The tensile modulus and strength for jute reinforced PLA samples were reported to be 5.11±0.41 GPa and 57.1±5.3 MPa, respectively, an increase of 157% and 134%, respectively, compared to the tensile

strength and modulus of pure PLA specimens, respectively. In this study, continuous carbon fiber was found to be more effective in reinforcing PLA compared to jute fiber.

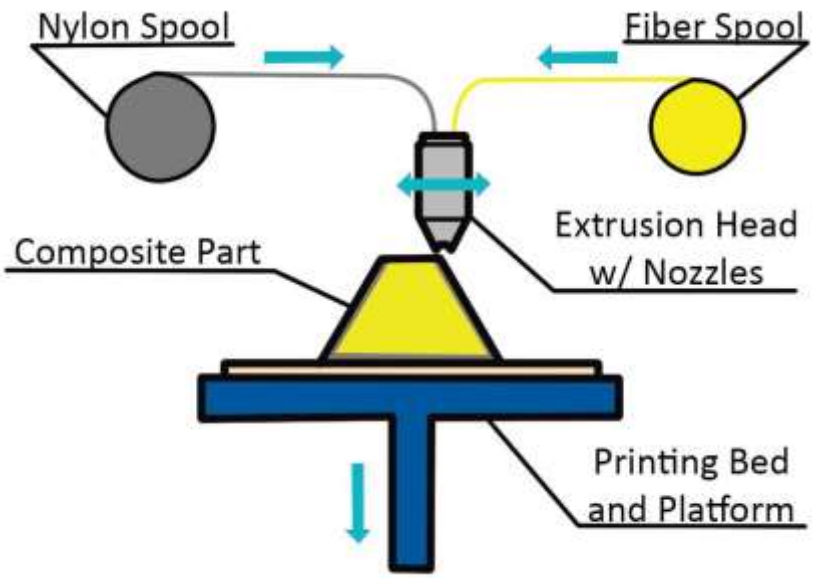

Figure 2-3: Schematic of fiber-impregnation method to reinforce using continuous fiber [66].

In another example of the fiber impregnation mechanism, Tian et al. [40] obtained a flexural strength of 335 MPa and modulus of 30 GPa on using continuous reinforcement of 27 wt.% carbon fiber in PLA. Li and coworkers [37] were able to improve the tensile strength and modulus by 14% and 164%, respectively, on reinforcing PLA with continuous carbon fiber.

Currently, Markforged is the only company that offers machines that are capable of printing continuously reinforced parts using direct impregnation technology [15]. Their machines are capable of using carbon, glass, and Kevlar fiber as continuous reinforcements [15]. Researchers have used machines sold by Markforged to print continuously reinforced parts. Melenka and coworkers [39] used a Markforged machine to reinforce nylon-6 with Kevlar and obtained tensile

moduli of 1.8, 6.9, and 9.0 GPa on using fiber volume fractions of 4.0, 8.1 and 10.1% respectively [68]. Similarly, Klift et al. [41] used carbon fiber to reinforce Nylon-6 using a Markforged printer and reported significant improvement in the tensile properties [41].

2.3.3 Print Patterns used to Print Composite Parts in FFF

The use of short fiber reinforced composite filaments regardless of the fiber type is not restricted by the print pattern. This is because severing can occur effortlessly during the printing process. However, the use of continuous fiber reinforcement poses restrictions on the selection of the print patterns. Several researchers have reported that the stiffness of the fibers prevents taking sharp turns on using continuous reinforcements. Dickson and coworkers [36] demonstrated using continuous Kevlar, carbon and glass fiber that only two patterns are possible with the use of continuous fibers, as shown in Figure 2-4. The fibers can be deposited using either the concentric pattern or the isotropic pattern. It was shown that glass fiber and Kevlar could be deposited using both patterns, whereas carbon fiber could only be deposited using the concentric pattern. This is because the isotropic pattern requires a very sharp change in the direction of the print head during the reinforcement deposition. Additionally, regardless of the type of the pattern used, the continuous fibers require a severing mechanism to detach the nozzle from the print surface. Klift et al. [41] printed a square plaque, as shown in Figure 2-5, using continuous carbon fiber. It was reported that the stiffness of the fiber prevented deposition of the fiber in the inter region of the plaque.

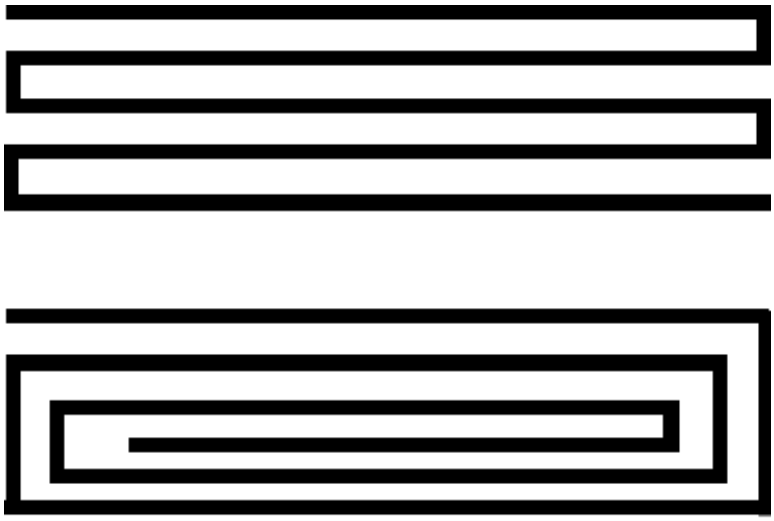

Figure 2-4: Print patterns possible with the use of continuous fibers. The top pattern has been named as the isotropic pattern, whereas the bottom pattern has been named the concentric pattern [36].

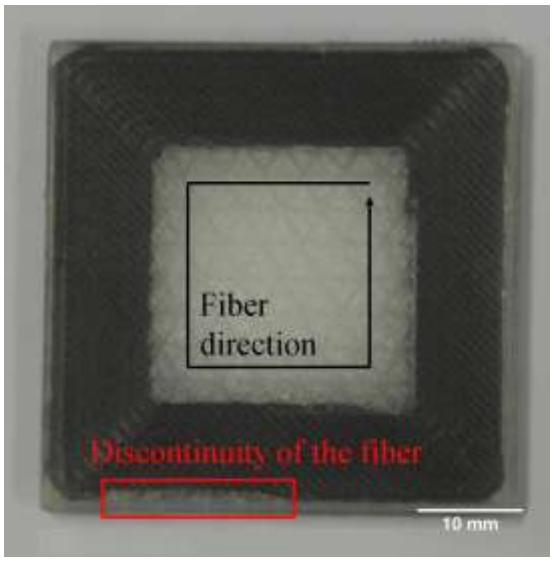

Figure 2-5: A square plaque printed by reinforcing continuous carbon fiber that demonstrates that the interior regions cannot be reinforced as they require sharp change in the direction of the printer during reinforcement deposition [41].

2.3.4 Major disadvantages of using Continuous Fibers in FFF

As discussed in subsection 2.3.2, researchers reported encouraging results on using continuous fibers due to a significant improvement in the tensile properties. However, several disadvantages are also associated with the use of continuous fibers. Briefly mentioned in subsection 2.3.3 is the inability to print all patterns. The stiffness of the fibers prevents sharp turns during material deposition. Additionally, a severing mechanism is also required to detach the nozzle from the print surface. A detailed discussion is included in chapter 4.

Because the use of the continuous fibers demands a major modification of the printers, the adoption of the continuous fibers becomes expensive in comparison with the use of short fibers. Researchers have also reported poor adhesion between the matrix and the fiber as both are separately dispensed from separate nozzles. A solution to mitigate these problems formed the major motivation of this research. The adoption of nearly continuously reinforced filaments without the modification of the printers has been demonstrated in chapter 4 and 5. Therefore, a class of non-conventional reinforcement called thermotropic liquid crystalline polymers (TLCP) that were used in the work discussed in chapters 3-5 forms the topic of discussion in section 2.4. TLCPs have been discussed as a subclassification of a broader class of polymers called Liquid Crystalline Polymers (LCPs).

2.4 Liquid Crystalline Polymers (LCPs)

Liquid crystalline polymers (LCPs) form structured fluids in the molten state or in solution and exhibit a phase of matter intermediate to the solid and the liquid crystals [69, 70]. The LCPs possess excellent properties such as low dielectric constant, dimensional stability, good barrier properties, and high thermal and chemical resistance [71]. The phase of matter exhibited by the

LCPs is called the mesophase or the mesomorphic phase and has been classified by Friedel [72] into 3 types, depending on the type of ordering. These are nematic, smectic and cholesteric phases, as shown in Figure 2-6 [73]. The nematic phase exhibits long range orientational order and no positional order such that the chains, consisting of rod-like monomers, are parallel to each other [71, 72, 74-76]. The smectic phase exhibits a long range orientational and positional order, such that the polymer chains are aligned in one direction in addition to being layered. The cholesteric phase consists of a stack of nematic layers, such that each layer is at an angle with the neighboring layer [77]. Moreover, LCPs exhibit a polydomain structure, as shown in Figure 2-7 [78]. The orientation within each domain is represented by a vector **n**. Although, within each domain, the orientation is uniform, but it varies heterogeneously from domain to domain. The domain size can be on the order of several microns [79].

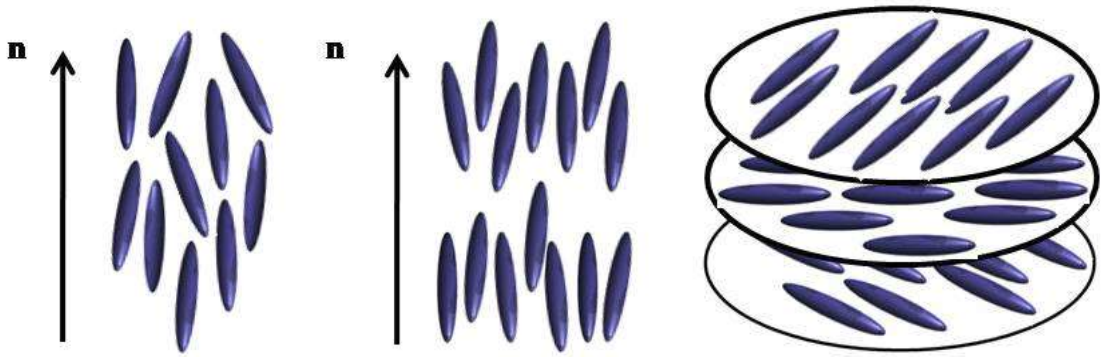

Figure 2-6: Types of mesophases. Left) Nematic phase, Center) Smectic Phase, and Right) Cholesteric phase. This image has been adapted from Qian's dissertation [77].

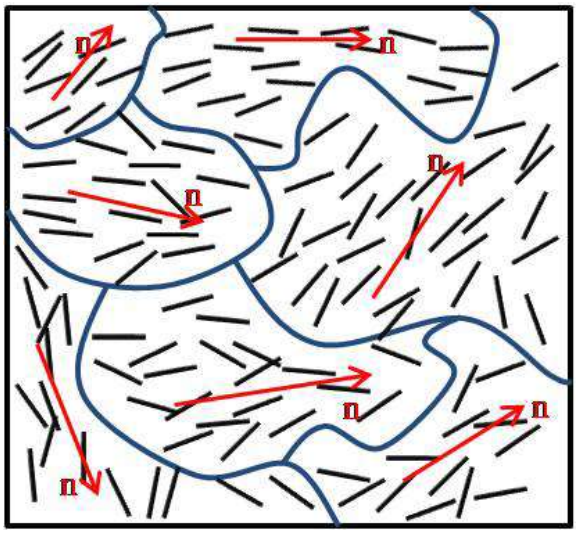

Figure 2-7: Polydomain structure of LCPs. Arrows represent orientation within each domain. The orientation varies randomly from domain to domain [77].

2.4.1 Thermotropic Liquid Crystalline Polymers (TLCPs)

The liquid crystalline polymers are subcategorized into lyotropic and thermotropic based on whether the ordering is exhibited in the solution or in the molten state, respectively. The mesophases of lyotropic liquid crystalline polymers (LLCPs) are controlled using the type of solvent, the solution temperature and the polymer concentration [69, 80]. The LLCPs typically do not exhibit liquid crystallinity in the molten state because their degradation temperature is below their melting temperature [81-83]. The type of LCPs relevant to the current work are TLCPs, and therefore, a discussion on the LLCPs is beyond the scope of this dissertation.

The melting temperature of the LCPs can be brought below the degradation temperature by two different methods. The first method is to use different mesogenic groups in the polymer and the second method is to use flexible spacers. The morphology of the mesogens in TLCPs

depends on the temperature, thermal history, shear history etc. [69, 80] . An example of a TLCP which doesn't use a flexible spacer is Vectra A950, which is composed of 73 mole% hydroxybenzoic acid and 27 mole% 2-hydroxy-6-naphthoic acid [84]. On the other hand, examples of a TLCP which use flexible spacers are copolyesters of polyethylene terephthalate (PET) and hydroxybenzoic acid (HBA), in which the HBA content ranged between 40 to 80 mole%. In these TLCPs ethylene acts as a flexible spacer [69].

TLCPs possess versatile properties that enable their use in many applications. One important property possessed by TLCPs is low permeability to gasses. However, this advantage is irrelevant for application in additive manufacturing due to the introduction of multiple voids and weld lines which may lead to increased permeability of the printed parts. Researchers have taken advantage of the low permeability of TLCPs to gasses in developing membranes as well as hydrogen storage applications [85, 86]. A study showed that Vectra A900 film, a commercial TLCP, has a permeability over 100 times lower than that of polyethylene terephthalate (PET) and around 5000 times lower than the permeability of polypropylene (PP) [87, 88].

The TLCPs also possess excellent tensile properties that attract their application to form composites. Additionally, their low density (~1.4 g/cm^3) leads to a further increase in the specific properties, which is a density-normalized property. TLCPs possess high tensile properties due to the rod-like monomers. The rod-like monomers can be highly aligned under extensional flow kinematics to impart excellent one-dimensional properties due to the steric hindrance of the monomers [69]. The chemical compositions of some of the commercially available TLCPs have been shown in Table 2-2 [89].

Table 2-2: Chemical composition of commercially available thermotropic liquid crystalline polymers (TLCPs). This table has been reproduced from Qian's dissertation [77].

Material	**Chemical Composition**		**Comments**
Rodrun	HBA: 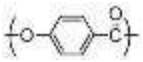 PET: 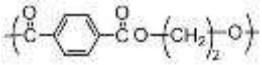		Rodrun was developed under the codename of X7G by Eastman Kodak, it is now manufactured by Unitika, Japan. It is the first commercial TLCP available, containing either 60 mol% 4-hydroxy benzoic acid (HBA) -40 mol% polyethylene terephthalate (PET) or 80 mol% HBA-20 mol% PET. X7G was withdrawn from the US market soon after its commercialization due to its poor performance at high temperatures.
Vectra	Vectra A	HNA:  HBA: 	Vectra series is a broad range of TLCPs developed by Hoechst, which is now marketed by Ticona-Celanese. The well-studied Vectra A 950 is a

	Vectra B	HNA: 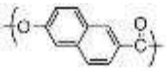 TA: 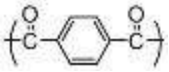 AP: 	copolyester containing 27 mol% 2-hydroxy-6-naphthoic acid (HNA) and 73 mol% HBA [90]. Vectra B 950 is a polyesteramide of 60 mol% HNA, 20mol% terephthalic acid (TA) and 20 mol% 4-aminophenol (AP) [86]. The Vectra series has been extensively discussed in the literature.
Zenite	HBA: 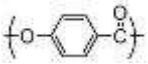 TA: 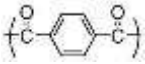 HQ: 	Zenite is a class of TLCPs originally developed by Dupont, then it was brought by Ticona-Celanese. Zenite molecules contain various amount of HBA, TA and hydroquinone (HQ), but the detailed monomer contents belong to the proprietor. Some grades of Zenite show good high temperature properties, such as HX-3000 and HX-6000 (melting point above 330 °C).

2.4.2 *In situ* composites based on TLCPs

The advantage of the superior properties of TLCPs, discussed in subsection 2.4.1, is taken by forming *in-situ* composites of TLCPs with matrices that are lower in tensile properties. The resulting composites differ from the traditionally used glass and carbon fiber reinforced composites because the fibrils that form the reinforcement are generated the during processing stage. The *in-situ* composites can be generated by either imposing a single thermal history on the

TLCP and the matrix polymer during processing (by direct blending in a single extruder) or using different thermal histories (by using two different extruders prior to blending). The method of imposing separate thermal histories was invented by Baird and coworkers [91] using a technology called the dual extrusion technology, which is discussed in the section 2.5. It was carried out to avoid the degradation of the matrix polymer due to higher processing temperature of the TLCPs.

There are several advantages of *in-situ* composites relative to the glass and carbon fiber composites. *In-situ* composites are lighter in weight, have smaller fibril diameter, lead to a lesser wear of the processing equipment, enable addition of the interfacial agents easily, can be potentially recycled, and exhibit a low blend viscosity [92, 93]. The density of the *in-situ* composites is lower than the composites reinforced with traditional fibers due to lower reinforcement density. To compare, the density of the commercially available TLCP's is around 1.4 g/cm^3, lower in comparison with that of carbon fiber (density: 1.8 g/cm^3) and glass fiber (density: 2.55 g/cm^3) [44, 58, 69]. The major disadvantage of the *in-situ* composites is the high anisotropy of the composites [82, 91-106]. The properties in the transverse direction are significantly lower than that in the axial direction.

TLCP reinforced composites have been extensively studied by researchers. Subsequently, the *in-situ* composites have been used for postprocessing in injection molding, blow molding [88], extrusion [93], and even in FFF [92]. Researchers studied in detail the improvement in the physical properties and the morphologies that were developed. An extended list of tensile properties obtained has been listed in Table 2-3 [89]. The table also lists the processing method that was used.

Table 2-3**:** Tensile properties of the TLCP reinforced *in-situ* composites in the machine direction, obtained on using various matrices. This table has been reproduced from Qian's work to emphasize the improvement in the tensile properties that is possible with TLCPs [89].

Thermoplastic matrix	**TLCP content Wt.%**	**Tensile strength (MPa)**	**Tensile modulus (GPa)**	**Processing method**	**Ref**
LLDPE/HDPE blend	0	16.0	0.4	Film blowing	[107]
	10% Vectra RD-501	25.0	1.2	Film blowing with a rotating die	[107]
	10% Vectra RD-501	22.0	1.0	Film blowing with a non-rotating die	[107]
PP	0	31.2	1.4	Injection molding (tensile bars)	[108]
	30% Vectra A950	36.6	3.8		[108]
	20% 60/40 HBA/PET	28.7	2.1		[108]
	30% Vectra B950	23.1	3.7		[109]
	0	42.9	0.7	Film extrusion	[110]
	15% 80/20 HBA/PET	25.1	1.7		[110]
	0	0.7	N/A	Extrusion strand	[111]
	26% Vectra B950	13.5	N/A		[111]

	28% Vectra A950	4.7	N/A		[111]
	24% 60/40 HBA/PET	2.7	N/A		[111]
PVC	0	44.5	1.4	Injection molding (tensile bars)	[112]
	5% 60/40 HBA/PET	48.0	1.8		[112]
	10% 60/40 HBA/PET	46	1.6		[112]
	35% 60/40 HBA/PET	25.0	1.7		[112]
PS	0	32.0	3.1	Injection molding (tensile bars)	[113]
	25% Vectra A950	32.0	3.6		[113]
	25% Vectra B950	35.0	4.6		[113]
	0	28.0	1.5	Compression molded film	[114]
	10%60/40 HBA/PET	22.5	1.7		[114]
	0	43.5	2.0	Fiber spinning	[114]
	10% 60/40 HBA/PET	37.5	2.6		[114]
PET	0	61.0	2.6	Injection molding (tensile bars)	[115]
	30% Vectra A950	74.0	4.1		[115]
PET	0	40.0	0.9	Compression molded film	[114]

	10% 60/40 HBA/PET	43.7	1.17		[114]
	0	60.5	1.9	Fiber spinning	[114]
	10% 60/40 HBA/PET	67.8	2.5		[114]
PBT	0	51.7	2.6	Injection molding (tensile bars)	[116]
	30% Vectra A950	37.9	3.5		[116]
PA66	0	62.0	1.1	Compression molded film	[117]
	20% Vectra A950	81.0	1.2		[117]
PA6	0	31.5	0.9	Injection molding (end-gated plaque)	[118]
	35% HX-8000	42.5	2.9	Standard nozzle	[118]
	35% HX-8000	54.0	3.5	Static mixer nozzle	[118]
PC	0	66.9	2.3	Injection molding (tensile bar)	[116]
	30% Vectra A950	121.0	5.7		[116]
	30% Vectra B950	154.0	6.6		[116]
PEN	0	83.0	N/A	Injection molding (tensile bar)	[119]
	30% Vectra A950	112.0	N/A		[119]
PEEK	0	84.1	3.5	Injection molding	[116]

	30% Vectra A950	71.7	4.3	(tensile bar)	[116]
	0	116.0	5.0	Injection molding (tensile bar)	[120]
	25% Vectra A950	125.0	17.0		[120]
PES	0	64.3	2.5	Extrusion strands	[116]
	30% Vectra A950	115.8	4.1		[116]
	30% Vectra B950	164.1	5.7		[116]
PPS	0	82.0	3.7	Injection molding (tensile bar)	[121]
	25% Vectra A950	87.0	4.8		[121]
PEI	0	91.0	3.1	Injection molding (tensile bar)	[116]
	30 % Vectra A950	129.0	5.2		[116]
	30 % Vectra B950	95.8	7.5		[116]
	0	100.0	3.0	Injection molding (end-gated plaque)	[122]
	30 % HX-4000	135.0	5.8		[122]
	30 % Granular	129.0	9.0		[122]

LLDPE = linear low-density polyethylene; HDPE = high density polyethylene; PP = polypropylene; PVC = polyvinyl chloride; PS = polystyrene; PET = polyether terephthalate; PBT = polybutylene terephthalate; PA66 = polyamide 66, PA6 = polyamide 6; PC = polycarbonate;

PEN = polyethylene naphthalate; PEEK = polyether ether ketone; PES = polyether sulfone; PPS = polyphenylene sulfide; PEI = polyether imide.

The table shows the dependency of the tensile properties on the type of processing technology used. The tensile properties also depend on the concentration of TLCPs, type of matrix used, and the processing history. From the table, improvement in the tensile properties is noticeable on using TLCPs as reinforcement. However, researchers have reported that the processing temperatures of the commercially available TLCPs are significantly above the degradation temperature of the commodity plastics [92, 102]. To avoid such processing hurdles, researchers have used dual extrusion technology, which is discussed in detail in next subsection.

2.5 Dual Extrusion Technology

There are several disadvantages in using direct blending to form *in-situ* composites. First, it is required to have an overlapping processing temperature to blend TLCPs with the matrix polymers. Second, to melt all the residual crystallites, processing temperatures need to be higher than the melting temperature of the TLCPs. Such conditions have been reported to result in the matrix degradation [92, 102, 123]. Third and the most important is that the fibrillation depends on the droplet formation and dispersion [123]. To avoid these problems, Baird and coworkers [91] developed the dual extrusion technology.

In the dual extrusion technology, shown by the schematic in Figure 2-8, TLCP and the matrix polymer are plasticated in separate extruders. The TLCP extruder temperature is generally chosen to be higher than that of the matrix extruder. TLCP is then continuously injected into the

matrix polymer using a multiport injection nozzle to form a continuous stream of reinforcement. Because the injection of TLCP-stream is continuous, requirement for drop formation is avoided. Contrarily, in direct blending techniques, the viscosity ratio of TLCP (μ_D) and the matrix polymer (μc) is required to be fractional to promote droplet formation [100, 124]. After the TLCP is injected, the blend passes through a series of static mixers that blend and striate the TLCP streams into finer streams. A die is used to extrude either a monofilament that has a matrix-fibril morphology or to extrude multiple strands that have sheath core morphology. The extrudate is drawn at high draw ratios to impart orientation in the TLCP phase, following which the extrudate is cooled in a water bath to lock in the orientation. Researchers have reported the formation of fibrils that are smaller in diameter than those of carbon and glass fiber [100].

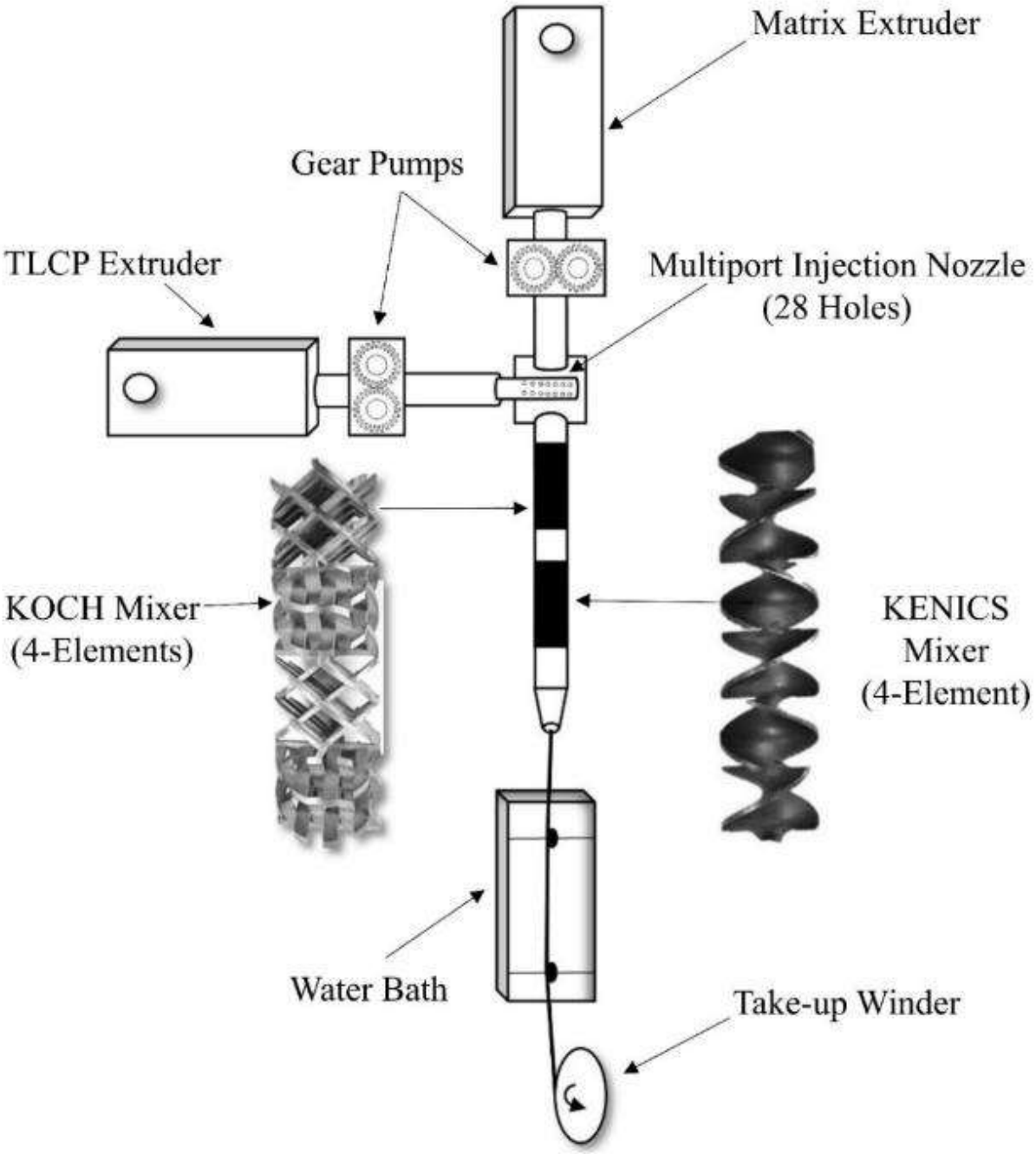

Figure 2-8: Schematic of dual extrusion technology.

In-situ composites generated using dual extrusion have been used as feedstock for postprocessing in many polymer processing technologies, such as compression molding, injection molding, blow molding and FFF [84, 91, 92, 97, 100-102]. The schematic shown in Figure 2-9 shows the procedure that is followed. The matrix polymer is reinforced with TLCP in the dual extrusion technology, following which, the composite strand is pelletized for postprocessing in injection molding, compression molding, blow molting, sheet extrusion and FDM/FFF.

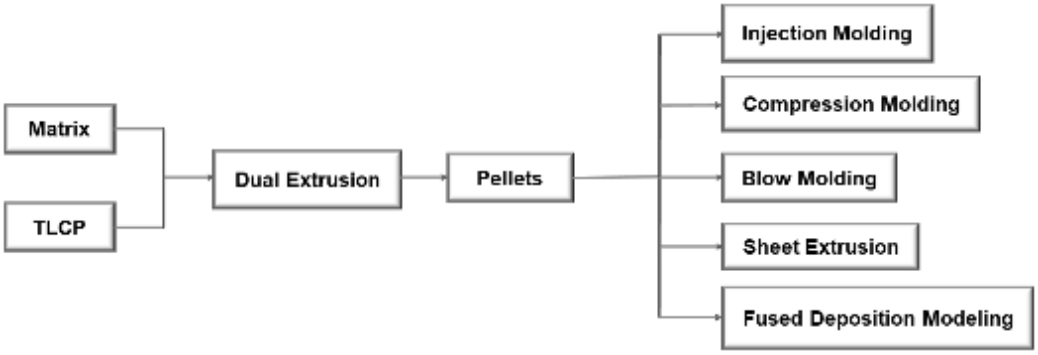

Figure 2-9: Schematic showing the procedure that is followed to postprocess composites generated using dual extrusion technology.

There is only one reported paper concerning the use of TLCP reinforced composite in FFF, and this was by Gray and coworkers [92, 93]. In this work, a TLCP composed of hydroxybenzoic acid (73 mole%) and 2-hydroxy-6-napthoic acid (27 mole%) was used to reinforce polypropylene using the dual extrusion technology. The reinforced filaments generated were pelletized to fabricate monofilaments, which were used to print specimens. The tensile modulus and strength of the filaments generated using the dual extrusion technology, monofilaments generated after re-extruding the pellets, and the properties of the printed specimen are listed in Table 2-4. On comparing the tensile modulus and strength of the specimen listed in the table with those of pure polypropylene (tensile modulus: 1.0±0.2 GPa and tensile strength: 23.2±3.9 MPa), a significant

improvement can be noticed. However, the additional step of monofilament generation leads to a drop in the tensile properties by an order in magnitude, as can be seen in the table. This is because the continuity of the reinforcing fibrils is disrupted due to pelletization. Therefore, the motivation of the work discussed in chapter 4 and 5, pertaining to the use of TLCP-reinforced filaments in FFF, is to avoid disrupting the continuity of the reinforcing fibrils.

Table 2-4: Tensile properties of the filaments generated using dual extrusion technology, monofilaments obtained after re-extruding pelletized strands obtained using dual extrusion technology, and the specimens printed using the monofilaments [92].

Concentration Vectra A/PP (wt.%)	**Filament**		**Monofilament**		**Printed**	
	Tensile Modulus (GPa)	**Tensile Strength (MPa)**	**Tensile Modulus (GPa)**	**Tensile Strength (MPa)**	**Tensile Modulus (GPa)**	**Tensile Strength (MPa)**
20	9.5±0.5	116.0±16.0	1.9±0.1	25.6±1.3	1.6	33
40	22.8±1.6	321.0±39.0	2.2±0.1	21.1±2.3	2.7	37

2.5.1 Rheology of TLCPs required for Filament Generation

The study of the rheological behavior of TLCPs is very important in determining the processing temperatures required for the generation of composites using the dual extrusion technology. A detailed overview of the work is presented in Chapters 3-5. Researchers have

reported that the TLCPs exhibit processing temperatures higher than their melting temperatures. This is due to the presence of higher melting crystallites in the melt [91, 92, 100]. Also, researchers have identified a method of lowering the processing temperatures below the melting temperature of the TLCPs and the degradation temperature of the matrices [77, 86, 125]. In this method, TLCPs are heated above their melting temperatures to remove residual crystallites. Following which, the melt is cooled to temperatures below their melting temperatures. This is because the TLCPs have been reported to exhibit a molten state even below their melting temperatures, a property referred to as super-cooling behavior [102]. The advantage of the super-cooling behavior is taken to lower the processing temperatures of the TLCPs. Therefore, identification of the equilibration temperatures to remove residual crystallites and identification of temperatures below the TLCP melting temperature where TLCPs exhibit a stable melt is required for filament generation.

Small amplitude oscillatory shear (SAOS) in isothermal conditions has been used by researchers to study the crystallization behavior of TLCPs below the melting temperature to determine the solidification temperatures. Done and Baird [126] studied the solidification behavior of TLCPs by preheating the TLCP's above the melting temperature and cooling it to temperatures below the melting point. In these experiments, the storage and loss modulus were tracked as a function of temperature to determine the cross-over point of the curves, which was taken as the solidification temperature. Similarly, Chen et al. [86, 125] studied the transient shear rheology of TLCP below the melting temperature in isothermal conditions to determine the stability of the TLCP melt below its melting temperature. Identification of the solidification time and temperature windows using SAOS tests in the cooling mode and under isothermal conditions has been demonstrated in chapters 3-5.

Identification of the equilibration temperatures to remove residual crystallites can be performed using shear step strain tests. Done and Baird [127] conducted transient shear step strain on two liquid crystalline polymers, a copolyester of 60 mol% p-hydroxybenzoic acid (PHB) and 40 mol % poly(ethylene terephthalate) (PET), and 60/40 PHB/PET [127]. These tests indicated the presence of tails in the melt which were associated with the presence of solid structures. The advantage of the shear step strain test can be taken in determining equilibration temperatures.

2.5.2 Identification of Post-processing Temperatures of TLCP Reinforced Filaments

After filaments are generated using dual extrusion technology, a knowledge of the post-processing temperature is important. This is to avoid melting the TLCPs on postprocessing. Moreover, identification of temperatures that induce flexibility of the TLCP fibrils on printing is important to allow printing features that require sharp turns by the printer. In the past, post-processing temperatures have been determined using conventional polymer processing technologies, such as compression molding and injection molding [52, 69, 92, 105]. McLeod and coworkers [105] reported that the tensile properties drop on post processing due to fiber breakage and orientation relaxation of the TLCPs at elevated temperatures. Similarly, Gray IV et. al [52, 92] reported a drop in tensile properties and attributed the drop to orientation relaxation. However, no attempt was made to study the effect of temperatures on the dynamic mechanical properties of the TLCPs. In the work carried out previously, the reasons cited for the drop in the tensile properties on post processing has been vaguely explained. Therefore, a method to narrow down the effect of elevated temperatures and exposure times on the dynamic properties of TLCPs is required and has been demonstrated in Chapter 3.

References

[1] A. Standard, ISO/ASTM 52900: 2015 Additive manufacturing-General principles-terminology, ASTM F2792-10e1 (2012).

[2] U.K. uz Zaman, M. Rivette, A. Siadat, S.M. Mousavi, Integrated product-process design: Material and manufacturing process selection for additive manufacturing using multi-criteria decision making, Robotics and Computer-Integrated Manufacturing 51 (2018) 169-180.

[3] W.E. Frazier, Metal additive manufacturing: a review, Journal of Materials Engineering and Performance 23(6) (2014) 1917-1928.

[4] I. Gibson, D. Rosen, B. Stucker, Additive manufacturing technologies: 3D printing, rapid prototyping, and direct digital manufacturing, Springer2014.

[5] G.N. Levy, R. Schindel, J.-P. Kruth, Rapid manufacturing and rapid tooling with layer manufacturing (LM) technologies, state of the art and future perspectives, CIRP Annals-Manufacturing Technology 52(2) (2003) 589-609.

[6] N. Hopkinson, P. Dickens, Rapid prototyping for direct manufacture, Rapid prototyping journal 7(4) (2001) 197-202.

[7] T. Wohlers, I. Campbell, O. Diegel, Wohlers Report 2018, Fort Collins: Wohlers Associates (2018).

[8] E. Atzeni, A. Salmi, Economics of additive manufacturing for end-usable metal parts, The International Journal of Advanced Manufacturing Technology 62(9) (2012) 1147-1155.

[9] B.P. Conner, G.P. Manogharan, A.N. Martof, L.M. Rodomsky, C.M. Rodomsky, D.C. Jordan, J.W. Limperos, Making sense of 3-D printing: Creating a map of additive manufacturing products and services, Additive Manufacturing 1 (2014) 64-76.

[10] I. Gibson, D.W. Rosen, B. Stucker, Additive manufacturing technologies: rapid prototyping to direct digital manufacturing, Springer Publishing Company, Incorporated2009.

[11] S.H. Huang, P. Liu, A. Mokasdar, L. Hou, Additive manufacturing and its societal impact: a literature review, The International Journal of Advanced Manufacturing Technology (2013) 1-13.

[12] C. Klahn, B. Leutenecker, M. Meboldt, Design strategies for the process of additive manufacturing, Procedia CIRP 36 (2015) 230-235.

[13] I. Gibson, D. Rosen, B. Stucker, Extrusion-Based Systems, Additive Manufacturing Technologies: 3D Printing, Rapid Prototyping, and Direct Digital Manufacturing, Springer New York, New York, NY, 2015, pp. 147-173.

[14] D. Chakraborty, B.A. Reddy, A.R. Choudhury, Extruder path generation for curved layer fused deposition modeling, Computer-Aided Design 40(2) (2008) 235-243.

[15] M. Chapiro, Current achievements and future outlook for composites in 3D printing, Reinforced Plastics 60(6) (2016) 372-375.

[16] https://www.ge.com/reports/ge-fired-its-3d-printed-advanced-turboprop-engine/, Accessed 17 January 2019.

[17] M. Candi, A. Beltagui, Effective use of 3D printing in the innovation process, Technovation (2018).

[18] S.-Y. Oh, D. Suh, H.-G. Kim, Last Design for Mens Shoes using 3D Foot Scanner and 3D Printer, The Journal of the Korea Contents Association 16(2) (2016) 186-199.

[19] M. Motta, R. Gaddi, G. Conti, 3D technology and industrial design to breathe new life into product design. Is this the future of fashion and textiles?, International Conference on Design (CODE 2016), 2017, pp. 97-113.

[20] E.R. Fitzharris, I. Watt, D.W. Rosen, M.L. Shofner, Interlayer bonding improvement of material extrusion parts with polyphenylene sulfide using the Taguchi method, Additive Manufacturing 24 (2018) 287-297.

[21] J.C. Nelson, S. Xue, J.W. Barlow, J.J. Beaman, H.L. Marcus, D.L. Bourell, Model of the selective laser sintering of bisphenol-A polycarbonate, Industrial & Engineering Chemistry Research 32(10) (1993) 2305-2317.

[22] J.D. Williams, C.R. Deckard, Advances in modeling the effects of selected parameters on the SLS process, Rapid Prototyping Journal 4(2) (1998) 90-100.

[23] J.-Y. Lee, J. An, C.K. Chua, Fundamentals and applications of 3D printing for novel materials, Applied Materials Today 7 (2017) 120-133.

[24] C. Esposito Corcione, A. Greco, A. Maffezzoli, Photopolymerization kinetics of an epoxy-based resin for stereolithography, Journal of applied polymer science 92(6) (2004) 3484-3491.

[25] I. Gibson, D.W. Rosen, B. Stucker, Powder Bed Fusion Processes, Additive Manufacturing Technologies: Rapid Prototyping to Direct Digital Manufacturing, Springer US, Boston, MA, 2010, pp. 120-159.

[26] M. Agarwala, R. Weeren, A. Bandyopadhyay, P. Whalen, A. Safari, S. Danforth, Fused deposition of ceramics and metals: an overview, Proceedings of the Solid Freeform Fabrication Symposium, Austin, Texas, 1996.

[27] M.K. Agarwala, V.R. Jamalabad, N.A. Langrana, A. Safari, P.J. Whalen, S.C. Danforth, Structural quality of parts processed by fused deposition, Rapid Prototyping Journal 2(4) (1996) 4-19.

[28] C.E. Duty, C.E. Duty, V. Kunc, V. Kunc, B. Compton, B. Compton, B. Post, B. Post, D. Erdman, D. Erdman, Structure and mechanical behavior of Big Area Additive Manufacturing (BAAM) materials, Rapid Prototyping Journal 23(1) (2017) 181-189.

[29] A.A. Hassen, J. Lindahl, X. Chen, B. Post, L. Love, V. Kunc, Additive manufacturing of composite tooling using high temperature thermoplastic materials, SAMPE Conference Proceedings, Long Beach, CA, May, 2016, pp. 23-26.

[30] V. Kishore, X. Chen, C. Ajinjeru, A.A. Hassen, J.M. Lindahl, J. Failla, V. Kunc, C.E. Duty, Additive manufacturing of high performance semicrystalline thermoplastics and their composites, Oak Ridge National Lab.(ORNL), Oak Ridge, TN (United States), 2016.

[31] V. Kunc, R.B. Dinwiddie, B.K. Post, L.J. Love, C. Duty, M. Matlack, R. Fahey Jr, A.A. Hassen, Investigation of In-autoclave Additive Manufacturing Composite Tooling.

[32] L.J. Love, V. Kunc, O. Rios, C.E. Duty, A.M. Elliott, B.K. Post, R.J. Smith, C.A. Blue, The importance of carbon fiber to polymer additive manufacturing, Journal of Materials Research 29(17) (2014) 1893-1898.

[33] V. Kishore, C. Ajinjeru, C.E. Duty, A.A. Hassen, J.M. Lindahl, P. Liu, V. Kunc, Rheological Characteristics of Fiber Reinforced Poly (ether ketone ketone)(PEKK) for Melt Extrusion Additive Manufacturing, Oak Ridge National Lab.(ORNL), Oak Ridge, TN (United States), 2017.

[34] H.L. Tekinalp, V. Kunc, G.M. Velez-Garcia, C.E. Duty, L.J. Love, A.K. Naskar, C.A. Blue, S. Ozcan, Highly oriented carbon fiber–polymer composites via additive manufacturing, Composites Science and Technology 105 (2014) 144-150.

[35] J.-W. Tseng, C.-Y. Liu, Y.-K. Yen, J. Belkner, T. Bremicker, B.H. Liu, T.-J. Sun, A.-B. Wang, Screw extrusion-based additive manufacturing of PEEK, Materials & Design 140 (2018) 209-221.

[36] A.N. Dickson, J.N. Barry, K.A. McDonnell, D.P. Dowling, Fabrication of continuous carbon, glass and Kevlar fibre reinforced polymer composites using additive manufacturing, Additive Manufacturing 16 (2017) 146-152.

[37] N. Li, Y. Li, S. Liu, Rapid prototyping of continuous carbon fiber reinforced polylactic acid composites by 3D printing, Journal of Materials Processing Technology 238 (2016) 218-225.

[38] R. Matsuzaki, M. Ueda, M. Namiki, T.-K. Jeong, H. Asahara, K. Horiguchi, T. Nakamura, A. Todoroki, Y. Hirano, Three-dimensional printing of continuous-fiber composites by in-nozzle impregnation, Scientific reports 6 (2016) 23058.

[39] G.W. Melenka, B.K. Cheung, J.S. Schofield, M.R. Dawson, J.P. Carey, Evaluation and prediction of the tensile properties of continuous fiber-reinforced 3D printed structures, Composite Structures 153 (2016) 866-875.

[40] X. Tian, T. Liu, C. Yang, Q. Wang, D. Li, Interface and performance of 3D printed continuous carbon fiber reinforced PLA composites, Composites Part A: Applied Science and Manufacturing 88 (2016) 198-205.

[41] F. Van Der Klift, Y. Koga, A. Todoroki, M. Ueda, Y. Hirano, R. Matsuzaki, 3D printing of continuous carbon fibre reinforced thermo-plastic (CFRTP) tensile test specimens, Open Journal of Composite Materials 6(01) (2015) 18.

[42] E.L. Gilmer, D. Miller, C.A. Chatham, C. Zawaski, J.J. Fallon, A. Pekkanen, T.E. Long, C.B. Williams, M.J. Bortner, Model analysis of feedstock behavior in fused filament fabrication: Enabling rapid materials screening, Polymer 152 (2018) 51-61.

[43] R.T.L. Ferreira, I.C. Amatte, T.A. Dutra, D. Bürger, Experimental characterization and micrography of 3D printed PLA and PLA reinforced with short carbon fibers, Composites Part B: Engineering 124 (2017) 88-100.

[44] S.-Y. Fu, B. Lauke, E. Mäder, C.-Y. Yue, X. Hu, Tensile properties of short-glass-fiber-and short-carbon-fiber-reinforced polypropylene composites, Composites Part A: Applied Science and Manufacturing 31(10) (2000) 1117-1125.

[45] R.W. Gray IV, D.G. Baird, J. H. Bøhn, Effects of processing conditions on short TLCP fiber reinforced FDM parts, 4(1) (1998) 14-25.

[46] W. Zhong, F. Li, Z. Zhang, L. Song, Z. Li, Short fiber reinforced composites for fused deposition modeling, Materials Science and Engineering: A 301(2) (2001) 125-130.

[47] M. Dawoud, I. Taha, S.J. Ebeid, Mechanical behaviour of ABS: An experimental study using FDM and injection moulding techniques, Journal of Manufacturing Processes 21 (2016) 39-45.

[48] A.C. de Leon, Q. Chen, N.B. Palaganas, J.O. Palaganas, J. Manapat, R.C. Advincula, High performance polymer nanocomposites for additive manufacturing applications, Reactive and Functional Polymers 103 (2016) 141-155.

[49] J.R.C. Dizon, A.H. Espera Jr, Q. Chen, R.C. Advincula, Mechanical characterization of 3D-printed polymers, Additive Manufacturing 20 (2018) 44-67.

[50] J.T. Cantrell, S. Rohde, D. Damiani, R. Gurnani, L. DiSandro, J. Anton, A. Young, A. Jerez, D. Steinbach, C. Kroese, Experimental characterization of the mechanical properties of 3D-printed ABS and polycarbonate parts, Rapid Prototyping Journal 23(4) (2017) 811-824.

[51] M. Ivey, G.W. Melenka, J.P. Carey, C. Ayranci, Characterizing short-fiber-reinforced composites produced using additive manufacturing, Advanced Manufacturing: Polymer & Composites Science 3(3) (2017) 81-91.

[52] R.W. Gray IV, The Effects of Processing Conditions on Thermoplastic Prototypes Reinforced with Thermotropic Liquid Crystalline Polymers, Virginia Tech, 1997.

[53] M. Nikzad, S. Masood, I. Sbarski, Thermo-mechanical properties of a highly filled polymeric composites for fused deposition modeling, Materials & Design 32(6) (2011) 3448-3456.

[54] M. Allahverdi, S. Danforth, M. Jafari, A. Safari, Processing of advanced electroceramic components by fused deposition technique, Journal of the European Ceramic Society 21(10) (2001) 1485-1490.

[55] S. Masood, W. Song, Development of new metal/polymer materials for rapid tooling using fused deposition modelling, Materials & design 25(7) (2004) 587-594.

[56] K. Gnanasekaran, T. Heijmans, S. Van Bennekom, H. Woldhuis, S. Wijnia, G. de With, H. Friedrich, 3D printing of CNT-and graphene-based conductive polymer nanocomposites by fused deposition modeling, Applied Materials Today 9 (2017) 21-28.

[57] M. Shofner, K. Lozano, F. Rodríguez-Macías, E. Barrera, Nanofiber-reinforced polymers prepared by fused deposition modeling, Journal of applied polymer science 89(11) (2003) 3081-3090.

[58] X. Yao, C. Luan, D. Zhang, L. Lan, J. Fu, Evaluation of carbon fiber-embedded 3D printed structures for strengthening and structural-health monitoring, Materials & Design 114 (2017) 424-432.

[59] F. Ning, W. Cong, J. Qiu, J. Wei, S. Wang, Additive manufacturing of carbon fiber reinforced thermoplastic composites using fused deposition modeling, Composites Part B: Engineering 80 (2015) 369-378.

[60] A. Hassan, N.M. Salleh, R. Yahya, M.R.K. Sheikh, Fiber length, thermal, mechanical, and dynamic mechanical properties of injection-molded glass-fiber/polyamide 6,6: plasticization effect, Journal of Reinforced Plastics and Composites 30(6) (2011) 488-498.

[61] M.A. Anwer, H.E. Naguib, Study on the morphological, dynamic mechanical and thermal properties of PLA carbon nanofibre composites, Composites Part B: Engineering 91 (2016) 631-639.

[62] D. Bigg, Effect of compounding on the properties of short fiber reinforced injection moldable thermoplastic composites, Polymer composites 6(1) (1985) 20-28.

[63] P. Cloud, PRIMER ON REINFORCING AND FILLING IM PLASTICS, Plastics World 33(9) (1975) 36-40.

[64] A. Rezadoust*, M. Esfandeh, Study of fiber breakage and length distribution during compounding glass-NBR-Phenolic composites, Polymer-Plastics Technology and Engineering 44(1) (2005) 63-71.

[65] K.-i. Mori, T. Maeno, Y. Nakagawa, Dieless forming of carbon fibre reinforced plastic parts using 3D printer, Procedia Engineering 81 (2014) 1595-1600.

[66] A. Imeri, Investigation of the Mechanical Properties for Fiber Reinforced Additively Manufactured Components, Tennessee Technological University, 2017.

[67] X. Wang, M. Jiang, Z. Zhou, J. Gou, D. Hui, 3D printing of polymer matrix composites: A review and prospective, Composites Part B: Engineering 110 (2017) 442-458.

[68] T. Vaneker, Material extrusion of continuous fiber reinforced plastics using commingled yarn, Procedia CIRP 66 (2017) 317-322.

[69] M.A. McLeod, Injection molding of pregenerated microcomposites, Virginia Tech, 1997.

[70] H.K.F. Cheng, T. Basu, N.G. Sahoo, L. Li, S.H. Chan, Current advances in the carbon nanotube/thermotropic main-chain liquid crystalline polymer nanocomposites and their blends, Polymers 4(2) (2012) 889-912.

[71] G.R. Luckhurst, T.J. Sluckin, Biaxial nematic liquid crystals: theory, simulation and experiment, John Wiley & Sons2015.

[72] G. Friedel, The mesomorphic states of matter, Annales de Physique, 1922, p. 5.

[73] A. Isayev, M. Modic, Self-Reinforced melt processible polymer composites: Extrusion, compression, and injection molding, Polymer composites 8(3) (1987) 158-175.

[74] C.V. por seleção Equivalência, D.T. Outros, EM QUÍMICA, MINISTÉRIO DA EDUCAÇÃO UNIVERSIDADE FEDERAL DA GRANDE DOURADOS UNIVERSIDADE

ESTADUAL DE GOIÁS UNIVERSIDADE FEDERAL DE GOIÁS/REGIONAL CATALÃO (2016) 38.

[75] D. Andrienko, Introduction to liquid crystals, IMPRS school, Bad Marienberg (2006).

[76] V.P. Shibaev, L. Lam, Liquid crystalline and mesomorphic polymers, Springer Science & Business Media2012.

[77] C. Qian, Linking the Rheological Behavior to the Processing of Thermotropic Liquid Crystalline Polymers in the Super-cooled State, Virginia Tech, 2016.

[78] W.R. Burghardt, Molecular orientation and rheology in sheared lyotropic liquid crystalline polymers, Macromolecular Chemistry and Physics 199(4) (1998) 471-488.

[79] A.M. Donald, A.H. Windle, S. Hanna, Liquid crystalline polymers, Cambridge University Press2006.

[80] C. Qian, Linking the Rheological Behavior to the Processing of Thermotropic Liquid Crystalline Polymers in the Super-cooled State, (2016).

[81] A.I. Isayev, Self-reinforced composites involving liquid-crystalline polymers: Overview of development and applications, ACS Publications1996.

[82] K. Blizard, D. Baird, R. Ramanathan, SPE ANTEC Tech, Papers 33 (1987) 1399.

[83] G. Kiss, In situ composites: blends of isotropic polymers and thermotropic liquid crystalline polymers, Polymer Engineering & Science 27(6) (1987) 410-423.

[84] A. Handlos, D.G. Baird, Sheet extrusion of microcomposites based on thermotropic liquid crystalline polymers and polypropylene, 17(1) (1996) 73-85.

[85] T.-S. Chung, Thermotropic Liquid Crystal Polymers: Thin-film Poly Chara Blends, CRC Press2001.

[86] C. Qian, D.G. Baird, The transient shear rheology of a thermotropic liquid crystalline polymer in the super-cooled state, Polymer 102 (2016) 63-72.

[87] L. Thomas, D. Roth, Films from liquid-crystals, Chemtech 20(9) (1990) 546-550.

[88] C. Qian, C. Mansfield, D. Baird, Extrusion Blow Molding of Polymeric Blends Based on Thermotropic Liquid Crystalline Polymer and High Density Polyethylene, International Polymer Processing 32(1) (2017) 112-120.

[89] C. Qian, Connecting the Rheological Behavior to the Processing of Thermotropic Liquid Crystalline Polymers in the Super-Cooled State, PhD Dissertation, Virginia Tech, Blacksburg, 2016.

[90] S. Pisharath, X. Hu, S.-C. Wong, Rheology–morphology relationships in nylon–LCP hybrid composites, Composites science and technology 66(15) (2006) 2971-2979.

[91] D.G. Baird, A. Sukhadia, Mixing process for generating in-situ reinforced thermoplastics, U.S. Patent, 5225488, 1991.

[92] R.W. Gray IV, D.G. Baird, J. Helge Bøhn, Effects of processing conditions on short TLCP fiber reinforced FDM parts, Rapid Prototyping Journal 4(1) (1998) 14-25.

[93] R. Gray, D.G. Baird, J.H. Bøhn, Thermoplastic composites reinforced with long fiber thermotropic liquid crystalline polymers for fused deposition modeling, Polymer composites 19(4) (1998) 383-394.

[94] M.Q. Ansari, C.D. Mansfield, D.G. Baird, A Process for Generating Composites of Acrylonitrile-Butadiene-Styrene Reinforced with a Thermotropic Liquid Crystalline Polymer for Use in Fused Filament Fabrication.

[95] S. Bafna, T. Sun, D. Baird, The role of partial miscibility on the properties of blends of a polyetherimide and two liquid crystalline polymers, Polymer 34(4) (1993) 708-715.

[96] S. Bafna, T. Sun, J. De Souza, D. Baird, The effect of miscibility on the morphology and properties of blends of poly (ether imide) with liquid crystalline polymers, Polymer 36(2) (1995) 259-266.

[97] A. Datta, H. Chen, D.G. Baird, The effect of compatibilization on blends of polypropylene with a liquid-crystalline polymer, Polymer 34(4) (1993) 759-766.

[98] D. Baird, S. Bafna, J. De Souza, T. Sun, Mechanical properties of in situ composites based on partially miscible blends of polyetherimide and liquid crystalline polymers, Polymer composites 14(3) (1993) 214-223.

[99] W. DePolo, D. Baird, Flow-induced warpage of injection-molded TLCP fiber-reinforced polypropylene composites, Polymer composites 27(3) (2006) 239-248.

[100] A. Handlos, D. Baird, Processing and associated properties of in situ composites based on thermotropic liquid crystalline polymers and thermoplastics, Journal of Macromolecular Science, Part C: Polymer Reviews 35(2) (1995) 183-238.

[101] J. Huang, D. Baird, Injection molding of polypropylene reinforced with thermotropic liquid crystalline polymer microfibrils. Part III: Combination of glass and TLCP, Journal of Injection Molding Technology 6(3) (2002) 187.

[102] R.K. Krishnaswamy, D.G. Baird, Wholly thermoplastic composites from woven preforms based on nylon-11 fibers reinforced in situ with a hydroquinone-based liquid crystalline polyester, Polymer composites 18(4) (1997) 526-538.

[103] M. McLeod, D. Baird, The crystallization behavior of blends of thermotropic liquid crystalline polymers, Polymer 40(13) (1999) 3743-3752.

[104] M. Mcleod, D. Baird, Coinjection molded pregenerated microcomposites, Journal of Elastomers & Plastics 31(2) (1999) 143-161.

[105] M. McLeod, D. Baird, Injection molding of poly (ethylene terephthalate) reinforced with pregenerated thermotropic liquid crystalline polymer microfibrils, Polymer composites 20(1) (1999) 3-18.

[106] E. Sabol, A. Handlos, D. Baird, Composites based on drawn strands of thermotropic liquid crystalline polymer reinforced polypropylene, Polymer composites 16(4) (1995) 330-345.

[107] W. Chinsirikul, T.C. Hsu, I.R. Harrison, Liquid crystalline polymer (LCP) reinforced polyethylene blend blown film: Effects of counter-rotating die on fiber orientation and film properties, Polym. Eng. Sci. 36(22) (1996) 2708-2717.

[108] A. Datta, D.G. Baird, Compatibilization of thermoplastic composites based on blends of polypropylene with two liquid crystalline polymers, Polymer 36(3) (1995) 505-514.

[109] H.J. O'Donnell, D.G. Baird, In situ reinforcement of polypropylene with liquid-crystalline polymers: effect of maleic anhydride-grafted polypropylene, Polymer 36(16) (1995) 3113-26.

[110] S. Saengsuwan, S. Bualek-Limcharoen, G.R. Mitchell, R.H. Olley, Thermotropic liquid crystalline polymer (Rodrun LC5000)/polypropylene in situ composite films: rheology, morphology, molecular orientation and tensile properties, Polymer 44(11) (2003) 3407-3415.

[111] A.M. Sukhadia, A. Datta, D.G. Baird, Mixing history on the morphology and properties of thermoplastic/LCP blends, Int. Polym. Proc. 7(3) (1992) 218-28.

[112] Y.Z. Meng, S.C. Tjong, Preparation and properties of injection-molded blends of poly(vinyl chloride) and liquid crystal copolyester, Polymer 40(10) (1999) 2711-2718.

[113] G. Crevecoeur, G. Groeninckx, Morphology and mechanical properties of thermoplastic composites containing a thermotropic liquid crystalline polymer, Polymer Engineering and Science 30(9) (1990) 532-542.

[114] P. Zhuang, T. Kyu, J.L. White, Characteristics of hydroxybenzoic acid-ethylene terephthalate copolymers and their blends with polystyrene, polycarbonate, and polyethylene terephthalate, Polymer Engineering and Science 28(17) (1988) 1095-106.

[115] J. Seppala, M. Heino, C. Kapanen, Injection-molded blends of a thermotropic liquid-crystalline polymer with poly(ethylene terephthalate), polypropylene, and poly(phenylene sulfide), J. Appl. Polym. Sci. 44(6) (1992) 1051-60.

[116] G. Kiss, In situ composites: Blends of isotropic polymers and thermotropic liquid crystalline polymers, Polym. Eng. Sci. 27(6) (1987) 410-423.

[117] D. Dutta, R.A. Weiss, J. He, Compatibilization of blends containing thermotropic liquid crystalline polymers with sulfonate ionomers, Polymer 37(3) (1996) 429-35.

[118] R.K. Krishnaswamy, S.E.B. Wadud, D.G. Baird, Influence of a reactive terpolymer on the properties of in situ composites based on polyamides and thermotropic liquid crystalline polyesters, Polymer 40(3) (1998) 701-716.

[119] S.H. Jang, B.S. Kim, Morphology and mechanical properties of liquid crystalline copolyester and poly(ethylene 2,6-naphthalate) blends, Polymer Engineering and Science 35(6) (1995) 538-45.

[120] A.I. Isayev, P.R. Subramanian, Blends of a liquid-crystalline polymer with poly(ether ether ketone), Polymer Engineering and Science 32(2) (1992) 85-93.

[121] T.G. Gopakumar, S. Ponrathnam, A. Lele, C.R. Rajan, A. Fradet, In situ compatibilization of poly(phenylene sulfide)/wholly aromatic thermotropic liquid crystalline polymer blends by reactive extrusion: morphology, thermal and mechanical properties, Polymer 40(2) (1998) 357-364.

[122] S.S. Bafna, T. Sun, J.P. de Souza, D.G. Baird, The effect of miscibility on the morphology and properties of blends of poly(ether imide) with liquid crystalline polymers, Polymer 36(2) (1995) 259-266.

[123] A.A. Handlos, The processing of microcomposites based on polypropylene and two thermotropic liquid crystalline polymers in injection molding, sheet extrusion, and extrusion blow molding, Virginia Tech, 1994.

[124] H.P. Grace, Dispersion phenomena in high viscosity immiscible fluid systems and application of static mixers as dispersion devices in such systems, Chemical Engineering Communications 14(3-6) (1982) 225-277.

[125] C. Qian, G. Wan, C.E. Frazier, D.G. Baird, Isothermal crystallization of blends containing two thermotropic liquid crystalline polymers, Materials Today Communications 9 (2016) 16-21.

[126] D. Done, D. Baird, Solidification behavior and recovery kinetics of liquid crystalline polymers, Polymer Engineering & Science 30(16) (1990) 989-995.

[127] D. Done, D.G. Baird, Transient flow of thermotropic liquid crystalline polymers in step strain experiments, Journal of Rheology 34(5) (1990) 749-762.

3 Generation and Post-Processing of Acrylonitrile Butadiene Styrene Reinforced with a Thermotropic Liquid Crystalline Polymer

Chapter 3: Generation and Post-Processing of Acrylonitrile Butadiene Styrene Reinforced with a Thermotropic Liquid Crystalline Polymer

Mubashir Q. Ansari,[1] Craig D. Mansfield[1], Donald G. Baird[1,2]

[1]Department of Chemical Engineering, Virginia Tech, Blacksburg, VA 24061, USA.

[2]Macromolecules Innovation institute, Virginia Tech, Blacksburg, VA 24061, USA.

3.1 Abstract

In this work, dynamic shear rheology was used to select an appropriate thermotropic liquid crystalline polymer (TLCP) and processing conditions to reinforce acrylonitrile butadiene styrene (ABS). Due to non-overlapping processing conditions, the generation of the TLCP-reinforced ABS filaments was carried out in a dual extrusion technique. This method allowed processing of the matrix polymer and the selected TLCP in separate extruders before injecting the TLCP into ABS at a lower temperature. Small amplitude oscillatory shear (SAOS) tests performed on the selected TLCP in the cooling mode identified the extent of supercooling, an important factor to determine if the TLCP has a processing temperature overlap with that of the polymer matrix. Because the TLCP melt is unstable below its melting temperature and starts crystallizing, the temperature at which the selected TLCP is injected into ABS was determined by SAOS tests carried out in the isothermal mode. Tensile strength and modulus of the 40.0 wt.% TLCP/ABS improved by 4.3 and 17.3 times to 169.2±4.0 MPa and 39.9±3.7 GPa, respectively, in comparison with those of pure ABS. A dynamic mechanical analysis (DMA) test was developed to identify the postprocessing conditions of the TLCP/ABS composite which minimized loss in properties occurring due to orientation relaxation of the TLCP phase at the elevated temperatures. On using the conditions determined by DMA to process 40.0 wt.% TLCP/ABS strands in compression molding at 240 °C,

the maximum tensile properties were obtained. The compression molded plaques exhibited a tensile strength and modulus of 79.6±4.4 MPa and 12.3±1.2 GPa, respectively.

3.2 Introduction

Thermotropic Liquid Crystalline Polymers (TLCPs) have been in some cases used to improve the physical properties of matrix polymers due to their superior tensile properties. A number of polymer matrices such as polyphenylene sulfide (PPS) [1], polypropylene (PP) [2], nylon 11 [3] and polyethylene terephthalate (PET) [4, 5] have been reinforced using TLCPs. One of the most important advantages of using TLCPs is the generation of *in-situ* composites that allows the formation of the reinforcing fibrils during the processing stage [6]. This leads to avoiding fiber breakage problems during the compounding stage, which otherwise is very common when using traditional fibers such as carbon fiber [7]. Highly aligned TLCPs under extensional flow conditions result in composites with excellent one-dimensional tensile properties [8].

An important consideration for reinforcing polymer matrices with TLCPs is the selection of TLCPs such that there exists a temperature difference between the melting temperature of the TLCP and the postprocessing temperatures of the composite. This is to allow processing of the TLCP-reinforced composite as solid filled system like carbon and glass fiber reinforced composites. Handlos and coworkers [9] processed a pregenerated composite of PP and a TLCP in an extruder to generate sheets. The sheet extrusion was carried out below the melting temperature of the reinforcing TLCP at 165 and 185 °C, whereas the reinforcing TLCP was reported to melt at 320 °C.

A wide range of commercially available TLCPs offer to satisfy this criterion to reinforce lower melting polymers. However, the processing temperatures of the commercially available TLCPs are significantly higher than the processing temperatures of most matrix polymers, which

prevents blending in a single extruder [3, 5, 6, 10, 11]. To overcome the processing challenge of blending polymers with non-overlapping temperatures, Baird and coworkers [11] invented dual extrusion technology. In this technology, a lower melting polymer can be reinforced with a higher melting TLCP without degrading the matrix polymer. This is because the constituent polymers are plasticated in separate extruders at different temperatures. Following this, the temperature of the TLCP-melt is lowered before injecting into the matrix polymer by taking advantage of a unique property exhibited by TLCPs, known as supercooling behavior [8, 10]. By virtue of this property, TLCPs exhibit a molten state even below their melting temperature. It was reported by Krishnaswamy et al. [3] that melt stability of TLCP below the melting temperature is strongly dependent on the temperature. Later, Qian and coworkers [10] studied the temperature dependency of the melt stability by using isothermal Small Amplitude Oscillatory Shear (SAOS) test in the supercooled regime of TLCP after cooling from a temperature well above the TLCP melting temperature. This study demonstrated that a threshold temperature exists below the TLCP melting temperature above which the melt is stable for longer time periods.

This paper discusses our effort in reinforcing a commodity polymer, acrylonitrile butadiene styrene, using dual extrusion technique. Due to numerous advantages of ABS such as its amorphous structure, low processing temperature and easy processability, ABS can be processed in both conventional polymer processing technologies as well as in FDM [12, 13]. However, a major limitation is its poor tensile properties [7]. Numerous efforts have been made to improve the physical properties of ABS by taking advantage of not only traditional fibers such as carbon [7] and glass fiber [14] but also by using self-reinforcing TLCP fibrils [15, 16].

Das and coworkers [15] studied blends of ABS and TLCP and reported an improvement in the storage modulus. In this work, the authors used a commercially available TLCP that was

reported to melt at 280 °C. It was not mentioned how the blending operation was carried out in a single mixer below the TLCP melting temperature at 250 °C. In another work carried out by Xia et al. [16], a lab-synthesized lower melting TLCP was used for blending with ABS. Although the lower melting TLCP alleviates concerns of ABS-degradation, such blends are not desired for processing as a solid-filled system due to a small temperature difference between the postprocessing temperature and the melting temperature of the TLCP.

The work reported previously by researchers involving reinforcement of polymers with lower degradation temperature than the processing temperature of TLCPs, using the dual extrusion method did not fully utilize rheology for the selection of TLCPs. For example, Handlos et al. [9] reinforced PP with a TLCP that was reported to melt at 320 °C. The selected TLCP required processing of PP at 270 °C to avoid solidification of the TLCP during processing. The repercussion of selection of the TLCP and processing condition on the degradation of PP was not investigated. It has been reported by González-González and coworkers [17] that PP degrades appreciably in the temperature range of 230-250 °C and severely above 250 °C.

TLCP reinforced matrices generated using the dual extrusion method have been postprocessed in a wide range of polymer processing technologies such as injection molding [5], compression molding [6], blow molding [18] and even in Fused Deposition Modeling (FDM) [8], a form of additive manufacturing (AM) technology. In all these attempts, the postprocessing temperatures were randomly selected to process the composites below the melting temperature of TLCPs. These researchers reported a drop in the tensile properties on postprocessing TLCP-reinforced composites, which was attributed to fiber breakage and orientation relaxation of the TLCPs. No attempt was made to investigate orientation relaxation of TLCPs that leads to a drop in tensile properties.

Our goal in this work is to use Small Amplitude Oscillatory Shear (SAOS) testing in the cooling mode on several available TLCPs and isothermal SAOS tests in the supercooled regime of the selected TLCP to identify a TLCP and processing conditions, respectively, for reinforcing ABS in the dual extrusion technique. The resulting composite is required to be postprocessed below the melting temperature of the TLCPs. A dynamic mechanical analysis test is also developed to enable identification of postprocessing conditions that lead to minimizing orientation relaxation of the TLCP phase when the composite is postprocessed in conventional technologies such as compression molding.

3.3 Experimental

3.3.1 Materials

ABS used in this work was provided by Trinseo (Grade: Magnum^{TM} 555). Before using, the ABS was dried at 85 ℃ for at least 4 hours as recommended by the supplier. The available TLCPs, Zenite HX3000, HX6000 and HX8000 were originally supplied by DuPont and are believed to be composed of unspecified ratios of hydroxybenzoic acid, terephthalic acid, hydroquinone and hydroquinone derivatives [5, 9, 10]. The TLCPs were dried overnight at 110 ℃ before using.

3.3.2 Differential scanning calorimetry (DSC)

The glass transition temperature of ABS determined using differential scanning calorimetry, DSC (model: TA instrument's DSC2500 Discovery series), was found to be 105 ℃. The melting temperatures of HX3000, HX6000 and HX8000 were also determined using DSC and were found to be 330, 338 and 280 ℃, respectively.

3.3.3 Thermogravimetric Analysis (TGA)

Isothermal TGA (model: TA instrument's TGA5500 Discovery series) was performed on ABS at 240, 250, 260 and 270 °C in a nitrogen atmosphere. In the TGA tests, the samples were heated at 10 °C/min to the test temperature following which the percentage weight loss was tracked as function of time for 20 minutes.

3.3.4 Rheological tests

All rheological tests were carried out using a TA instrument's ARES-G2 rheometer in a nitrogen atmosphere. The fixtures were heated at the starting test temperatures for two hours to allow for thermal expansion before loading samples. The samples were loaded in the form of pellets between the fixtures. After loading, the samples were equilibrated before each test and compressed between the fixtures. The excess material outside the fixtures was trimmed before starting the tests. All tests were carried out using a 25 mm diameter cone and plate fixture (cone angle: 0.1002 radian). The strain used in all SAOS tests was 5%, and the angular frequency used was 1 radian/sec. The strain used is in the linear viscoelastic range.

SAOS tests in the cooling mode were performed on HX3000, HX6000 and HX8000 after equilibrating at 360, 350 and 310 °C, respectively, for 5 minutes. The cooling rate used was 10 °C/minute. During the tests, the storage and loss moduli were tracked as a function of temperature. This test was used to select a TLCP for reinforcing ABS. Based on the results, as will be discussed later in the results and discussion section, HX8000 was the only desired TLCP to be used as a reinforcement for ABS in the dual extrusion technique. SAOS in the cooling mode was also carried out on pure ABS from 270 to 200 °C, and the resulting complex viscosity was plotted as a function of temperature for comparing with values of HX3000, HX6000 and HX8000. Isothermal SAOS

tests were also performed on ABS at 240, 250, 260, 270, 300 and 330 °C for 20 minutes. The complex viscosity was tracked as a function of time during the 20-minute time sweeps to study melt stability at the test temperatures.

3.3.5 Dual Extrusion Technique

HX8000/ABS composite strands were generated using the dual extrusion method, a schematic of which is shown in Figure 3-1. ABS and HX8000 were processed in two separate 2.54 cm diameter and L/D=24 extruders (model: Killion KL-100). Both polymers were metered using two separate gear pumps (model: Zenith HD-556) with designed flow rate of 1.725 cm^3/revolution. A 28-hole injection nozzle was used to inject HX8000 into ABS, following which the blend was passed through a 4-element Koch and 4-element Kenics mixers. A L/D=20 and 3 mm diameter die was used to extrude a monofilament into a water bath. A custom made 48 cm diameter take-up winder was used to collect filaments at a controlled rpm. Three concentrations of HX8000/ABS (10.0, 20.0 and 40.0 wt.%) strands were generated using the conditions discussed in the result and discussion section of this paper.

3.3.6 Extrusion

Pure ABS was extruded using zones 1-4 temperatures of 220, 230, 240 and 240 °C, respectively, in a 2.54 cm diameter and L/D=24 extruders (model: Killion KL-100). The 3 mm die temperature used was maintained at 240 °C. The pure ABS strands were used for tensile testing for use as a control for comparing improvement in the tensile properties of the ABS-HX800 composite strands.

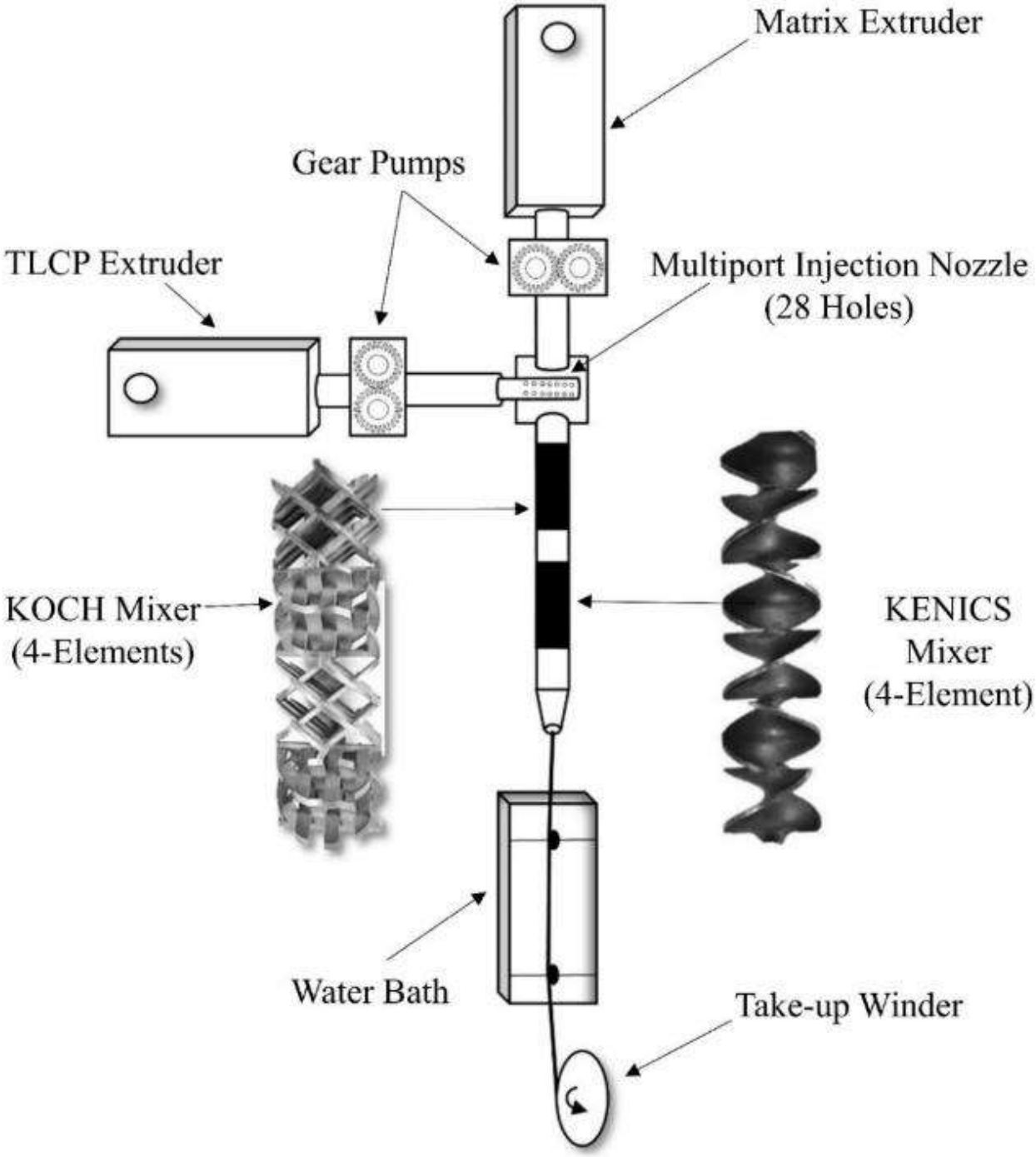

Figure 3-1: Dual extrusion schematic.

3.3.7 Dynamic mechanical analysis (DMA)

DMA was performed using a TA instrument's ARES-G2 rheometer on the strips cut out from injection molded pure HX8000 plaques, as shown in Figure 3-2. The dimensions of the strips were 50 mm x 8 mm x 2 mm and were loaded using the instrument supplier's rectangular fixture. The DMA tests were carried out in a nitrogen atmosphere using a strain of 0.5% and an angular frequency of 1 radian/sec. In these tests, the HX8000 strips were exposed to 240 °C for 0, 300 and 600 seconds following which the temperature was dropped at a rate of 30 °C/min and the resulting storage modulus was tracked as a function of cooling temperature to compare the effects of exposure duration at 240 °C. In the second set of tests, HX8000 was exposed to 240, 250 and 260 °C for a constant exposure time of 10 minutes, following which the temperature was dropped at 30 °C/min. The resulting storage modulus was plotted as a function of cooling temperature.

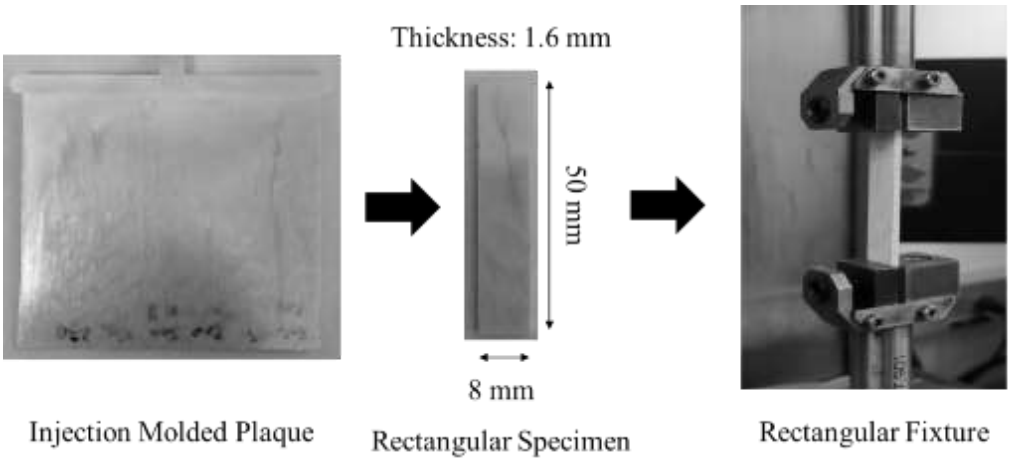

Figure 3-2: Sample preparation for DMA tests carried out on pure HX8000.

3.3.8 Compression Molding

A 76.2 mm square mold was used to carry out compression molding using a Carver hot press (model: 2696) to generate plaques 2.0 mm in thickness. Before loading the samples, the

molds were heated at the molding temperatures for 2 hours. 40.0 wt.% HX8000/ABS composite strands were cut into 76.2 mm lengths and were uniaxially loaded into the hot mold as shown in Figure 3-3. Long strands were used to take the advantage of the high aspect ratio of the fibers. A Kapton® film was used at the top and bottom of the samples to allow for easy removal of the plaques after cooling. The molding pressure and time were 1.7 MPa and 5 minutes, respectively. The compression molding temperatures used were 240, 250, 260 and 280 °C.

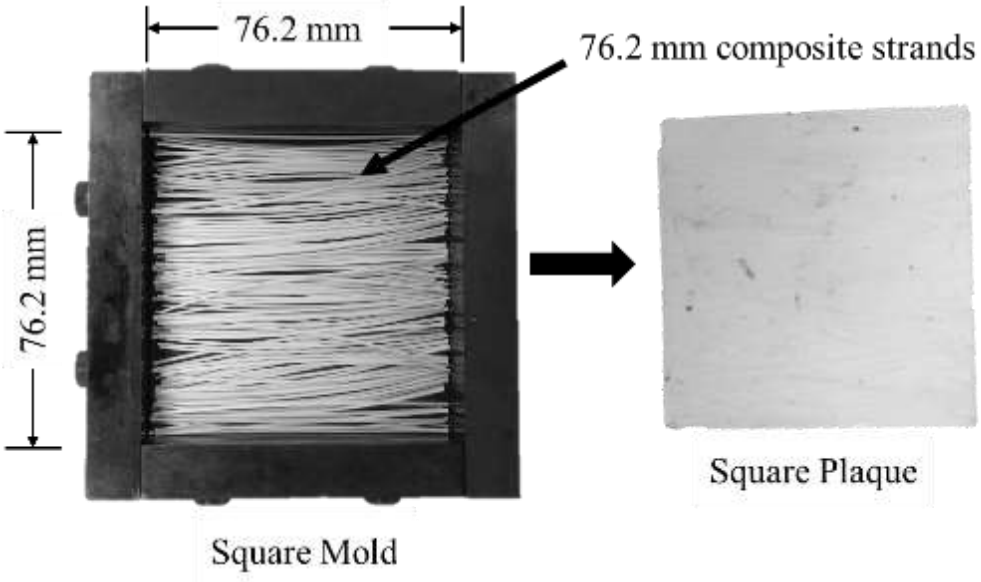

Figure 3-3: Compression molding of 40.0 wt.% HX8000/ABS strands generated using dual extrusion technology.

3.3.9 Tensile Testing

The tensile properties of all samples were measured using an Instron Mechanical Tester (model: 4468). The crosshead speed used was 1 mm/minute and a 5kN load cell was used. A 50%

maximum strain extensometer (model: MTS 634.12E-54) was used only for testing the injection and compression molded samples as it was difficult to mount the extensometer on the circular cross section of the composite strands. The HX8000/ABS composite strands were tested on 150 mm long samples. To carry out tensile testing in the fiber-alignment direction of the compression molded plaques, samples of dimensions 76.2 mm x 8.0 mm x 2 mm (dimensions represent: length x width x thickness) were cut from the compression molded plaques. For all tensile property data reported, at least 5 tests were carried out and the outlier data points were removed before calculating the average with 95% confidence intervals.

3.4 Results and Discussions

3.4.1 SAOS in cooling mode on available TLCPs

Figure 3-4 shows results for SAOS tests performed in the cooling mode on HX3000, HX6000 and HX8000. As the temperature is dropped from the equilibration temperature, both the storage and loss moduli increase and eventually crossover. The equilibration temperatures were selected to be well above the melting temperatures of the corresponding TLCP to get rid of all residual crystallites. At temperatures above the melting temperature of the TLCPs, the loss modulus is above the storage modulus. This signifies that the dissipative energy is higher than the stored energy, suggesting the viscous nature is dominant. At the crossover point, both quantities become equal, which has been taken as the onset of crystallization by Qian and coworkers [10]. Based on the crossover point, the solidification temperatures determined for HX3000, HX6000 and HX8000 were 285, 300 and 235 °C, respectively. This information was used as a determining factor for the selection of a TLCP to reinforce ABS as will be discussed later in the ABS rheology section.

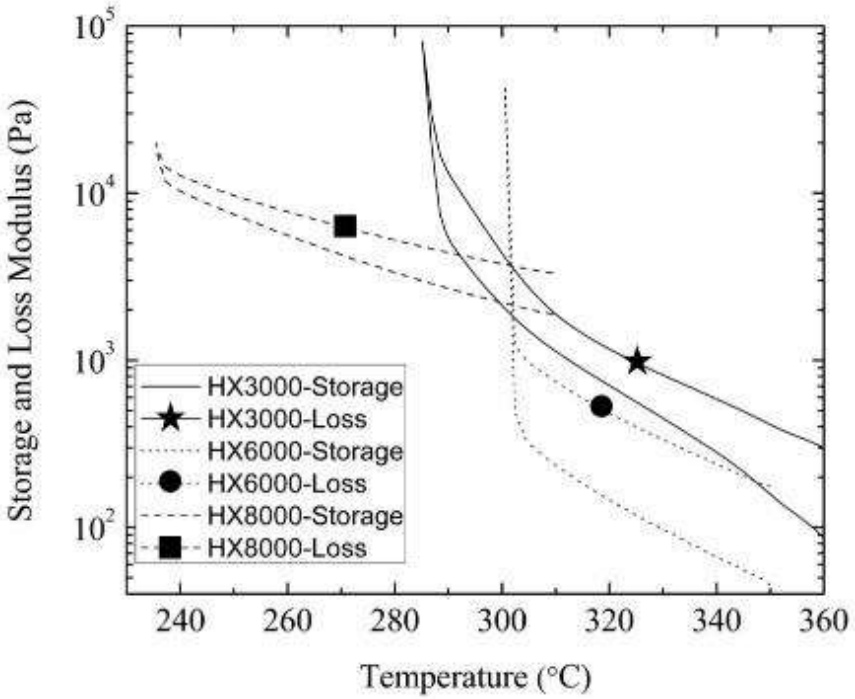

Figure 3-4: SAOS tests carried out on HX3000, HX6000 and HX8000 in the cooling mode in a nitrogen atmosphere using a cooling rate of 10 °C/min. The top and bottom curve for each TLCP represent loss (G″) and storage modulus (G′), respectively.

The complex viscosities obtained by performing SAOS tests in the cooling mode on HX3000, HX6000, HX8000 and ABS are plotted as a function of cooling temperature in Figure 3-5. This comparison of the complex viscosities shows that only HX8000 exhibits a complex viscosity less than that of ABS in the temperature range of 270 to 240 °C. It has been reported previously by Handlos et al. [4] that to obtain a longer aspect ratio of the TLCP fibrils, it is desired to have a viscosity ratio of the TLCP phase to that of the matrix phase to be less than unity. This is required to obtain larger deformation in the TLCP phase under extensional kinematics during

the drawing of the filaments. Therefore, only HX8000 serves as the desired reinforcing TLCP for ABS.

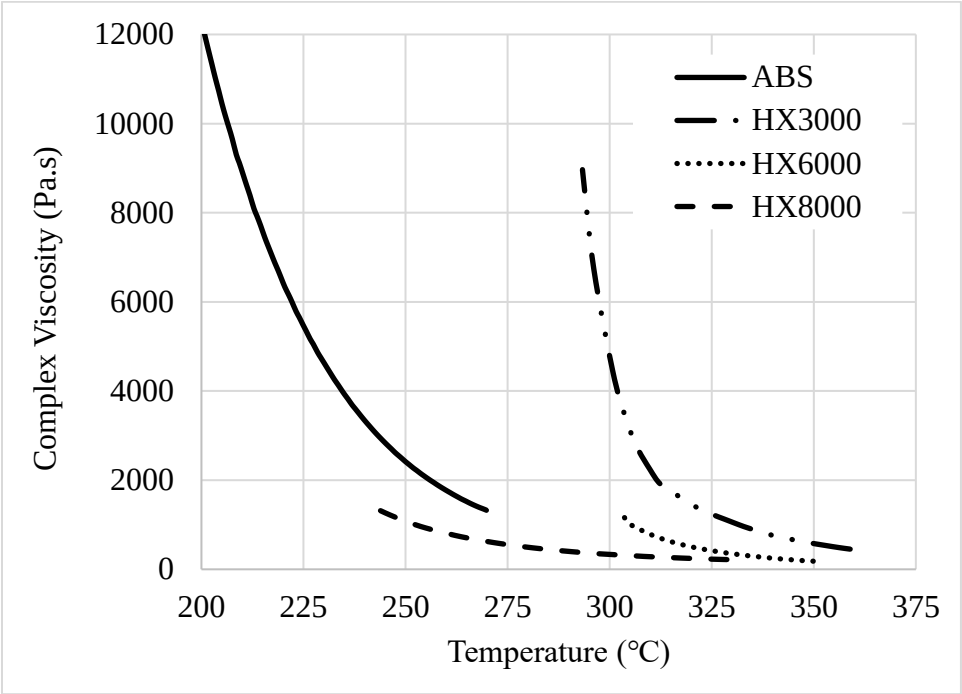

Figure 3-5: A comparison of complex viscosity of ABS with that of HX3000, HX6000 and HX8000 as the samples were cooled during the SAOS tests in nitrogen atmosphere. A cooling rate of 10 °C/min was used.

3.4.2 ABS Rheology

The reinforcement of any matrix polymer with a TLCP requires knowledge of the matrix stability at the blending temperatures. The residence time distribution during the processing of HX8000/ABS strands, calculated based on the volumetric flow rate required ABS-melt to be stable for 10-20 minutes. To investigate ABS-melt stability, isothermal time sweeps (SAOS tests in the

isothermal mode) were carried out on ABS at 240, 250, 260, 270, 300 and 330 ℃ in a nitrogen atmosphere. Figure 3-6 shows that the complex viscosity is stable for 20 minutes at all temperatures below 270 ℃. At 300 ℃, which has been used as the HX8000 processing temperature in the past [3, 10], it can be seen that there is a drop in complex viscosity, signifying the onset of degradation. The complex viscosity drops from 573 to 368 Pa.s. At 330 ℃, which is the melting temperature of HX3000 and below that of HX6000, the complex viscosity drops more severely as represented by a steeper curve in comparison with other temperatures. At 330 ℃, the complex viscosity drops from 133 to 21 Pa.s. Based on the results shown in Figure 3-6, it is desired to maintain the ABS processing temperature at or below 270 ℃. Moreover, the presence of bubbles and discoloration effects were also observed for the ABS samples tested at 270 ℃.

The previous studies carried out to study ABS degradation involved use of TGA/FTIR under the temperature ramp mode [19, 20]. Such tests do not capture prolonged isothermal exposure effects on the melt stability as the samples are exposed for significantly smaller time scales. Moreover, TGA tests are also diffusion limited at the sample surface and do not capture the degradation effects on the flow behavior of the melt. Suzuki and coworkers [20] studied the degradation behavior of different constituents of ABS, polyacrylonitrile (PAN), polybutadiene (PBD), polystyrene (PS). It was reported that different constituents respond differently to temperature ramps. Degradation products were reported to be eliminated in the ABS constituents over a wide range of temperatures. HCN from PAN was reported to be eliminated at 290 ℃, whereas the elimination of acrylonitrile begins at 400 ℃. Numerous degradation products were reported such as ammonia, nitrile, butadiene etc. which is speculated to have led to drop in the complex viscosity as seen in Figure 3-6 for the samples tested at 300 and 330 ℃. It is not desirable

to have gaseous degradation products in the composite strands as it may lead to stress concentration effects due to the presence of bubbles, leading to a drop in tensile properties.

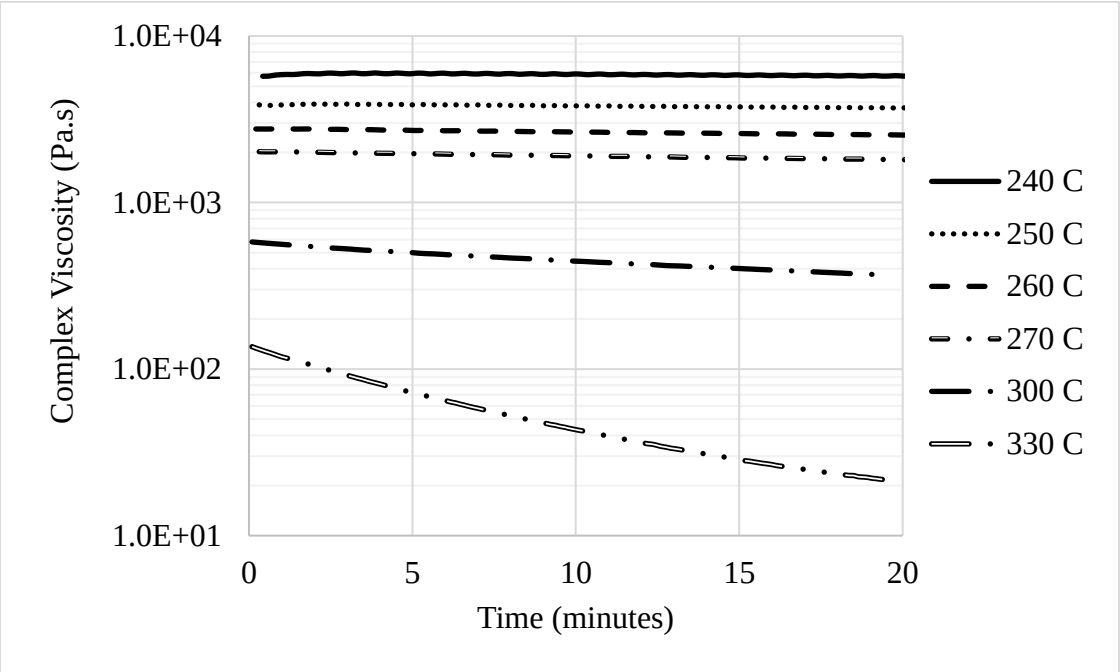

Figure 3-6: Complex viscosity obtained by performing SAOS test on ABS in nitrogen atmosphere at 240, 250, 260, 270, 300 and 330 °C.

To confirm melt stability of ABS at and below 270 °C, TGA analysis was also carried out under isothermal conditions in a nitrogen atmosphere at 240, 250, 260 and 270 °C. It was found that the weight drops are minimal at these temperatures as seen in Figure 3-7, signifying a stable melt. Based on the results obtained using the isothermal SAOS test and isothermal TGA performed on ABS, HX3000 and HX6000 cannot be used for direct blending in a single extruder as the ABS melt is not stable at 330 °C, which is the melting temperature of HX3000 and below the melting temperature of HX6000. Moreover, the use of HX3000 and HX6000 as reinforcing TLCPs in the

dual extrusion technique is also not allowable as their solidification temperatures (285 and 300 ℃, respectively) are well above the temperatures where ABS exhibits a stable melt. This leads to confirming HX8000 as reinforcing candidate for two reasons. First, its viscosity is lower than that of ABS, leading to longer fibrils. Second, HX8000 supercools to 235 ℃, which is within the stable melt temperature range of ABS.

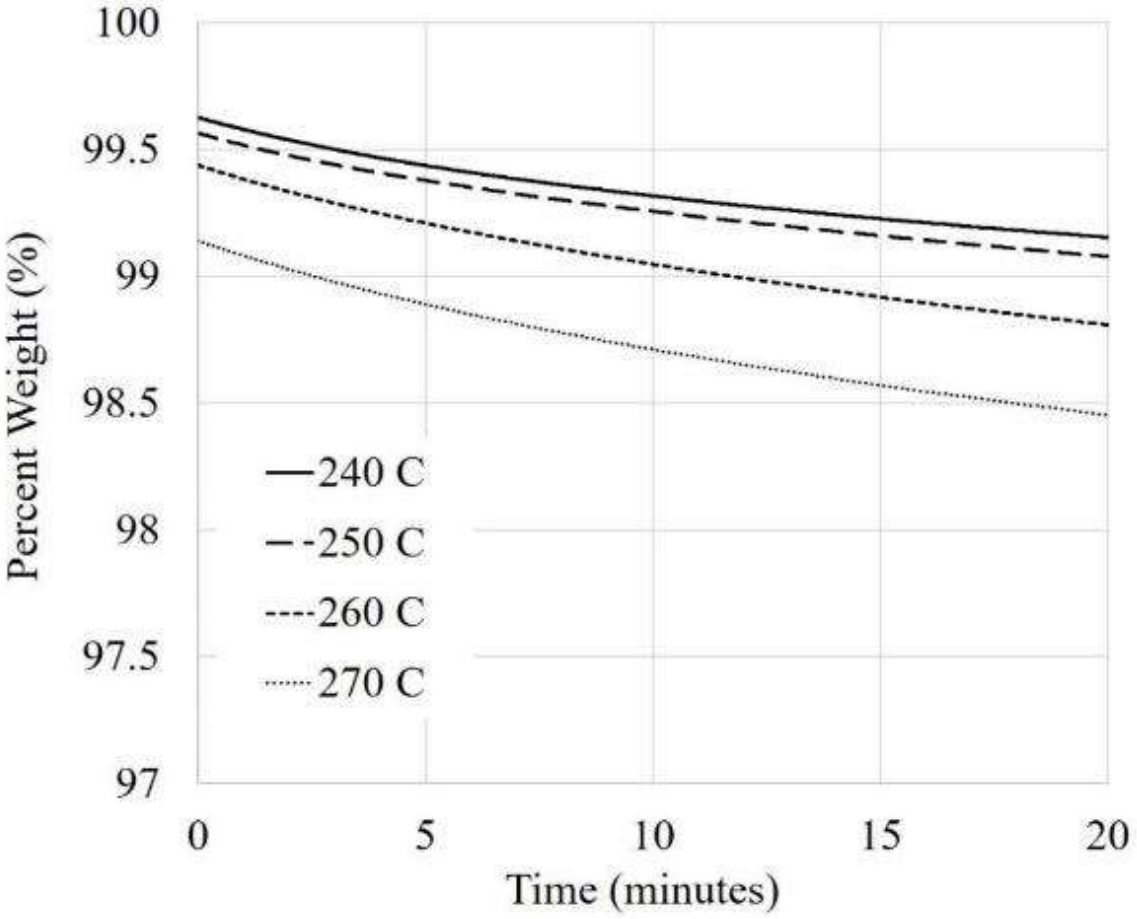

Figure 3-7: Isothermal TGA performed on ABS in Nitrogen atmosphere at 240, 250, 260 and 270 ℃ for 60 minutes.

3.4.3 Selection of temperatures for reinforcing ABS with HX8000 in dual extrusion technology

The processing temperatures used for generating HX8000/ABS composites were determined using a combination of rheological and calorimetric results discussed earlier. The data obtained has been summarized in Table 3-1. The melting temperatures shown in the table were determined using DSC. The equilibration temperatures were selected to get rid of all residual crystallites from the melt and were determined using SAOS tests in the cooling mode using different starting equilibration temperatures. The equilibration temperature that led to the maximum degree of supercooling was taken as final equilibration temperature. The degree of supercooling listed in the table is the difference of the equilibration temperature and the solidification temperature obtained using crossover of storage and loss modulus in the SAOS tests carried out in cooling mode.

Table 3-1: Summary of the temperatures obtained using DSC and rheological tests.

TLCP	**Melting Temperature (°C)**	**Equilibration Temperature (°C)**	**Solidification Temperature (°C)**	**Degree of supercooling (°C)**
HX3000	330	360	285	45
HX6000	338	350	300	32
HX8000	280	310	235	45

It is worth mentioning that the TLCP melt-stability in the supercooled regime is highly dependent on the temperatures below the melting temperature of the TLCP. Qian and coworkers

[10] studied the melt stability of HX8000 at 250, 260 and 270 °C after cooling from 310 °C by performing isothermal SAOS tests. It was found that storage and loss moduli crossed over at 250 °C with time, whereas no crossover was reported for the test temperatures of 260 and 270 °C. This work was originally carried out to enable increasing melt strength during blow molding process as the TLCP viscosity is comparatively higher in the supercooled state compared to that at temperatures above its melting temperature [18]. In our work, advantage of temperature dependent melt stability is taken to match processing temperatures of ABS and HX8000 for processing in the dual extrusion technology. Based on the tests carried out in this work and those carried out by Qian and coworkers, processing temperature used in dual extrusion technology for reinforcing ABS is represented by the schematic shown in Figure 3-8.

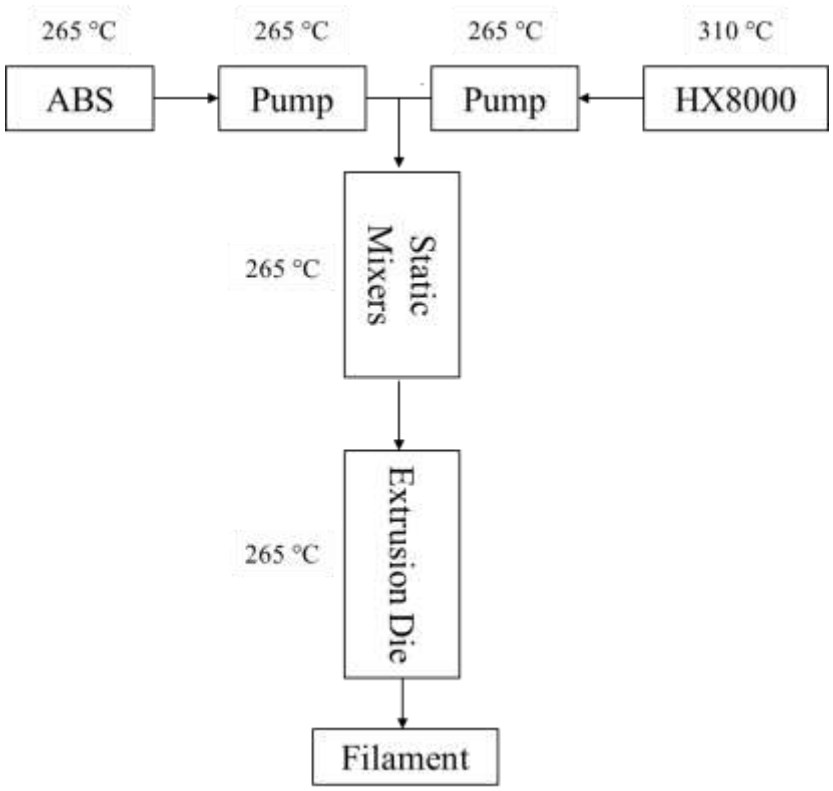

Figure 3-8: Temperature schematic for reinforcing ABS in dual extrusion technology.

ABS was processed at 265 ℃ in the matrix extruder, whereas HX8000 was processed at 310 ℃ in the TLCP extruder. Following this, HX8000 melt temperature was dropped to 265 ℃ before injecting into ABS. The static mixers (Koch and Kenics mixers) and the die were maintained at 265 ℃. Temperature schematic shown in Figure 3-8 ensures stable ABS melt as the use of the supercooling property of HX8000 is taken to an extent that ABS doesn't degrade at the blending temperature. In addition, it is ensured that the blend is maintained at a temperature where HX8000 exhibits stable melt in the supercooled regime to avoid premature solidification during processing.

3.4.4 Tensile properties of HX8000/ABS composite strands

The tensile properties of the HX8000/ABS strands obtained using the dual extrusion technology are listed in Table 3-2. This table shows tensile strength and modulus at different concentrations. It also lists the draw ratios that were used for generating the filaments. The tensile strength and modulus of pure ABS strands were 39.3±3.3 MPa and 2.3±0.4 GPa, respectively. On comparing the tensile properties of the HX8000/ABS strands with those of the pure ABS, a significant improvement in properties can be noticed. The tensile properties also increased with increasing HX8000 concentration. Comparing 40.0 wt.% tensile properties with those of the pure ABS strands, there was almost 4.3 times increase in the tensile strength and around 17.3 times increase in the tensile modulus. Krishnaswamy and coworkers [3] reported tensile properties of pure HX8000 as a function of draw ratio. They reported that the tensile properties are highly dependent on the draw ratio and eventually the properties plateau at the draw ratio of around 75. The maximum tensile strength and modulus of pure HX8000 were reported to be 825 MPa and 47 GPa, respectively. Although the tensile strength of 40.0 wt.% HX8000/ABS is far from that of

pure HX8000, the tensile modulus is 85% of the pure HX8000 maximum tensile modulus. Thus, there exists a scope of improvement in the tensile strength by using a higher draw ratio compared to what is listed in the Table 3-2.

Table 3-2: Tensile properties of HX8000/ABS filaments at different concentrations.

TLCP Concentration (wt.%)	**Draw Ratio**	**Tensile Strength (MPa)**	**Tensile Modulus (GPa)**
10.0	45.0	88.7±1.5	4.0±0.3
20.0	31.9	115.3±3.9	5.7±0.2
40.0	34.8	169.2±4.0	39.9±3.7

3.4.5 Identification of postprocessing conditions of HX8000/ABS strands

The use of TLCP reinforced pregenerated composites is to use as feedstock in conventional polymer processing technologies such as injection molding and compression molding. The postprocessing step involves the identification of conditions that lead to higher properties. An important consideration is to select conditions lower than the melting temperature of the TLCP such that orientation relaxation is minimal. The work reported previously involved random selection of postprocessing conditions for use in compression and injection molding [3, 5]. In such applications, drop in tensile properties has been reported arising due to orientation relaxation and fiber breakage. Mcleod et al. [5] reported drop in the tensile properties on injection molding PET reinforced with a TLCP. In this work, the author cited three reasons for drop in properties, molecular relaxation of TLCPs at elevated temperatures, TLCP agglomeration and loss in the aspect ratio of the TLCP fibers. Moreover, it was reported that lower injection molding

temperature resulted in higher tensile properties. Krishnaswamy et al. also reported drop in tensile properties on compression molding TLCP-reinforced nylon-11. This drop was attributed to loss in orientation. The attribution to drop in tensile properties was not investigated in any of the previously reported work.

In this work, the development of the DMA test is primarily to avoid factors other than orientation relaxation such as fiber breakage and fibril-aggregation. The use of pure HX8000 for carrying out DMA focused on the drop in properties arising only due to the TLCP phase in the matrix phase. Injection molding imparted initial orientation in the TLCP phase, which was constant in every samples as the samples were cut from a constant location of the plaques. Moreover, a high cooling rate was used to achieve quenching effects to minimize transient thermal effects on the samples during cooling.

Figure 3-9 shows results for the HX8000 samples that were exposed to 240 ℃ for 0, 300 and 600 seconds. As the samples were cooled, the storage modulus increased with cooling temperature. On comparing the storage moduli of the samples, a drop can be noticed for the sample that was exposed for 600 seconds. The sample exposed for 300 seconds shows minimal loss in storage modulus in comparison with that of the sample exposed for zero seconds. This suggests that loss in orientation is minimal if the exposure duration can be maintained below five minutes. The results for the HX8000 samples that were exposed to 240, 260 and 270 ℃ for a constant exposure time of 10 minutes is shown in Figure 3-10. This result shows a slight drop in the storage modulus as the exposure temperature is increased. In conclusion, Figure 3-9 and 3-10 suggest that to obtain higher properties, exposure temperatures should be minimized as much as possible. These findings are in alignment with that of the work reported previously by Mcleod et al. [5] and

Krishnaswamy et al. [3]. At 240 °C, the tensile property obtained on postprocessing can be higher if the exposure duration is kept lower than five minutes.

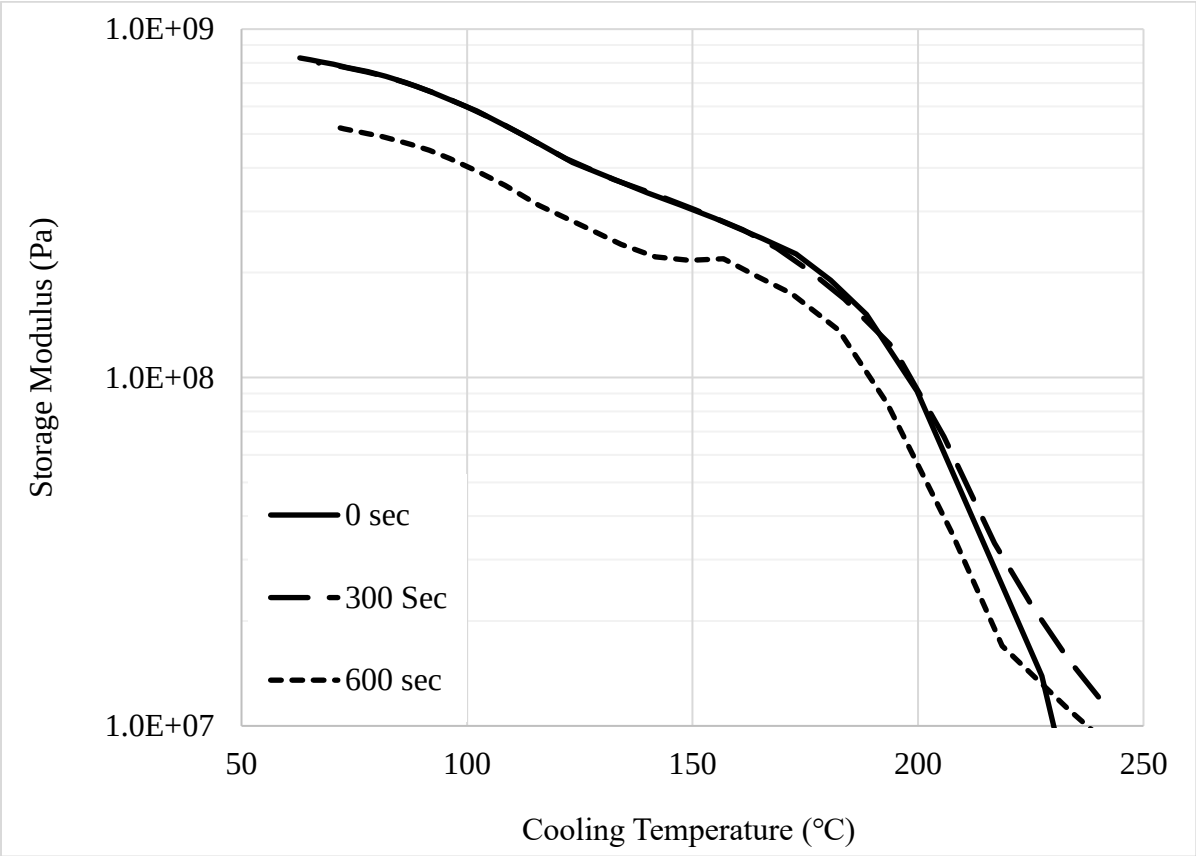

Figure 3-9: DMA performed on HX8000 by exposing to 240 °C for 0, 300 and 600 seconds. Following exposure, the samples were cooled at 30 °C/min and the resulting storage moduli were recorded as a function of cooling temperature.

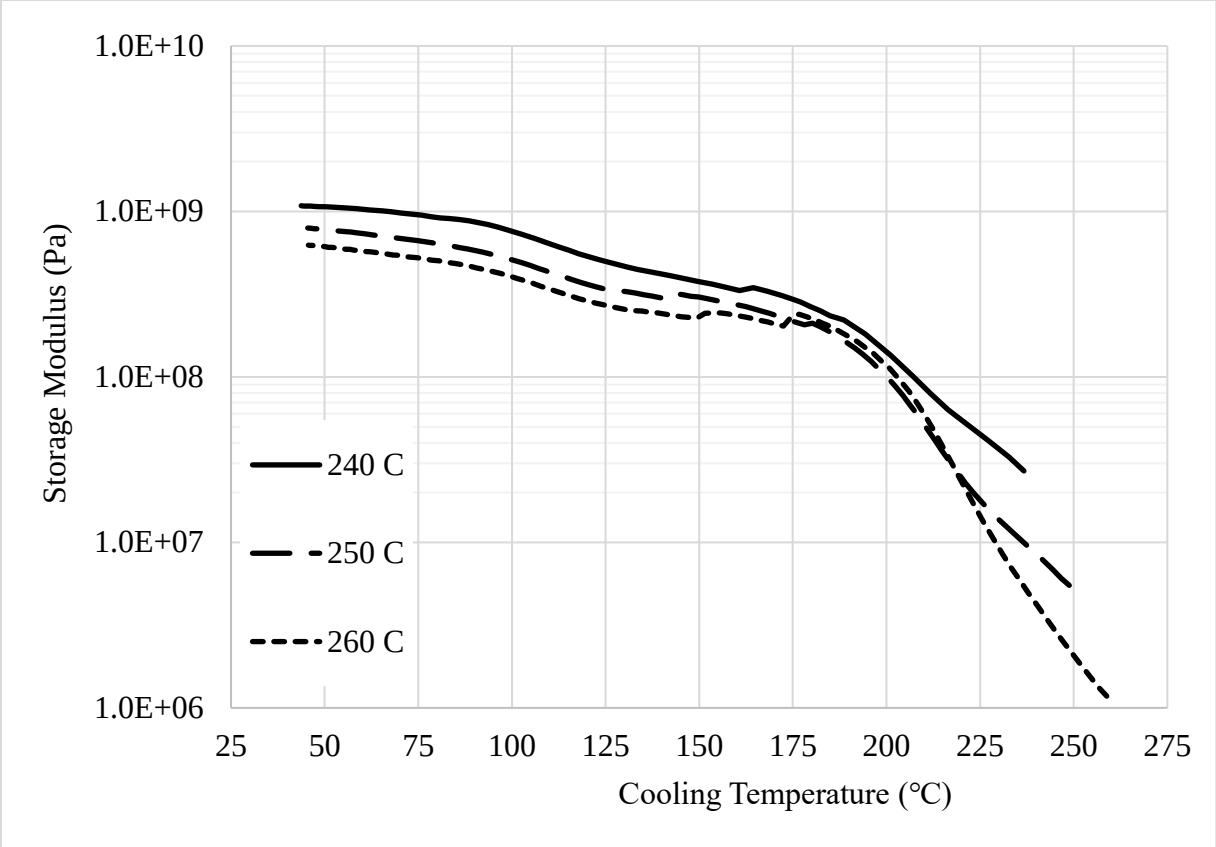

Figure 3-10: DMA performed on HX8000 by exposing to 240, 250 and 260 °C for 600 seconds. Following exposure, the samples were cooled at 30 °C/min and storage moduli were recorded as a function of cooling temperature.

3.4.6 Tensile properties of the compression molded plaques

Figure 3-11 and 3-12 show tensile strength and modulus of the compression molded 40.0 wt.% HX8000/ABS as a function of compression molding temperature. The molding time used was five minutes as obtained by performing DMA on the samples that were exposed to 240 °C. The maximum average tensile strength and modulus were at the lowest compression molding temperature of 240 °C and was found to be 79.6±4.4 MPa and 12.3±1.2 GPa, respectively. It is

important to notice that there is a significant drop in the tensile properties in comparison with those of the strands. The tensile strength and modulus at the molding temperature of 240 °C is only 47% and 31% of the strand properties. Tekinalp et al. [7] compression molded 40.0 wt.% carbon fiber/ABS and obtained a tensile strength and modulus of 75 MPa and 17 GPa (data obtained from plots), respectively. The tensile strength of 40.0 wt.% HX8000/ABS compression molded plaques, molded at 240 °C are higher than that of 40.0 wt.% Carbon fiber/ABS. On the other hand, the tensile modulus is 72% of the 40.0 wt.% carbon fiber/ABS compression molded plaques. With the use of higher draw ratios during strand generation in dual extrusion method, it might be possible to attain even better properties on the compression molded 40.0 wt.% HX8000/ABS. This is because draw ratio used was only, whereas Krishnaswamy et al. [3] reported that the tensile properties of HX8000 attains its maximum at a draw ratio of 75.

The drop in tensile properties on compression molding in comparison with the strand properties may be due to a combination of temperature induced loss in orientation as well as fiber breakage occurring due to consolidation pressure. Although the effect of consolidation pressure was not explored, there may be property dependency on the consolidation pressure as well.

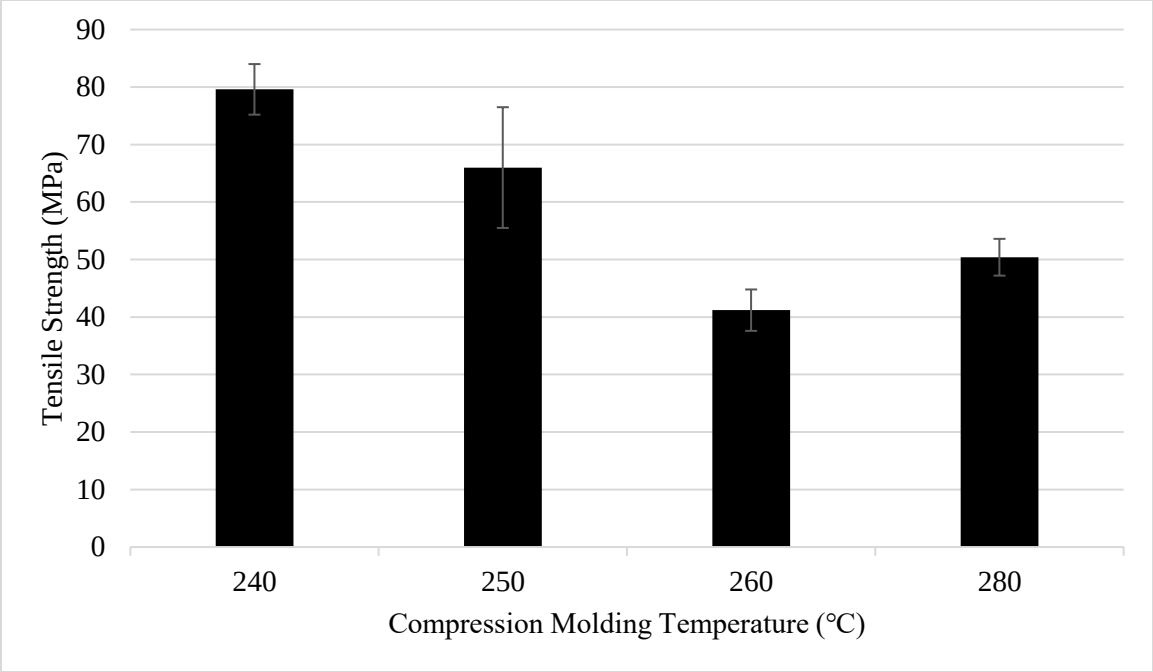

Figure 3-11: Tensile strength of 40.0 wt.% HX8000/ABS as a function of compression molded temperature in the alignment direction.

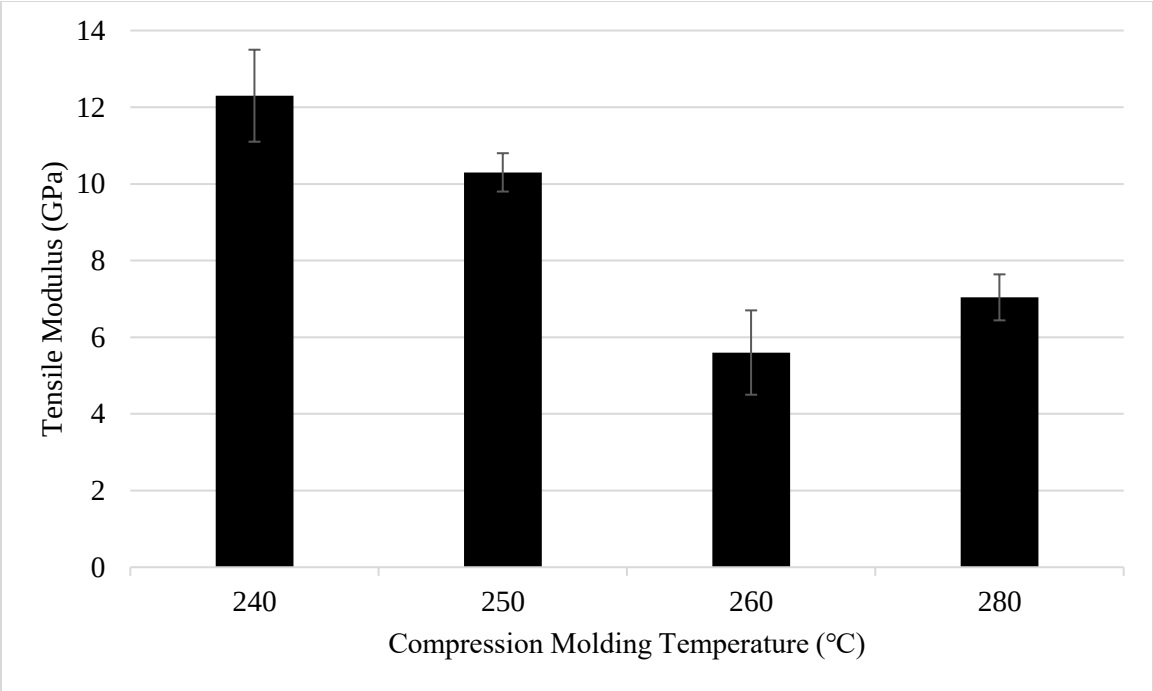

Figure 3-12: Tensile modulus of 40.0 wt.% HX8000/ABS as a function of compression molded temperature in the alignment direction.

The compression molding temperatures of 240, 250 and 260 °C, were such that the composites were processed as a solid filled system as the melting temperature of HX8000 was determined to be 280 °C. The average tensile properties dropped with increasing molding temperature up to the molding temperature 260 °C. This may be due to a combination of fiber breakage and orientation relaxation in the TLCP phase as previously reported by the researchers McLeod et al. and Krishnaswamy et al. [5, 21]. At the molding temperature of 280 °C, a slight increment in the tensile properties can be noticed. This increase might be due to TLCP-reorientation affects at the HX8000 melting temperature.

The results obtained by performing DMA on pure HX8000 and by performing tensile testing on the compression molded 40.0 wt.% HX8000/ABS serve as methods for the selection of conditions to process HX8000-reinforced ABS in various polymer processing technologies. These conditions can also be used to postprocess in injection molding as well as FDM.

3.5 Conclusions

In conclusion, this paper demonstrated the use of rheology in the selection of a TLCP and the processing conditions for reinforcing ABS using the dual extrusion technique. SAOS tests performed in the cooling mode on TLCPs allowed selection of the desired TLCP that avoided degradation of ABS. Moreover, the selected TLCP allowed processing of the composites as a solid filled system in compression molding. Isothermal SAOS test performed in the supercooled regime of HX8000 enabled matching of the processing conditions of ABS and HX8000 in the dual extrusion method. A significant improvement in tensile properties of the strands was obtained in comparison with those of pure ABS. Moreover, a DMA method was devised to study the effects of postprocessing conditions on the TLCP phase. This method is powerful in identifying postprocessing conditions required to process TLCP-reinforced matrix polymers. The conditions

generated using DMA enabled obtaining the highest tensile properties of the strands when used in compression molding of the 40.0 wt.% HX8000/ABS materials.

References

[1] T. Gopakumar, S. Ponrathnam, A. Lele, C. Rajan, A.J.P. Fradet, In situ compatibilisation of poly (phenylene sulphide)/wholly aromatic thermotropic liquid crystalline polymer blends by reactive extrusion: morphology, thermal and mechanical properties, 40(2) (1999) 357-364.

[2] E. Sabol, A. Handlos, D.G. Baird, Composites based on drawn strands of thermotropic liquid crystalline polymer reinforced polypropylene, 16(4) (1995) 330-345.

[3] R.K. Krishnaswamy, D.G. Baird, Wholly thermoplastic composites from woven preforms based on nylon-11 fibers reinforced in situ with a hydroquinone-based liquid crystalline polyester, 18(4) (1997) 526-538.

[4] A. Handlos, D.G. Baird, Part C: Polymer Reviews, Processing and associated properties of in situ composites based on thermotropic liquid crystalline polymers and thermoplastics, 35(2) (1995) 183-238.

[5] M. McLeod, D.G. Baird, Injection molding of poly (ethylene terephthalate) reinforced with pregenerated thermotropic liquid crystalline polymer microfibrils, 20(1) (1999) 3-18.

[6] M.A. McLeod, D.G. Baird, The influence of processing variables on the mechanical properties of injection molded pregenerated microcomposites, 30(3) (1999) 297-308.

[7] H.L. Tekinalp, V. Kunc, G.M. Velez-Garcia, C.E. Duty, L.J. Love, A.K. Naskar, C.A. Blue, S.J.C.S. Ozcan, Technology, Highly oriented carbon fiber–polymer composites via additive manufacturing, 105 (2014) 144-150.

[8] R.W. Gray IV, D.G. Baird, J. H. Bøhn, Effects of processing conditions on short TLCP fiber reinforced FDM parts, 4(1) (1998) 14-25.

[9] A. Handlos, D.G. Baird, Sheet extrusion of microcomposites based on thermotropic liquid crystalline polymers and polypropylene, 17(1) (1996) 73-85.

[10] C. Qian, D.G. Baird, The transient shear rheology of a thermotropic liquid crystalline polymer in the super-cooled state, 102 (2016) 63-72.

[11] D.G. Baird, A. Sukhadia, Mixing process for generating in-situ reinforced thermoplastics, U.S. Patent, 5225488, 1991.

[12] C.-S. Chen, T.-J. Chen, R.-D. Chien, S.-C.J.I.C.i.H. Chen, M. Transfer, Investigation on the weldline strength of thin-wall injection molded ABS parts, 34(4) (2007) 448-455.

[13] O.A. Mohamed, S.H. Masood, J.L.J.A.i.M. Bhowmik, Optimization of fused deposition modeling process parameters: a review of current research and future prospects, 3(1) (2015) 42-53.

[14] G. Ozkoc, G. Bayram, E.J.P.c. Bayramli, Short glass fiber reinforced ABS and ABS/PA6 composites: processing and characterization, 26(6) (2005) 745-755.

[15] T. Das, K. Pal, B. Adhikari, C.J.A.i.M.S. Das, Engineering, Effect of Compatibilizers on the Morphological Properties of ABS and LCP Blends, 2007 (2007).

[16] Y. Xia, H. Zhang, Q. Wang, J. Guo, Y.J.J.o.T.C.M. Gong, Study on in situ reinforced composites of thermoplastic resins: A novel TLCP with low melting temperature, 29(1) (2016) 37-47.

[17] V. González-González, G. Neira-Velázquez, J.J.P.d. Angulo-Sánchez, stability, Polypropylene chain scissions and molecular weight changes in multiple extrusion, 60(1) (1998) 33-42.

[18] C. Qian, C. Mansfield, D.G. Baird, Extrusion Blow Molding of Polymeric Blends Based on Thermotropic Liquid Crystalline Polymer and High Density Polyethylene, 32(1) (2017) 112-120.

[19] M.L. di Cortemiglia, G. Camino, L. Costa, M.J.T.a. Guaita, Thermal degradation of ABS, 93 (1985) 187-190.

[20] M. Suzuki, C.A.J.P.D. Wilkie, Stability, The thermal degradation of acrylonitrile-butadiene-styrene terpolymei as studied by TGA/FTIR, 47(2) (1995) 217-221.

[21] R.W. Gray IV, D.G. Baird, J.H. Bøhn, Thermoplastic composites reinforced with long fiber thermotropic liquid crystalline polymers for fused deposition modeling, 19(4) (1998) 383-394.

4 Application of Thermotropic Liquid Crystalline Polymer Reinforced Acrylonitrile Butadiene Styrene in Fused Filament Fabrication

Chapter 4: Application of Thermotropic Liquid Crystalline Polymer Reinforced Acrylonitrile Butadiene Styrene in Fused Filament Fabrication

Mubashir Q. Ansari[1], Alec Redmann[3], Tim A. Osswald[3], Michael Bortner[1,2], Donald G. Baird[1,2]

1. Department of Chemical Engineering, Virginia Tech, Blacksburg, VA 24061
2. Macromolecules Innovation Institute, Virginia Tech, Blacksburg, VA 24061
3. Polymer Engineering Center, University of Wisconsin-Madison, Madison, WI 53706

4.1 Abstract

In this work, acrylonitrile butadiene styrene (ABS) was reinforced with a thermotropic liquid crystalline polymer (TLCP) for use in Fused Filament Fabrication (FFF). As ABS and the selected TLCP do not exhibit overlapping processing temperatures, the composite filaments were generated using a dual extrusion technology which allows processing of such matrix-TLCP combinations. The 40.0 wt.% TLCP/ABS filaments exhibited a tensile strength and modulus of 169.2±4.0 MPa and 39.9±3.7 GPa, respectively, due to a nearly continuous reinforcement of the filament. The postprocessing of the filaments in FFF was carried out below the melting temperature of the TLCP, which allowed the printer to take sharp turns despite having nearly continuous reinforcement. On the contrary, the use of commercially available continuous carbon fiber/nylon 6 was found to avoid printing regions which required sharp turns. On printing with the 40.0 wt.% TLCP/ABS filaments, the tensile strength and modulus in the print direction were 74.9±2.4 MPa and 16.5±0.8 GPa, respectively. The compression molded specimens exhibited a tensile strength and modulus of 79.6±4.4 MPa and 12.3±1.2 GPa, respectively, whereas the injection molded specimens exhibited 51.3±3.0 MPa and 4.5±0.1 GPa, respectively.

4.2 Introduction

Fused Filament Fabrication (FFF) is a type of additive manufacturing (AM) technology wherein objects are fabricated using polymeric filaments as feedstock [1-4]. As shown in the schematic of FFF in Figure 4-1, the filament is fed into a chamber, commonly referred to as the hot end [4], where the matrix component of the filament melts and is pushed out due to the pressure exerted by the solid portion of the filament [1]. As the extrudate comes out of the nozzle, it is deposited to form various layers of the object being manufactured.

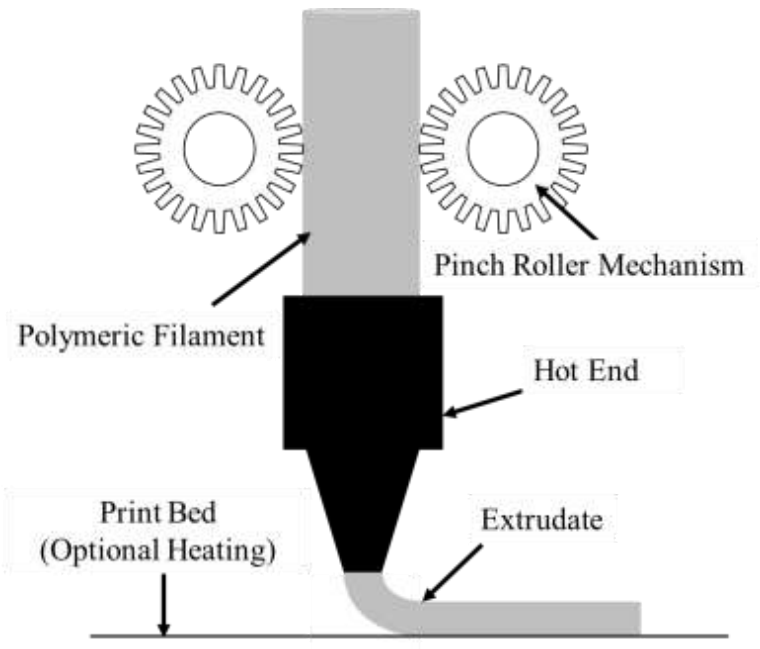

Figure 4-1: Schematic of Fused Filament Fabrication (FFF).

According to the Wohler report published in 2018 [5], the desktop printers, which are mostly comprised of FFF systems, contributed around 30% in revenues of all AM systems. A wider adoption of FFF is primarily due to the ease of operation, inexpensive feedstock and printers [4]. However, pure matrices commonly used to fabricate filament used in FFF, such as polylactic

acid (PLA), acrylonitrile butadiene styrene (ABS), and polycarbonate (PC) possess poor physical properties (especially relative to matrices reinforced with carbon or glass fibers) resulting in weaker printed parts [6].

To overcome using FFF as merely a rapid prototyping tool due to material limitations, significant effort has been expended to enable printing of stronger parts which can be used as functional components. These efforts can be broadly categorized into two approaches. The most commonly used approach is to use composite filaments reinforced with short fibers, such as carbon and glass fibers [3, 6, 7]. The second one, comparatively recent, takes advantage of long aspect ratios by using continuous fibers [4, 8-10]. In the following two paragraphs, an overview of the problems associated with each method will be provided. In FFF, short-fiber composites are usually preferred to avoid major modifications, apart from the requirement of abrasion resistant hot ends, in the 3D printers [3]. The composite filaments exhibit enhanced tensile properties, resulting in stronger printed parts. However, due to the small aspect ratio of the fibers, the tensile properties of the printed parts cannot be improved to the desired extent [3]. Moreover, during filament fabrication, the fiber-fiber, fiber-matrix and fiber-equipment interactions result in a further drop of aspect ratios of these fibers and, hence, limit the maximum achievable tensile properties [3]. For example, in the work carried out by Tekinalp et al. [3] to reinforce ABS with CF, it was reported that a drop in the fiber length from 3.2 mm to around 0.2-0.4 mm occurred. In addition, the fibers are randomly oriented in the matrix, which during printing, leads to additional problems such as nozzle clogging at higher fiber loading and the abrasion of the hot ends [3, 11]. Researchers have also reported a drop in the tensile properties after a certain concentration of fibers due to poor fiber-matrix interaction and the presence of voids [6]. These issues limit the use of higher fiber loading for reinforcing filaments.

To obtain comparatively higher tensile properties, the use of continuous fibers has recently emerged, and their use is enabled by modifying the printers [4, 8, 9]. The fibers are either impregnated in the hot end [9] or processed separately in an additional hot end [4]. While the former method has been reported to lead to poor fiber-matrix interaction [9, 12], the latter method alleviates this issue by feeding continuous fibers in the form of a fiber-matrix such that the fibers are fully encapsulated in the matrix prior to processing [4]. The resin component of the fiber-matrix tow bonds with the matrix deposited in the previous layer. Both methods have successfully resulted in significant improvement in the tensile properties. However, several difficulties arise during the printing process. Due to higher stiffness of the fibers, tighter loops of the reinforcements cannot be printed, which limit the geometric flexibility of the print patterns [4, 10]. Moreover, for enabling the movement of the print-head from one region of the part to another, a severing mechanism is required to allow detachment of the nozzle from the print surface [10].

The goal of this work is to generate composite filaments reinforced with a thermotropic liquid crystalline polymer (TLCP) for its application in FFF. TLCPs have been reported to possess excellent one-dimensional properties that arise due to polymer chain alignment under extensional kinematics [13-15]. TLCPs have also been used to reinforce numerous matrices to improve the tensile properties of the composites. However, most of the work carried out by former researchers was for application in the conventional processing technologies [13, 14, 16].

It was previously reported that the TLCP-thermoplastic composite generation is generally limited by incompatible processing temperatures [14]. This problem was overcome by using dual extrusion technology invented by Baird and coworkers [17]. In this technology, the TLCPs and the matrix polymers are plasticated in separate extruders, following which the TLCP stream is cooled below its melting temperature by taking advantage of the super-cooling behavior [14].

Following injection of the TLCP-stream using a multiport injection nozzle, the blend is passed through a series of static mixers that divide the streams into finer streams, eventually generating nearly continuously reinforced strands.

The use of TLCP as a reinforcement for use in FFF has been attempted before by Gray IV et al. [18]. In this work, polypropylene (PP) was reinforced with a higher melting TLCP to allow processing of the composite filaments as a solid-filled system. The strands obtained using the dual extrusion technology were pelletized and re-extruded to fabricate monofilaments of consistent diameters for use in FFF. Consequently, the additional step of monofilament generation led to a significant drop in the tensile properties as the monofilaments resembled short fiber reinforced filaments. The 40.0 wt.% TLCP/PP filaments generated using the dual extrusion technology exhibited a tensile strength and modulus of 321.0±39.0 MPa and 22.8+1.6 GPa, respectively. Due to the presence of short TLCP fibrils, the tensile strength and modulus dropped to 21.1±2.3 MPa and 2.2+0.1 GPa, respectively. Eventually, the poor tensile properties of the monofilaments translated into weaker printed parts. The maximum tensile strength and modulus obtained in the print direction of the parts were only 37.0 MPa and 2.7 GPa, respectively.

This work aims at enabling the printing of stronger parts by using ABS composite filaments that are nearly continuously reinforced with a TLCP. Consequently, the first objective is to reinforce ABS with a TLCP using dual extrusion technology to generate filaments. The second objective is to postprocess the filaments in FFF by taking advantage of nearly continuous reinforcement without modifying the 3D printer to minimize the cost associated with the adoption of novel TLCP/ABS filaments and to potentially enhance the generation of complex shaped parts. The third objective is to identify temperatures using compression molding, injection molding and FFF that lead to the maximum retention of the filament tensile properties. The fourth objective is

to determine whether all print orientations i.e. 0°, ±45° and 90° can be executed. It is important to assess if nearly continuous reinforcement does not restrict the print-head from taking sharp turns and if the reinforcement flexibility is dependent on the concentration of TLCP. A comparison will also be made using the commercially available continuous carbon fiber/nylon 6 composites by printing a part that requires sharp turns in certain regions.

4.3 Experimental

4.3.1 Materials

In this work, the ABS (Grade: Magnum™ 555) used was provided by Trinseo. Its glass transition temperature (T_g), identified using differential scanning calorimetry, DSC (model: TA instrument's DSC2500 Discovery series), was found to be 105 °C. ABS was dried for at least 4 hours at 85 °C before processing in a vacuum oven as recommended by the supplier. The density of ABS reported by the supplier was 1.04 g/cm^3. The TLCP used, HX8000, was originally supplied by DuPont and has been reported to be composed of unspecified ratios of hydroxybenzoic acid, terephthalic acid, hydroquinone and hydroquinone derivatives [19]. The melting temperature of HX8000, identified using DSC, is 280 °C and its density, as reported previously, is 1.38 g/cm^3 [19]. Before its use, the HX8000 was dried overnight in a vacuum oven at 110 °C.

Two types of filaments used in a MarkTwo printer were supplied by Markforged. The first type, composed of pure nylon 6, was fed into one hot end of the printer to print the pure matrix regions of the part. The second type, composed of nylon 6 reinforced with continuous carbon fibers, was fed into the other hot end of the printer to form the reinforced regions of a part. The fiber volume percent calculated using image analysis of a micrograph of the fiber reinforced filament was found to be approximately 22 volume%.

4.3.2 Filament Generation

ABS was reinforced with HX8000 using the dual extrusion technology, as described in [13, 16, 17], to generate 10.0 and 40.0 wt.% HX8000/ABS filaments. ABS and HX8000 were processed in two separate extruders of 2.5 cm diameter and L/D=24 (model: Killion KL-100) at 265 °C and 310 °C, respectively. Following this, the HX8000-stream temperature was lowered to 265 °C before injecting it into the ABS-stream with a 28-hole injection nozzle. This divided the HX8000-stream into 28 finer streams, each 0.6 mm in diameter. The HX8000/ABS blend was then passed through a 4-element Koch and a 4-element Kenics mixer to subdivide the incoming streams into smaller streams. A 3.0 mm diameter and L/D=20 die was used to generate the composite filaments. The extrudate was drawn and cooled in a water bath following which it was taken up on a custom made, 48 cm in diameter, and constant-rpm take-up winder.

Pure ABS filaments were also generated using a 2.54 cm diameter and L/D=24 extruder (model: Killion KL-100). The zone temperatures used were 220, 230, 240 and 240 °C, respectively. The die used was the same as used for generating HX8000/ABS filaments and was maintained at 240 °C.

4.3.3 Compression Molding

The 40.0 wt.% HX8000/ABS filaments generated using the dual extrusion technology were cut into 76.2 mm long strands for use in the consolidation of unidirectionally oriented 2.0 mm thick square plaques using a 76.2 mm square mold as shown in Figure 4-2. The consolidation temperatures used were 240, 250, 260, and 270 °C. This helped in identifying a temperature that lead to the maximum tensile properties in the alignment direction of the fibers.

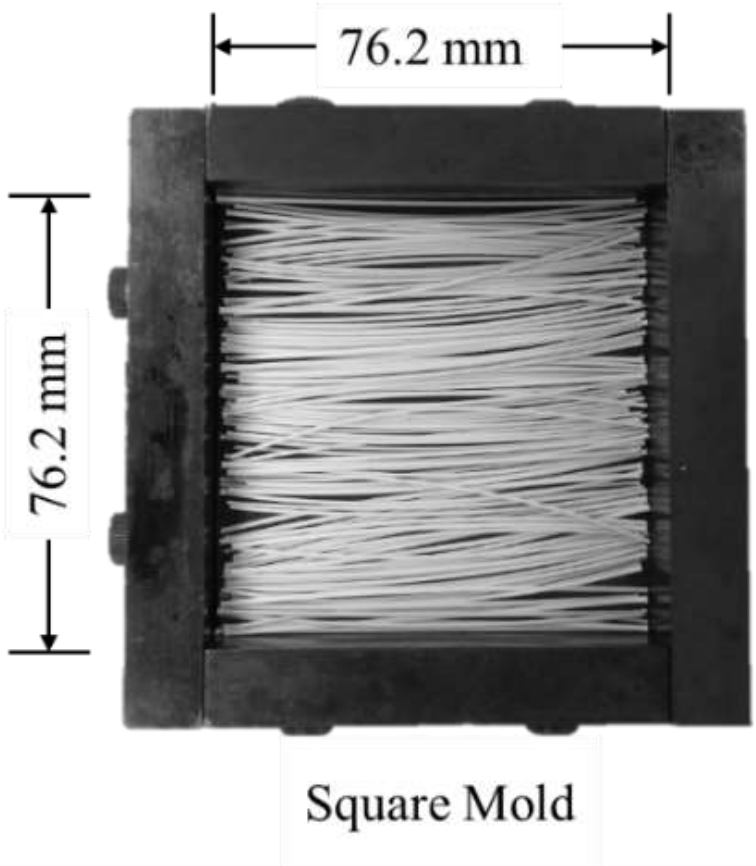

Figure 4-2: Schematic showing unidirectional compression molding of 76.2 mm-long 40.0 wt.% HX8000/ABS strands, into 2 mm thick square plaques, using a 76.2 mm square plaque.

4.3.4 Injection Molding

The 40.0 wt.% HX8000/ABS filaments were pelletized into 25.4 mm-long pellets and then injection molded (using a BOY 35 E machine) using an end-gated plaque. The plaque dimensions were 75.0 x 80.0 x 1.6 mm^3 (dimensions represent length x width x thickness). To study the effect of molding temperatures on the tensile properties of the plaques, two sets of zone temperatures were used for injection molding. The first set of injection molded plaques were obtained using

zone 1-4 temperatures of 220, 230, 240, 240 ℃, respectively, and the nozzle temperature of 240 ℃, while the second set of injection molded plaques were obtained using zone 1-4 temperatures of 240, 250, 260, 260 ℃, respectively, and the nozzle temperature of 260 ℃. In this paper, the former and the later conditions will be referred to as 240 ℃ and 260 ℃, respectively. The mold temperature and the cooling time in both cases were 60 ℃ and one minute, respectively. Pure ABS was also injection molded at 240 ℃ to use for comparing the tensile properties.

4.3.5 Fused Filament Fabrication (FFF)

To determine the print temperature that leads to a maximum retention of the filament tensile properties, rectangular specimens of dimensions 80 mm x 8 mm x 2 mm (dimensions represent length x width x thickness) were printed (3D printer model RoVa3D 5 Extruder 3D Printer by ORD Solutions, Canada) with 40.0 wt.% HX8000/ABS filaments at 240, 250, 260 and 270 ℃, using a zero degree, 0°, print orientation. For comparing the tensile properties, these rectangular specimens were also printed using pure ABS filaments at 240 ℃ in a 0° print orientation. 10 and 40.0 wt.% HX8000/ABS filaments were also printed in 0°, ±45° and 90° print orientations at the print temperature of 260 ℃. All specimens were printed using a 0.8 mm diameter nozzle and having the layer height and width of 0.5 mm and 0.6 mm, respectively. The printed roads overlapped by 0.1 mm and the scan speed used in every direction was 1200 mm/min. It was found that the filament diameter varied due to the inconsistencies in the flow rates of the extrudate and due to the variation in the rpm of the take-up winder. The diameters ranged between 0.7-0.98 mm.

Samples were printed using a MarkTwo printer from MarkForged with continuous carbon fiber reinforcement. The dimensions of the printed bars were 60.8 x 12.7 x 5 mm^3 and were printed

using a 0.1 mm layer height. Three layers of continuous carbon fiber were placed in concentric circles on the top and bottom surfaces of the bars with Markforged Nylon 6 material infill printed at 265 °C.

4.3.6 Scanning Electron Microscopy (SEM)

The morphology of the filaments generated using dual extrusion technology was studied using a field-emission scanning election microscope (model: LEO (Zeiss) 1550) with an accelerating voltage of 5 kV. The surfaces analyzed were sputter coated using a 5nm thick gold layer with a Cressington 208HR Sputterer. The images of 40.0 wt.% HX8000/ABS filaments were taken in the filament's length and transverse direction. The surface for imaging the cross section in the filament's transverse direction was obtained using cryofracture, whereas the surface in the filament's length direction was obtained by cutting, using a blade, in liquid nitrogen. In addition, imaging of the surface of the part printed using 40.0 wt.% HX8000/ABS filaments was also carried out.

Cross-sectional samples of continuous carbon fiber/nylon 6 filaments were cut to a length of approximately 15 mm and embedded in cylindrical test containers using clear Struers EpoFix resin system. The cured samples were polished using a Struers TegraPol 21 polisher. Injected water and polishing suspensions were used to drain the removed sample material and, thereby, preventing scratching of the sample surface. Similarly, the continuous carbon fiber/nylon 6 printed specimen was also cut perpendicular to its length and prepared for imaging. The cross sections were imaged with a BX41M incident light microscope from Olympus.

4.3.7 Tensile Testing

The tensile properties of the filaments, the compression molded and injection molded samples, and the printed specimens were measured using an Instron Mechanical Tester (model:

4468). The crosshead speed and the load cell used was 1 mm/minute and 5kN, respectively. A 50% maximum strain rated extensometer (model: MTS 634.12E-54) was also used for measuring the strains. The extensometer was only used for testing the compression molded, injection molded and the printed specimens as it was difficult to mount it on the cylindrical surface of the filaments. To test the filaments, 15.0 cm-long strands were used. The compression molded plaques were cut into 8.0 mm wide rectangular strips in the alignment direction of the fibers for tensile testing. To test injection molded specimens, 8.0 mm wide specimens were cut in the flow and transverse direction of the plaques. Because the flow pattern is very complex during mold filling in injection molding, the orientation of the fibers varies from region to region [15]. To avoid inconsistencies arising due to flow, tensile testing specimens were cut from the same location of each plaque. The printed specimens were tested by loading along the length. For all tensile property data reported, at least 5 tests were carried out and the outlier data points were removed before calculating the average value with 95% confidence intervals.

4.4 Results and Discussions

This section discusses the tensile property improvement and the morphology obtained on generating ABS filaments reinforced with HX8000 using the dual extrusion technology. Following this, identification of the post-processing temperature of the filaments is discussed. Finally, the performance of the HX8000/ABS filaments in FFF is noted, and their printability is compared with continuous carbon fiber reinforcement.

4.4.1 HX8000/ABS filament properties and morphology

The tensile properties of pure ABS and HX8000/ABS composite filaments are listed in Table 4-1. The HX8000/ABS filaments were generated using the dual extrusion technology, whereas pure ABS filaments were generated using a single extruder. The specific properties of the

filaments are also listed, which were calculated by dividing the tensile properties of the filaments by their densities. The filament densities were calculated based on the densities of pure ABS and pure HX8000. From Table 4-1, it can be seen that the tensile strength and modulus of 40.0 wt.% HX8000/ABS filaments improved by 4.3 and 17.3 times, respectively. Similarly, the tensile strength and modulus of 10.0 wt.% HX8000/ABS filaments improved by 2.6 and 1.7 times, respectively. This improvement is due to the reinforcing potential of HX8000, which on being oriented, exhibits superior tensile properties.

Table 4-1: Tensile and specific properties of pure ABS and HX8000/ABS filaments.

Concentration HX8000/ABS wt.%	**Draw Ratio**	**Tensile Strength (MPa)**	**Tensile Modulus (GPa)**	**Specific Strength (MPa.cm^3/g)**	**Specific Modulus (GPa.cm^3/g)**
0.0	-	39.3±3.3	2.3±0.4	37.7±3.2	2.2±0.4
10.0	45.0	88.7±1.5	4.0±0.3	79.2±1.4	3.6±0.2
40.0	34.8	169.2±4.0	39.9±3.7	143.4±3.4	33.8±3.1

Krishnaswamy and coworkers [14] studied the effect of drawing on the tensile properties of HX8000 and found that the properties were highly dependent on the draw ratios. It was reported that HX8000 attains the maximum tensile strength and modulus of 825.0 MPa and 47.0 GPa, respectively at a draw ratio of around 175. Table 4-2 compares the reinforcing potential of HX8000 with that of carbon and glass fiber. The tensile strength exhibited by highly-drawn HX8000 is around half of glass fiber and around one-fifth of the carbon fiber, whereas the tensile modulus is around three-fifths and one-fifth of glass and carbon fiber, respectively. Because the density of HX8000 is lower than both carbon and glass fiber, the specific properties of HX8000 approach

those of glass fiber but are significantly less than those of carbon fiber. The reinforcing potential of HX8000, in addition to its tailorable flexibility (because of its thermoplastic nature) makes its application in FFF very unique. This will be further discussed in the latter part of this section.

Table 4-2: Comparison of the reinforcing potential of HX8000 with carbon and glass fiber.

Reinforcement	**Density (g/cm^3)**	**Tensile Strength (MPa)**	**Tensile Modulus (GPa)**	**Specific Strength ($MPa.cm^3/g$)**	**Specific Modulus ($GPa.cm^3/g$)**
Pure HX8000 [14]	1.4	825.0	47.0	589.3	33.5
Glass Fiber [20]	2.6	1956.0	78.5	752.3	30.2
Carbon Fiber [20]	1.8	3950.0	238.0	2194.4	132.2

Figure 4-3 shows the morphology of 40.0 wt.% HX8000/ABS filaments. Figures 4-3a and 4-3b show the cross section in the length direction and perpendicular to the length direction of the filament, respectively. The filaments exhibit a fibrillar morphology as seen by the presence of HX80000 fibrils. These fibrils were generated during the processing stage of the filaments and can be seen running nearly continuously along the length of the filament leading to a nearly continuous reinforcement. This is primarily due to a continuous injection of HX8000 using a 28-hole injection nozzle into the ABS stream while processing in dual extrusion technology. The process of *in-situ* generation of HX8000 fibrils resulted in very high aspect ratio fibers which on contrary is unachievable by using carbon and glass fiber due to extensive fiber breakage that occurs during filament generation. Moreover, the fibrils are highly aligned along the length of the filament. The combined effect of nearly continuous fibrils and their allignment leads to a significant one-dimensional increment in the tensile properites of the composite filaments. The average fibril

diamter calculated from Figure 4-3b is 0.6±.1 μm and ranges between 0.3-1.4 μm. The average fibril diameter is an order of magnitude lower than that of carbon and glass fiber, which has been reported to be 7.5 and 13.8 μm, respectively [20]. HX8000 fibril diameters are low due to the fibrillation process that was used in the dual extrusion technology. The static mixers subdivided the 28 streams generated by the injection nozzle, into finer streams of HX8000. These streams were further drawn under extentional flow during the drawing phase of the filaments. From the literature lower fibril diameters lead to higher aspect ratio of the fibers, an essential requirement for obtaining higher tensile properties [21]. By using the rule of mixtures, the tensile moduli of 10.0 and 40.0 wt.% HX8000/ABS filaments were predicted to be 5.7 and 17.8 GPa, respectively. The prediction was based on the maximum modulus of pure HX8000, i.e. 47.0 GPa, as reported by Krishnaswamy and coworkers [14]. On comparing the predicted tensile moduli with the reported values in Table 4-1, an underprediction by the rule of mixtures is evident. The synergistic effect due to the presence of high aspect ratio fibrils that were generated due to the unique process of fibril generation in the dual extrusion technology may have led to obtaining tensile moduli greater than the predictions. On contrary, the tensile strength of 10.0 and 40.0 wt.% HX8000/ABS filaments is only 10.8 and 20.5 % of the maximum tensile strength of HX8000.

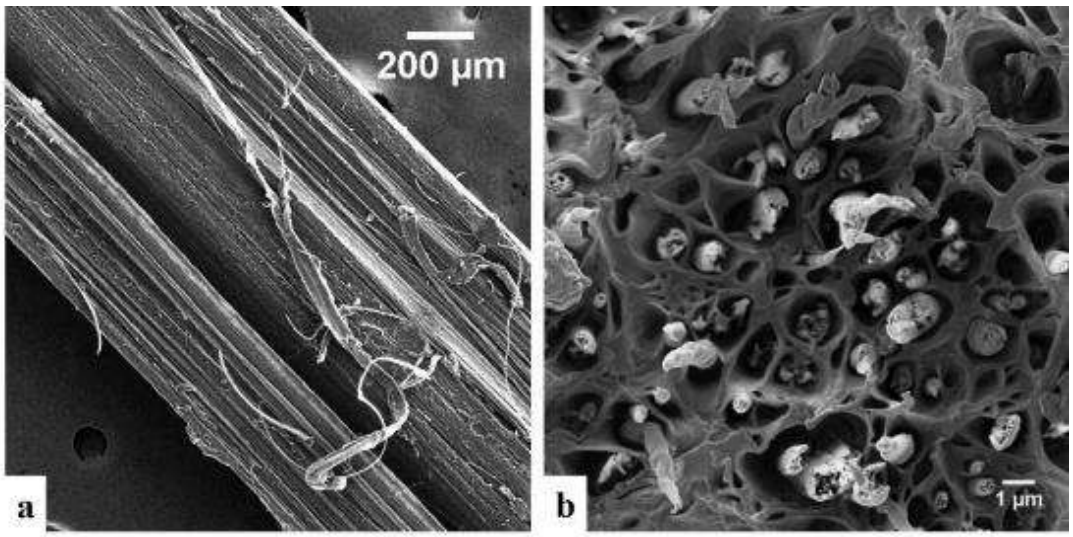

Figure 4-3: SEM image of 40.0 wt.% HX8000/ABS filaments showing the cross-sections in the filament's a) length direction and b) transverse direction.

Two reasons may have led to obtaining lower tensile strength of the composite filaments. The first reason is the lower draw ratios that were used to draw the 10.0 and 40.0 wt.% HX8000/ABS filaments, i.e. 45.0 and 34.8, respectively. On the other hand, the draw ratio used by Krishnaswamy and coworkers to achieve the highest tensile strength of 825.0 MPa for HX8000 was 175. Thus, there exists a scope of improving the tensile properties of the HX8000/ABS composite filaments even further by using higher draw ratios. The second reason is probably due to poor wetting of HX8000 fibrils. In Figure 4-3b, voids can be seen around the fibrils, which is believed to be due to poor interation of HX8000 and ABS. It is important that the matrix polymer interacts with the reinforcement to transmit the load from matrix to the reinforcement when the sample is loaded [22]. In the past, use of compatibilizers has been reported to increase TLCP-matrix interactions leading to improvement in the tensile properties [22]. Thus, the use of compatibilizers should be investigated to improve the HX8000-ABS interactions.

4.4.2 Identification of the postprocessing temperture of HX8000/ABS filaments

The goal of generating HX8000/ABS filaments was to postprocess them as a solid-filled system in FFF in a manner similar to that of glass and carbon fiber reinforced composites. This required the selection of a postprocessing temperature below the melting temperature of HX8000 to keep the fibrils in the solid state. The research carried out previously on TLCP-reinforced composites has reported orientation relaxation of the TLCP phase on postprocessing in conventional processing technologies such as compression and injection molding [14, 15, 18]. The orientation relaxation of the TLCP phase in combination with fiber breakage on postprocessing has been reported to result in the drop of the tensile properties. Thus, to estimate the postprocessing temperatures, 40.0 wt% HX8000/ABS filaments were compression molded and injection molded.

The reason for using 76.2 mm long strands in the consolidation of uniaxially oriented square plaques was to take maximum advantage of the long aspect ratio of the HX8000 fibrils in the filaments. Table 4-3 shows the tensile properties obtained on compression molding HX8000/ABS at 240, 250, 260 and 270 °C. On comparing the tensile properties of the compression molded plaques with those of the filaments, a significant drop in properties can be noticed. The drop is attributed to orientation relaxation and fiber breakage that occurred during the compression molding process. Moreover, the tensile properties obtained at the lowest molding temperature are the highest, suggesting the use of the lowest postprocessing temperature for compression molding.

Table 4-3: Tensile strength and modulus of uniaxially consolidated 76.2 mm long 40.0 wt.% HX8000/ABS strands in the fiber alignment direction at different consolidation temperatures.

Temperature (°C)	**Tensile Strength (MPa)**	**Tensile Modulus (GPa)**
240	79.6±4.4	12.3±1.2
250	66.0±10.5	10.3±0.5
260	41.2±3.6	5.6±1.1
270	55.3±6.7	7.1±0.4

The effect of injection molding was also studied to identify factors that lead to a drop in the tensile properties on postprocessing 40.0 wt.% HX8000/ABS. The tensile properties at the injection molding temperatures of 240 and 260 °C in the flow and transverese direction are shown in Table 4-4. The properties in the flow direction are significantly higher than those in the transverse direction because the TLCP fibrils are oriented preferentially in the flow direction. Additionally, the injection molded plaques exhibit lower tensile properties in comparison with the compression molded plaques due to the complex flow that occurs during mold filling. This leads to fiber breakage and random orientation of the fibrils. Moreover, long aspect ratio pellets could not be fed into the injection molder leading to lower properties. The tensile strength of the plaques molded at 260 °C are higher than the plaques molded at 240 °C. This is believed to be due to higher flexibility of HX8000 fibrils at higher temperatures which helps in minimizing fiber breakage on injection molding and, hence, leading to higher strength.

Table 4-4: Tensile properties obtained in the flow and transverse direction on injection molding 2.5 mm long 40.0 wt.% HX8000/ABS pellets.

Injection Molding Temp. (°C)	**Flow Direction**		**Transverse Direction**	
	Tensile Strength (MPa)	**Tensile Modulus (GPa)**	**Tensile Strength (MPa)**	**Tensile Modulus (GPa)**
240	48.5±4.0	4.5±0.5	22.5±1.1	3.2±0.6
260	51.3±3.0	4.5±0.1	23.6±0.3	2.8±0.1

The plaques generated using injection molding pure ABS exhibited a tensile strength and modulus of 26.9±0.6 MPa and 2.2±0.1 GPa, respectively. In comparison with pure ABS injection molded plaques, the tensile properties of 40.0 wt.% HX8000/ABS plaques is almost double. Thus, a significant improvement was obtained on postprocessing HX8000/ABS in injection molding that were pregenerated with HX8000 fibrils.

In conclusion, the postprocessing temperature required to achieve the highest tensile properties on postprocessing HX8000/ABS composite strands depends on the processing technology. The technology which did not require using the flexibility of the HX8000 fibrils, i.e. compression molding, resulted in the highest properties at the lowest postprocessing temperature. On the other hand, the processing technology which imposed complex flow on postprocessing the strands, i.e. injection molding, benefited from the temperature induced flexibility of the HX8000 fibrils. In such technologies, the lower processing temperature results in rigid fibrils which leads to fiber breakage on postprocessing.

4.4.3 Performance of HX8000/ABS filaments in FFF

The first step in assessing the printability of HX8000/ABS filaments is to identify the postprocessing temperature that leads to the maximum retention of filament tensile properties. Thus, basic rectangular specimens of dimensions 80 x 8 x 2 mm^3 were printed using the 0° print orientation at 240, 250, 260 and 270 °C, as shown in Figure 4-4. The lowest print temperature, i.e. 240 °C, led to poor adhesion between layers, which caused frequent delamination during the specimen removal from the print bed. On the other hand, the highest print temperature tested, 270 °C, led to the presence of bubbles in the part, which might be due to the degradation of ABS at elevated temperatures. Highly aligned HX8000 fibrils in HX8000/ABS filaments resulted in smooth printed parts due to their alignment parallel to the print surface.

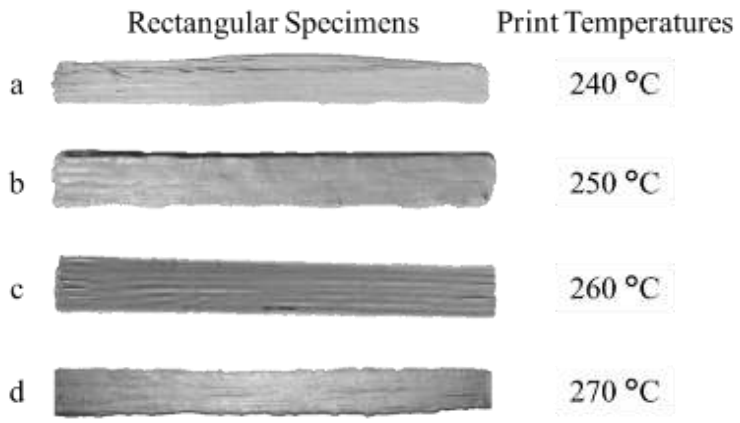

Figure 4-4: Rectangular bars of dimensions 80 mm x 8 mm x 2 mm, printed with 40.0 wt.% HX8000/ABS filaments using 0° print orientations at 240, 250, 260 and 270 °C.

Tensile testing of the specimens printed with 40.0 wt.% HX8000/ABS filaments was carried out to assess improvement in the tensile properties in comparison with those printed with

pure ABS filaments. The specimens printed with pure ABS exhibited tensile strength and modulus of 30.4±0.9 MPa and 2.2±0.1 GPa, respectively. Figure 4-5 shows the tensile properties of the specimens printed using 40.0 wt.% HX8000/ABS at 240, 250, 260, and 270 ℃. The properties are highest when using the print temperature of 260 ℃. As the print temperature is decreased or increased from 260 ℃, the tensile properties drop.

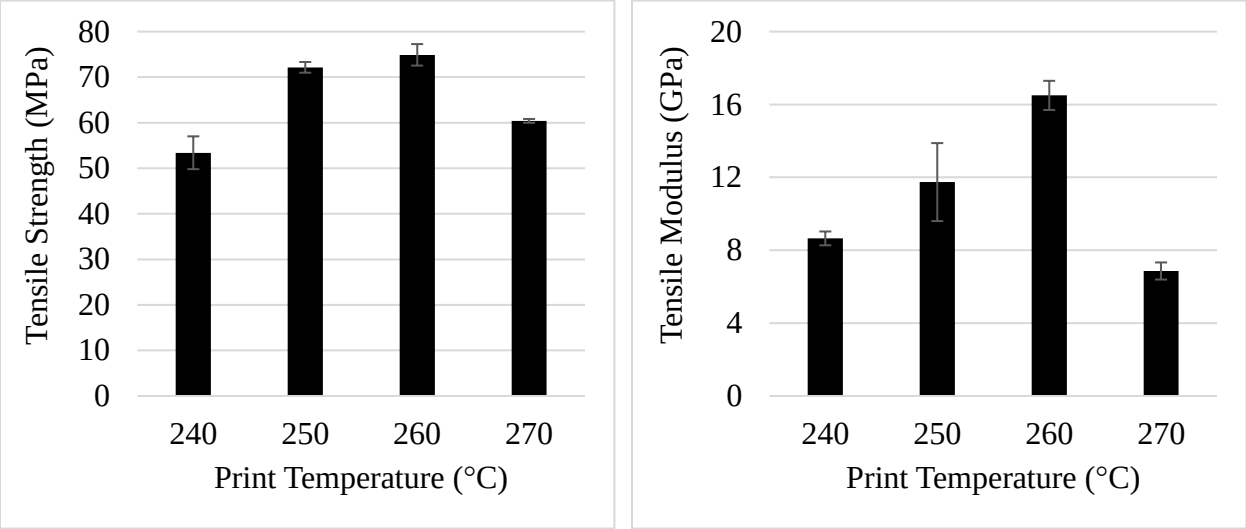

Figure 4-5: Tensile strength (left) and modulus (right) of the 40.0 wt.% HX8000/ABS specimens printed at 240, 250, 260 and 270 ℃. The properties are in the alignment direction of the roads, printed using 0° print orientation.

The properties are lower at lower print temperatures, likely due to fiber breakage that occurs due to a sharp change in the direction during material deposition, as explained by the schematics in Figure 4-6. As the extrudate exits the nozzle, it undergoes a 90° change in direction before the material is deposited. When the print temperatures are low, HX8000 fibrils are believed

to be stiffer, consequently more prone to breakage due to a 90° change in direction. Above 260 °C, the properties drop due to the orientation relaxation of HX8000 fibrils. The best tradeoff between temperature dependent fiber stiffness and orientation relaxation of the TLCP phase is found at 260 °C, thereby resulting in the maximum tensile properties in comparison with all print temperatures tested. This conclusion is also supported by the tensile property data of the injection molded plaques, which resulted in higher properties at 260 °C than those at 240 °C as can be seen in Table 4-4. The maximum tensile strength and modulus of the parts printed at 260 °C are 74.9±2.36 MPa and 16.5±0.8 GPa, respectively, which are around 2.5 and 7.5 times of the parts printed with pure ABS, respectively.

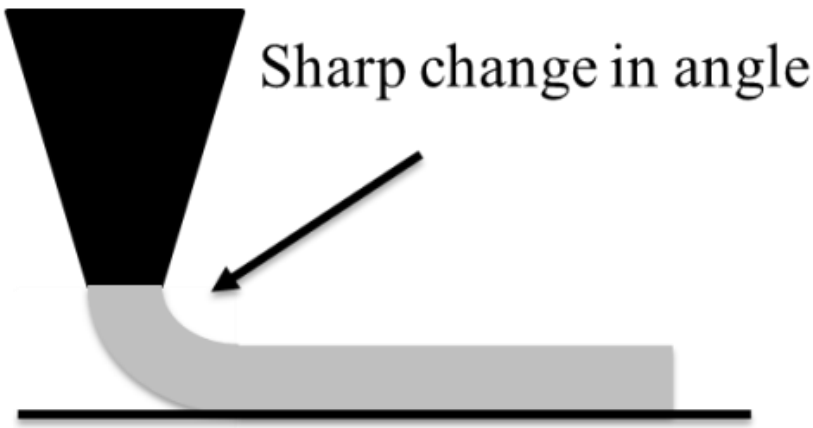

Figure 4-6: Schematic demonstrating a sharp change in angle during material deposition.

Table 4-5 summarizes the reported tensile properties of the printed parts reinforced with both short and continuous fiber reinforced composites. On comparing, the maximum tensile properties of 40.0 wt.% HX8000/ABS printed parts are higher than those of the short fiber reinforced composite parts. Although the tensile strength obtained on printing with 40.0 wt.%

HX8000/ABS is significantly lower, the tensile modulus is either greater or approaches that of the parts printed with continuous fiber reinforcement.

Table 4-5: Tensile properties of the printed parts reinforced with short and continuous fibers, as reported in the literature.

Composite	**Fiber Length**	**Tensile Strength (MPa)**	**Tensile Modulus (GPa)**
40.0 wt.% carbon fiber/ABS [3]	Short	67.0	14.0
40.0 wt.% Carbon Fiber/PP [20]	Short	59.3	14.8
48.5 wt.% Glass Fiber/PP [20]	Short	50.7	8.6
Glass fiber/nylon 6 [4]	Continuous	212.0±5.0	4.9±0.4
Carbon fiber/nylon 6 [4]	Continuous	198.0±12.0	8.5±0.4
Kevlar fiber/nylon 6 [4]	Continuous	161.0±9.0	4.8±0.6
Carbon fiber/PLA [12]	Continuous	185.2± 24.6	19.5± 2.1

HX8000 being a thermoplastic reinforcement, unlike carbon and glass fiber, form HX8000 fibrils in ABS which exhibit tunable flexibility that can be tailored during printing by using elevated temperatures. In order to ascertain if tunable flexibility can be taken advantage of in allowing the printer to take sharp turns during printing, rectangular bars were printed using 0°, ±45°, and 90° print orientations. Figure 4-7 shows that the desired specimens were successfully printed using 40.0 wt% HX8000/ABS filaments. Notably, nearly continuous reinforcement of HX8000 did not prevent the printer from taking sharp turns and also did not require any printer

modification. Figure 4-8 shows before and after pictures of 180° turn taken by the printer, required for printing certain geometries.

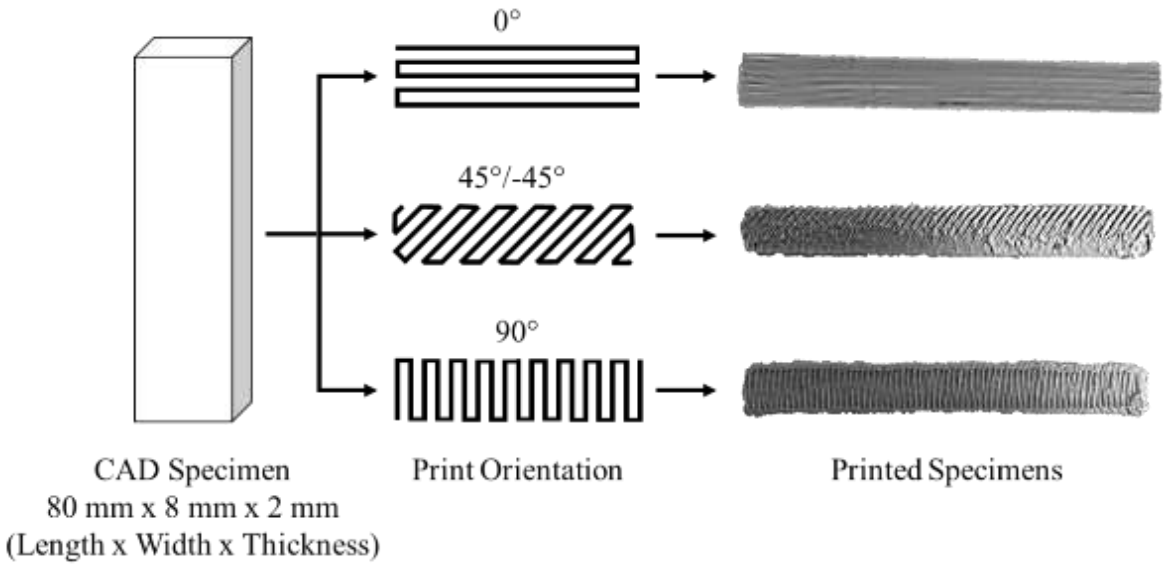

Figure 4-7: Rectangular bars of dimensions 80 mm x 8 mm x 2 mm, printed with 40.0 wt.% HX8000/ABS filaments using 0°, ±45° and 90° print orientations.

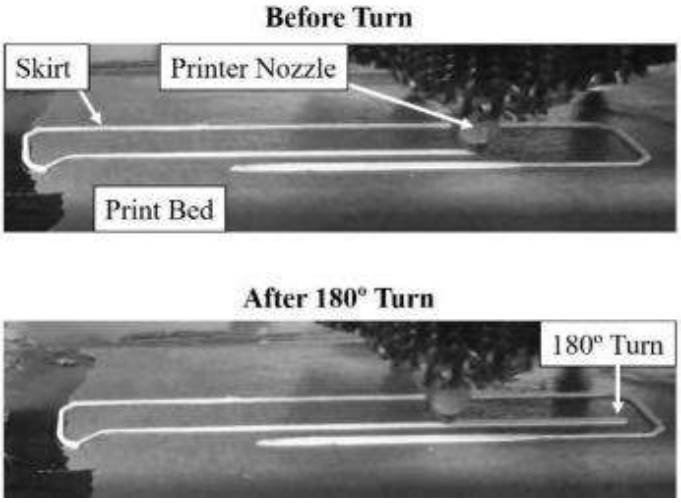

Figure 4-8: Before (top) and after (bottom) pictures of the printer, demonstrating ability to take sharp turns, in spite of nearly continuously reinforcement in the 40.0 wt.% HX8000/ABS filaments that were used for printing.

The printing performance of HX8000/ABS filaments is also compared with that of continuous carbon fiber reinforced filaments. A rectangular box of dimensions 50.8 x 12.7 x 5.0 mm^3 was printed using nylon 6 and continuous carbon fiber as shown in Figure 4-9a. Figure 4-9c shows the cross section that designates regions printed with continuous carbon fiber/nylon 6, pure nylon 6, and regions left as void after cross sectioning the bar as shown in Figure 4-9b. The designated reinforced regions were printed using continuous carbon fiber/nylon 6 in concentric circles shown in Figure 4-9e. The continuous carbon fiber reinforcement ran throughout the length of the rectangular bar in each reinforcement layer. Figure 4-9d shows the optical micrograph of the cross section of the printed rectangular bar in which several imperfections are highlighted. It shows the regions where continuous carbon fiber was not deposited because the stiffness of the fiber prevented the printer from taking sharp turns.

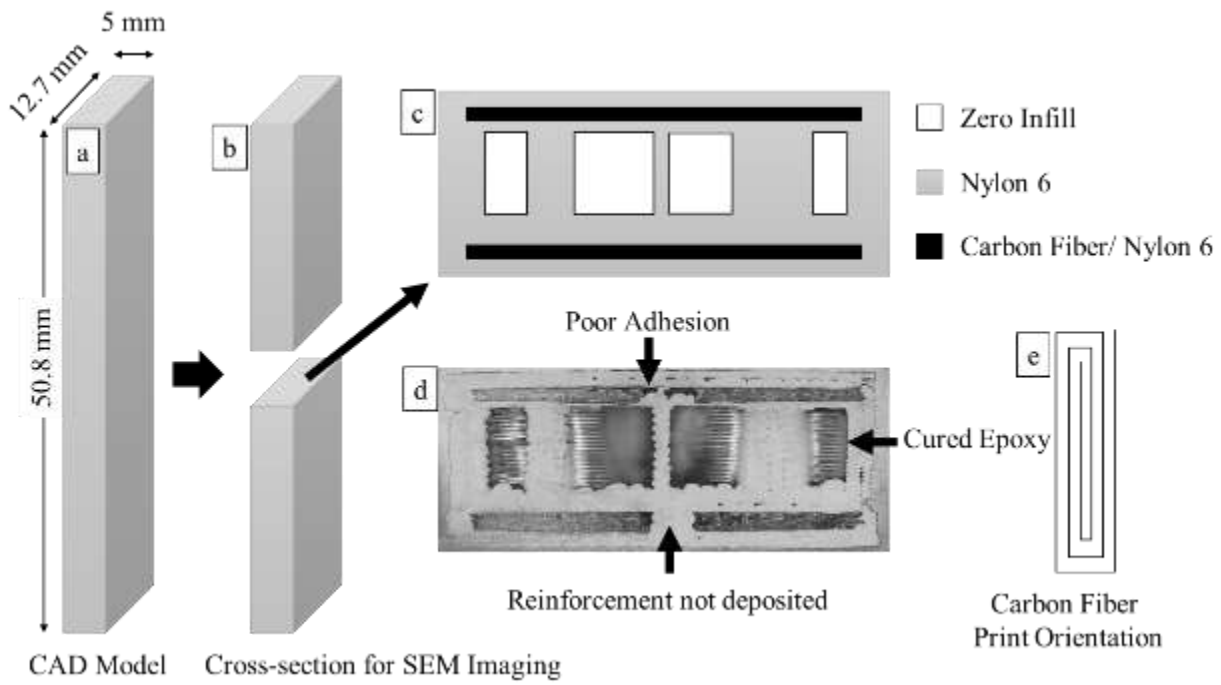

Figure 4-9: a) Rectangular bar of dimensions 50.8 x 12.7 x 5.0 mm^3, printed using continuous carbon fiber/ nylon 6. b) demonstration of cross sectioning, performed for imaging, c) demonstration of reinforcement, pure matrix and zero infill regions in the printed part, d) optical micrograph of the cross-section of the printed bar, printed with continuous carbon fiber/nylon 6, e) print orientation of continuous carbon fiber.

Other imperfections include poor adhesion between the fibers and the matrix, which can be further viewed in the magnified image of the reinforced region as shown in Figure 4-10. In this image, continuous carbon fiber/nylon 6 filament cross section highlighting the poor fiber distribution is also shown. This eventually translates into fiber rich and matrix rich areas in the printed specimens. Other flaws in the printed regions include fiber clustering, internal voids and external voids.

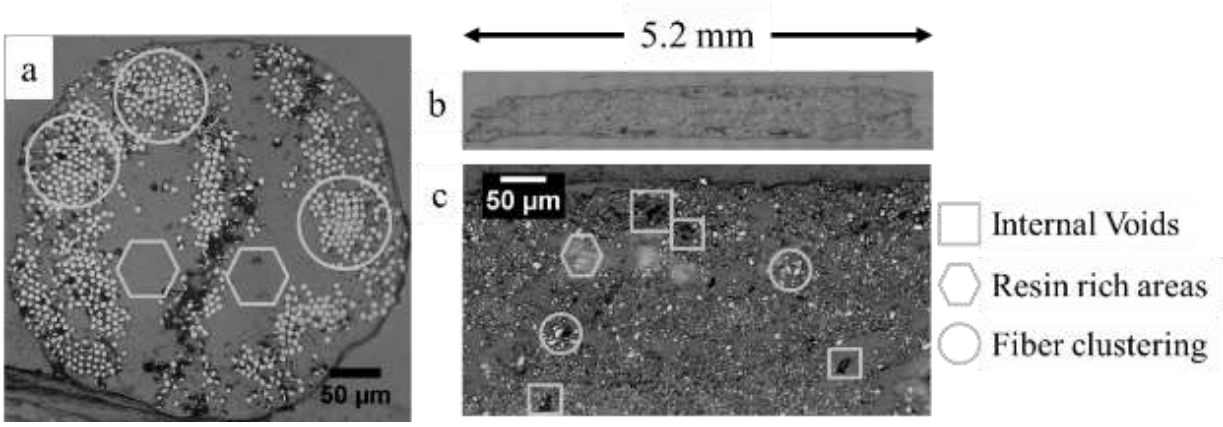

Figure 4-10: a) Cross section of the continuous carbon fiber/nylon 6 filaments, b and c) reinforcement region of the continuous carbon fiber in the printed part.

Figure 4-11 and Figure 4-12 show the tensile properties of the specimens printed using 40.0 and 10.0 wt.% HX8000/ABS filaments, respectively, using 0°, ±45° and 90° print orientations. The properties are highest on using a 0° print orientation, as all fibrils are aligned along the length of the part. As the print orientation is increased, the tensile properties drop. Moreover, the tensile properties obtained by printing with 40.0 wt.% HX8000/ABS using a 90° print orientation, i.e. transverse direction of the fiber alignment direction, are significantly lower in comparison with those of both the parts printed with 10.0 wt.% HX8000/ABS filaments as well as pure ABS filaments. As the concentration of HX8000 was lowered to 10.0 wt.%, the tensile properties of the parts printed using 90° print orientation regained the tensile properties of pure ABS. Because the fibrils are unidirectionally aligned along the length of the filaments, the tensile properties in the transverse direction cannot exceed those of pure ABS.

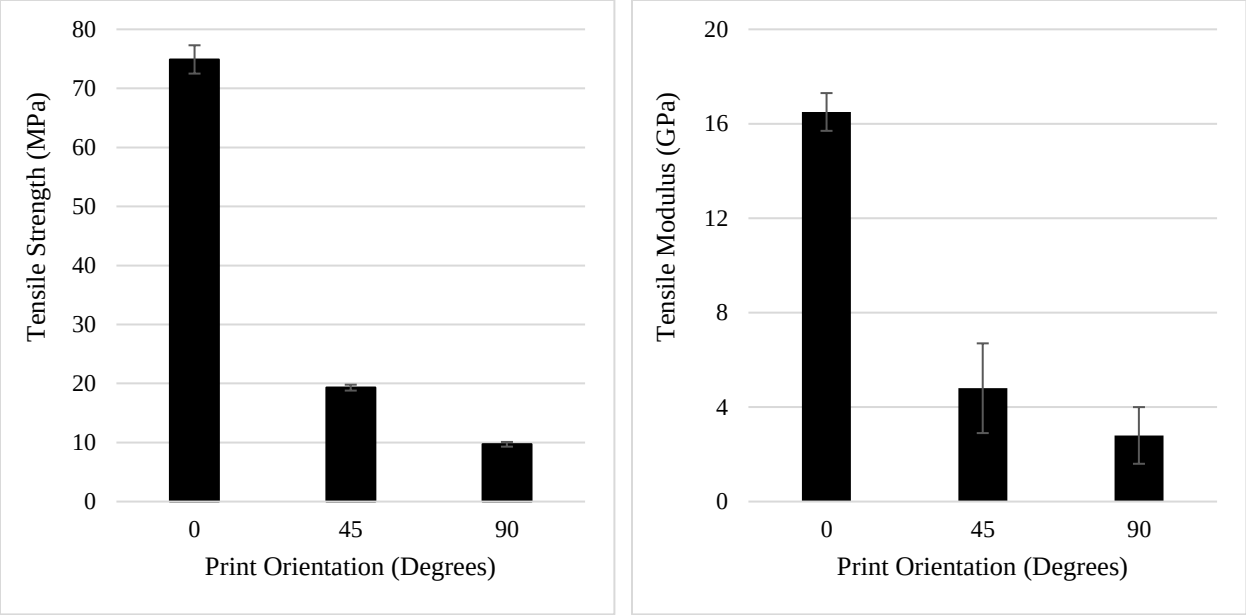

Figure 4-11: Tensile strength (left) and modulus (right) of the 40.0 wt.% HX8000/ABS specimens printed using 0°, ±45° and 90° print orientation. The samples were printed at 260 °C.

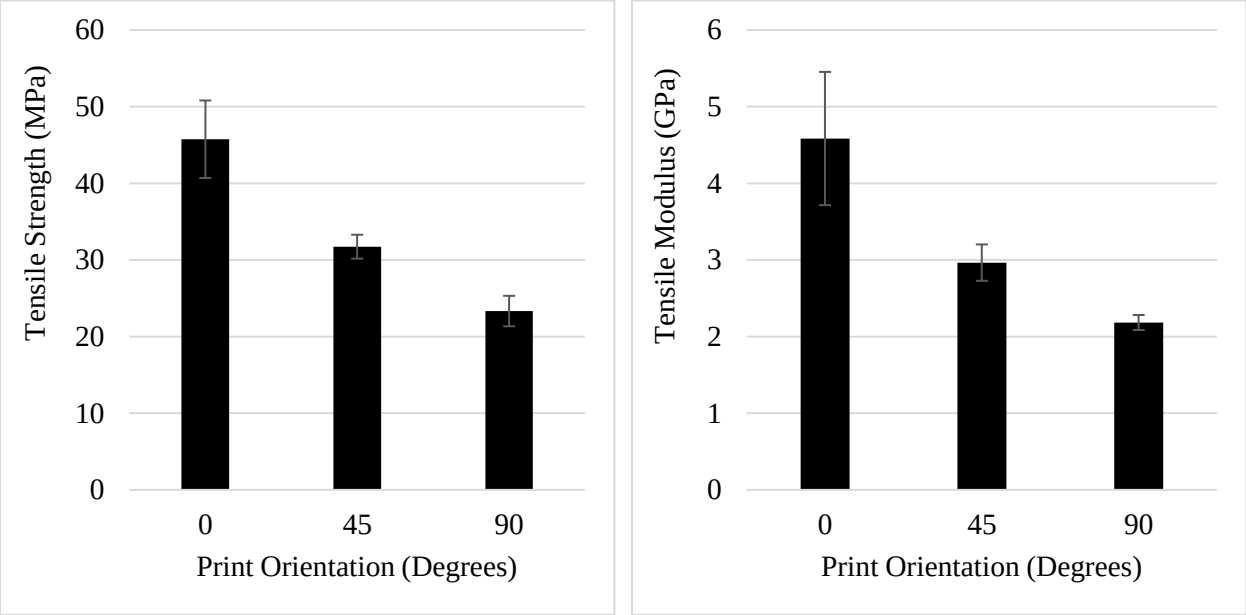

Figure 4-12: Tensile strength (left) and modulus (right) of the 10.0 wt.% HX8000/ABS specimens printed using 0°, ±45° and 90° print orientation. The samples were printed at 260 °C.

The increase in tensile properties in the transverse direction for lower HX8000 concentration is probably due to two factors. The first reason is that the lower concentration of ABS leads to better inter-layer adhesion. This is because only the ABS component of HX8000/ABS is in the molten state, which is essential for initiating bonding with the previous roads and layers. The higher concentration of HX8000 leads to a lower fraction of ABS on the surface, thereby leading to lesser available surface area for the entanglement at the interface. The second reason is the inconsistencies in the filament diameter that was used for printing, which translated into irregular contact between the roads, as shown by the SEM image of the printed part in Figure 13, leading to lower transverse direction tensile properties. The former problem can be solved by choosing a die design that promotes higher matrix concentration at the surface of the HX8000/ABS filaments even at higher HX8000 concentrations. The latter problem can be solved by generating consistent diameter filaments to achieve a consistent contact between the roads.

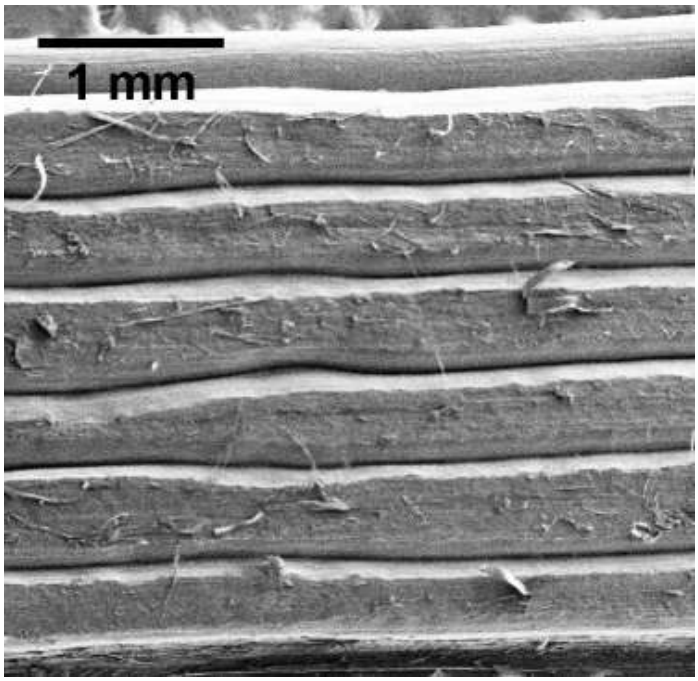

Figure 4-13: SEM image of the surface of the rectangular specimen printed with 40.0 wt. % HX8000/ABS filaments.

4.5 Conclusion

In this work, ABS was reinforced with HX8000 using dual extrusion technology, which resulted in nearly continuous reinforcement. The resulting fibrils averaged 0.6±0.1 μm in diameter, an order of magnitude lower than that of glass and carbon fiber fibers. 40.0 wt.% HX8000 improved the tensile strength and modulus of ABS by 4.3 and 17.3 times, respectively, to 169.2±4.0 MPa and 39.9±3.7 GPa, respectively. The postprocessing temperature of the filaments determined using compression molding led to maximum tensile properties at 240 ℃ above which the properties dropped, primarily due to orientation relaxation of HX8000 fibrils. On the other hand, the postprocessing temperature of 260 ℃ led to the maximum properties, when processed in injection molding and FFF. Below 260 ℃, the tensile properties dropped on postprocessing in FFF, probably due to rigid fibrils. The maximum unidirectional tensile properties of 40.0 wt. % HX8000/ABS printed parts were 74.9±2.36 MPa strength and 16.5±0.8 GPa modulus, which were 2.5 and 7.5 times, respectively, those of the parts printed with pure ABS. The unidirectional properties of the printed parts were higher than the flow direction properties of the injection molded parts. Moreover, nearly continuous reinforcement of HX8000 did not restrict the printer from taking sharp turns, unlike continuous carbon fiber which restricted depositing the reinforcement in the regions that required sharp turns.

References

[1] I. Gibson, D. Rosen, B. Stucker, Extrusion-Based Systems, Additive Manufacturing Technologies: 3D Printing, Rapid Prototyping, and Direct Digital Manufacturing, Springer New York, New York, NY, 2015, pp. 147-173.

[2] S.C. Ligon, R. Liska, J.r. Stampfl, M. Gurr, R. Mülhaupt, Polymers for 3D printing and customized additive manufacturing, Chemical reviews 117(15) (2017) 10212-10290.

[3] H.L. Tekinalp, V. Kunc, G.M. Velez-Garcia, C.E. Duty, L.J. Love, A.K. Naskar, C.A. Blue, S. Ozcan, Highly oriented carbon fiber–polymer composites via additive manufacturing, Composites Science and Technology 105 (2014) 144-150.

[4] A.N. Dickson, J.N. Barry, K.A. McDonnell, D.P. Dowling, Fabrication of continuous carbon, glass and Kevlar fibre reinforced polymer composites using additive manufacturing, Additive Manufacturing 16 (2017) 146-152.

[5] T. Wohlers, I. Campbell, O. Diegel, Wohlers Report 2018, Fort Collins: Wohlers Associates (2018).

[6] F. Ning, W. Cong, J. Qiu, J. Wei, S. Wang, Additive manufacturing of carbon fiber reinforced thermoplastic composites using fused deposition modeling, Composites Part B: Engineering 80 (2015) 369-378.

[7] W. Zhong, F. Li, Z. Zhang, L. Song, Z. Li, Short fiber reinforced composites for fused deposition modeling, Materials Science and Engineering: A 301(2) (2001) 125-130.

[8] G.W. Melenka, B.K. Cheung, J.S. Schofield, M.R. Dawson, J.P. Carey, Evaluation and prediction of the tensile properties of continuous fiber-reinforced 3D printed structures, Composite Structures 153 (2016) 866-875.

[9] N. Li, Y. Li, S. Liu, Rapid prototyping of continuous carbon fiber reinforced polylactic acid composites by 3D printing, Journal of Materials Processing Technology 238 (2016) 218-225.

[10] F. Van Der Klift, Y. Koga, A. Todoroki, M. Ueda, Y. Hirano, R. Matsuzaki, 3D printing of continuous carbon fibre reinforced thermo-plastic (CFRTP) tensile test specimens, Open Journal of Composite Materials 6(01) (2015) 18.

[11] J.P. Lewicki, J.N. Rodriguez, C. Zhu, M.A. Worsley, A.S. Wu, Y. Kanarska, J.D. Horn, E.B. Duoss, J.M. Ortega, W. Elmer, 3D-Printing of meso-structurally ordered carbon fiber/polymer composites with unprecedented orthotropic physical properties, Scientific reports 7 (2017) 43401.

[12] R. Matsuzaki, M. Ueda, M. Namiki, T.-K. Jeong, H. Asahara, K. Horiguchi, T. Nakamura, A. Todoroki, Y. Hirano, Three-dimensional printing of continuous-fiber composites by in-nozzle impregnation, Scientific reports 6 (2016) 23058.

[13] A. Handlos, D. Baird, Processing and associated properties of in situ composites based on thermotropic liquid crystalline polymers and thermoplastics, Journal of Macromolecular Science, Part C: Polymer Reviews 35(2) (1995) 183-238.

[14] R.K. Krishnaswamy, D.G. Baird, Wholly thermoplastic composites from woven preforms based on nylon-11 fibers reinforced in situ with a hydroquinone-based liquid crystalline polyester, Polymer composites 18(4) (1997) 526-538.

[15] M.A. McLeod, D.G. Baird, The influence of processing variables on the mechanical properties of injection molded pregenerated microcomposites, Composites Part B: Engineering 30(3) (1999) 297-308.

[16] A. Handlos, D.G. Baird, Sheet extrusion of microcomposites based on thermotropic liquid crystalline polymers and polypropylene, 17(1) (1996) 73-85.

[17] D.G. Baird, A. Sukhadia, Mixing process for generating in-situ reinforced thermoplastics, U.S. Patent, 5225488, 1991.

[18] R.W. Gray IV, D.G. Baird, J. H. Bøhn, Effects of processing conditions on short TLCP fiber reinforced FDM parts, 4(1) (1998) 14-25.

[19] M. McLeod, D. Baird, The crystallization behavior of blends of thermotropic liquid crystalline polymers, Polymer 40(13) (1999) 3743-3752.

[20] S.-Y. Fu, B. Lauke, E. Mäder, C.-Y. Yue, X. Hu, Tensile properties of short-glass-fiber-and short-carbon-fiber-reinforced polypropylene composites, Composites Part A: Applied Science and Manufacturing 31(10) (2000) 1117-1125.

[21] P.J. Hine, H.R. Lusti, A.A. Gusev, Numerical simulation of the effects of volume fraction, aspect ratio and fibre length distribution on the elastic and thermoelastic properties of short fibre composites, Composites science and technology 62(10-11) (2002) 1445-1453.

[22] A. Datta, H. Chen, D.G. Baird, The effect of compatibilization on blends of polypropylene with a liquid-crystalline polymer, Polymer 34(4) (1993) 759-766.

5 Generation of Polyphenylene Sulfide Reinforced with a Thermotropic Liquid Crystalline Polymer for Application in Fused Filament Fabrication

Chapter 5: Generation of Polyphenylene Sulfide Reinforced with a Thermotropic Liquid Crystalline Polymer for Application in Fused Filament Fabrication

Mubashir Q. Ansari[1], Michael J. Bortner[1,2], Donald G. Baird[1,2]

1. Department of Chemical Engineering, Virginia Tech, Blacksburg, VA 24061
2. Macromolecules Innovation Institute, Virginia Tech, Blacksburg, VA 24061

5.1 Abstract

In this work, polyphenylene sulfide (PPS) was reinforced with a thermotropic liquid crystalline polymer (TLCP) to generate composite filaments for use in Fused Filament Fabrication (FFF). Because of non-overlapping processing temperatures, rheology enabled taking advantage of the dual extrusion technology, which generated nearly continuously reinforced filaments that exhibited a tensile strength and modulus of 155.0±24.2 MPa and 40.4±7.5 GPa, respectively. On printing at the post-processing temperature determined using compression molding, maximum tensile strength and modulus of 108.5±19.4 MPa and 25.9±1.1 GPa, respectively, were obtained, higher than the properties of the reported use of short fiber composites. Moreover, the tensile strength was lower, and the tensile modulus was higher in comparison with the reported use of continuous fibers. Additionally, the tensile properties in the print direction were higher than those of compression molded samples. The nearly continuous reinforcement did not restrict the mobility of the printer, unlike the reported performance of the continuously reinforced carbon fiber thermoplastics in FFF.

5.2 Introduction

Additive Manufacturing (AM) or 3D printing encompasses a group of technologies that enable fabrication of objects by the successive addition of layers [1, 2]. AM has numerous

advantages, such as the ability to fabricate complex shapes, the generation of parts with minimal material waste, and no requirement of custom tooling [3, 4]. Of various AM technologies, material extrusion additive manufacturing (MEAM) is very common and is further classified into two parts: large format additive manufacturing (LFAM) or big area additive manufacturing (BAAM) and Fused Filament Fabrication (FFF). The LFAM/BAAM systems are much larger and use pellets as feedstock [5, 6]. On the other hand, the FFF systems are very common and desktop sized. In FFF, objects are fabricated using polymeric filaments as feedstock, which melt in a liquefier and then are extruded to form different layers of the object being printed [7].

Widely adopted filament matrices in FFF, such as acrylonitrile butadiene styrene (ABS), polylactic acid (PLA), and polycarbonate (PC) have been reported to exhibit poor tensile properties, which in addition to the artifacts introduced during printing such as poor interlayer adhesion and inclusion of voids lead to weaker printed parts [8, 9]. This problem is commonly addressed by taking advantage of the superior properties of traditionally used fibers such as carbon and glass fiber to form composite filaments [9, 10]. However, the property enhancement is not generally adequate to employ AM as a manufacturing technology. Unlike AM, the conventional manufacturing technologies, such as injection molding, have benefitted due to a wider material selection [9]. Available polymer matrices at disposal for conventional manufacturing technologies extend to include high-performance polymers and their composites to replace even metals in the automotive and aerospace industry [11, 12].

High-performance polymers are employed because of their excellent tensile properties and chemical and thermal resistance and are used to fabricate parts that demand such properties, e.g. under-the-hood automotive and aerospace components [8, 12]. The adoption of high-performance polymers in MEAM is slower, and the reported polymers being used include polyetherimide (PEI),

polyphenyl sulfone (PPSU), polyether sulfone (PES), polyphenylene sulfide (PPS), poly(etheretherketone) (PEEK), and poly(etherketoneketone) (PEKK) [8]. Geng and coworkers [13] used pure PPS in FFF to study the effect of heat treatment on the tensile properties of the printed specimens. In other work, Kishore et al. [8] printed with pure PPS as well as carbon fiber (CF) reinforced PEEK using FFF. However, in this work improvement in the properties of the printed specimens was not reported. The superior properties of high-performance polymers have been further improved by forming composites to enable printing tools for high temperature applications to broaden the application of MEAM. Kunc and coworkers [6] processed CF/PPS and CF/PPSU in LFAM to generate in-autoclave tools. The high temperature application of the high performance polymers resulted in the successful use of the printed tools in the two-hour long autoclave process which was conducted at 176.6 ºC and 620 kPa.

The goal of this work is to address the requirement of novel materials for use in FFF to enable printing stronger parts by using composites of PPS, which is a high-performance matrix. The reinforcing potential of thermotropic liquid crystalline polymers (TLCPs), which are composed of rod-like aromatic monomers, will be used [14-17]. TLCPs align under extensional flow kinematics leading to excellent one-dimensional tensile properties [18]. Although TLCP/PPS blends have been used in the past, their application was primarily in conventional manufacturing technologies such as injection molding [19, 20]. In this effort, TLCP/PPS composites will be investigated for their use in FFF.

Recently, continuously reinforced composites have gained attention in FFF [21-23]. In these technologies, continuous fibers such as Kevlar, glass and carbon fibers are impregnated with resin during printing using modified printers. These efforts have demonstrated improved tensile

properties of the printed parts in comparison with short fiber reinforced filaments [10, 21]. The first objective of this work is to generate nearly continuously reinforced TLCP/PPS composite filaments for use in FFF. This can be realized by using dual extrusion technology invented by Baird and coworkers [14, 24] that enables continuous injection of the TLCP-stream into the matrix-stream. The processing conditions required to reinforce PPS, nearly continuously, with a higher melting TLCP will be selected using rheology. The second objective is to determine the postprocessing conditions of the TLCP/PPS filaments which will allow for the processing of the filaments at temperatures in which the matrix will melt but the TLCP will retain its properties. This will be done using compression molding of the filaments under conditions that will lead to the retention of the filament properties to the maximum extent. The conditions selected will enable processing of the composite by only melting the PPS while the TLCP remains as a solid similar carbon and glass fiber reinforced composites. The third objective is to print basic specimens using TLCP/PPS filaments to study the improvement in the tensile properties. Finally, the tensile properties obtained on printing with TLCP/PPS filaments will be compared with the reported use of short and continuous fibers.

5.3 Experimental

5.3.1 Materials

The PPS used in this work, Ryton®, is a commercial grade and was generously supplied by Solvay. It's glass transition and melting temperatures, as reported by the supplier, are 90 and 280 °C, respectively. The TLCP used, HX3000, was supplied by Dupont and is reported to be composed of unspecified ratios of hydroxybenzoic acid, terephthalic acid, hydroquinone and hydroquinone derivatives [15]. It's melting temperature, determined using differential scanning

calorimetry, DSC (model: TA instrument's DSC2500 Discovery series), was found to be 330 °C. PPS and HX3000 were dried overnight at 120 °C in a vacuum oven prior to their use.

5.3.2 Rheological Measurements

All rheological tests were carried out using a TA instrument's ARES-G2 rheometer in a nitrogen atmosphere. A 25 mm parallel plate fixture was used for testing PPS whereas a 25 mm diameter cone and plate fixture (cone angle: 0.1002 radian) was used for testing HX3000. Small amplitude oscillatory shear (SAOS) measurements were carried out on PPS at 300, 310, 320, 330 and 340 °C to study the melt stability by tracking the complex viscosity for 1 hour. The strain used in the SAOS tests was 5%, which has been used by the researchers previously [15, 25].

HX3000 was subjected to SAOS measurements in the cooling mode after equilibrating at 360 °C for 3 minutes using cooling rates of 5, 10, 15 and 20 °C/min. In these tests, the complex viscosity was tracked as a function of temperature. HX3000 was also subjected to SAOS tests in the isothermal mode at 290, 295, 300, 305 and 310 °C after equilibrating at 360 °C for 3 minutes and then cooling at the rate of 10 °C/min.

HX3000 was subjected to shear step strain tests above its melting temperature at 340, 350, 360 and 370 °C. Shear step strain tests were also performed on HX3000 below its melting temperature at 290, 300, 310, and 320 °C after cooling at the rate of 10 °C/min from 360 °C.

5.3.3 Filament Generation using Dual Extrusion Technology

67.0 wt.% HX3000/PPS filaments were generated using dual extrusion technology. The higher concentration of HX3000 was used to take advantage of its reinforcing potential and to determine if it leads to nozzle clogging issues on printing, in comparison with the use of carbon fiber/ABS filaments by Tekinalp and coworkers [10]. As shown by the schematic in Figure 5-1a, PPS and HX3000 were plasticated in two separate single screw extruders (model: Killion KL-

100), and then the melts were metered using two gear pumps (model: Zenith HD-556). HX3000 was injected into PPS using a 28-hole injection nozzle, with each hole 0.6 mm in diameter. Following injection, the blend was passed through a 4-element Koch and a 4-element Kenics mixers. The filaments were drawn on extrusion from a L/D=20 and 3 mm diameter die, following which the extrudate was cooled in a water bath and taken up on a custom made 48 cm diameter winder shown in Figure 5-1b. The filaments and the assembled experimental setup are also shown in Figure 5-1c and Figure 5-1d, respectively. The conditions used for the generation of the filaments are discussed in the results and discussions section.

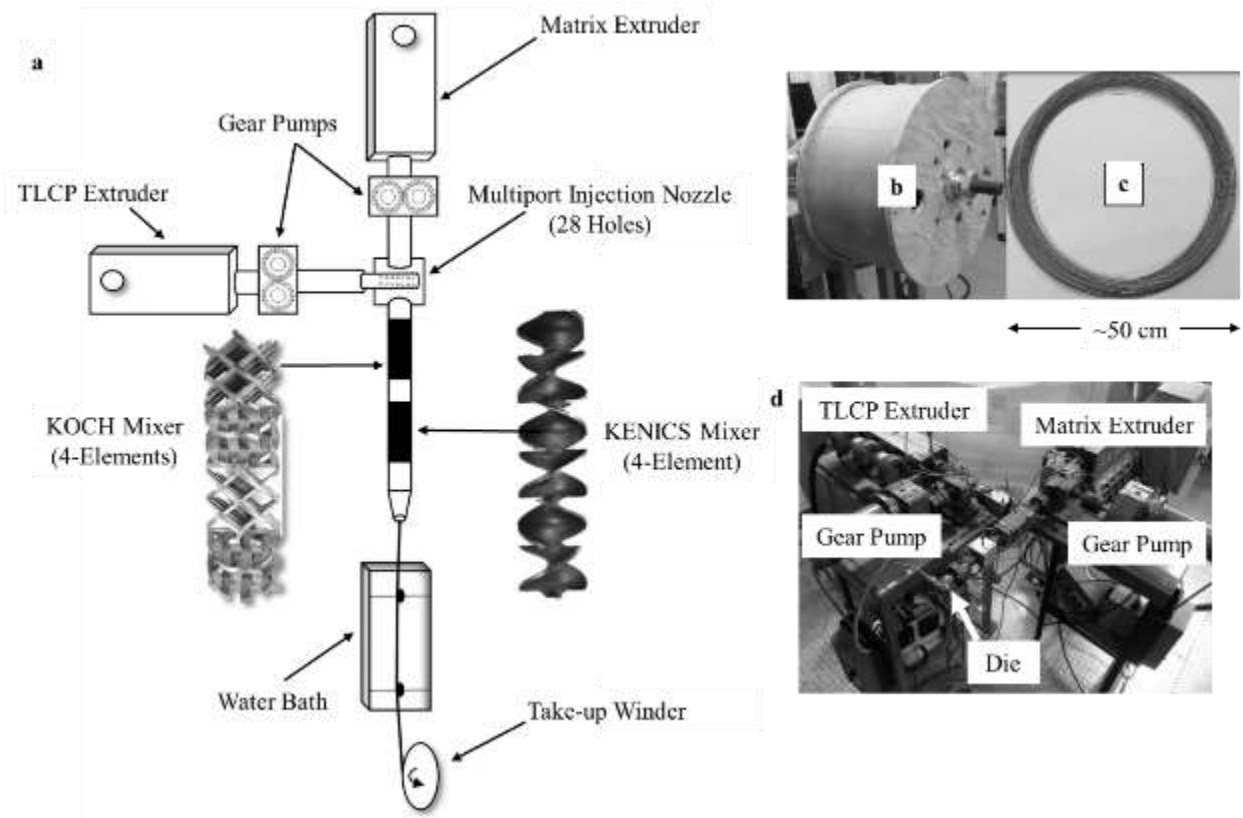

Figure 5-1: a) Schematic of dual extrusion technology, b) custom made take-up winder, c) 67.0 wt.% HX3000/PPS filaments, d) experimental setup.

5.3.4 Compression Molding

Compression molding was carried out by cutting 67.0 wt.% HX3000/PPS filaments into 76.2 mm long strands, which was the length of the mold, to take maximum advantage of the aspect ratio of the fibrils. The compression molded plaques were generated by consolidating the strands unidirectionally into 76.2 x 76.2 x 2.0 mm^3 plaques, using a Carver hot press (model: 2696). The molding temperatures used were 300, 310 and 320 ℃. Pure PPS was also compression molded at 310 ℃. The molding time and pressure used were 5 minutes and 1.7 MPa, respectively.

5.3.5 Fused Filament Fabrication (FFF)

To assess the performance of 67.0 wt.% HX3000/PPS filaments in FFF, rectangular specimens of dimensions 80.0 x 8.0 x 2.0 mm^3 were printed in a RoVa3D 5 Extruder printer (manufacturer: ORD Solutions, Canada). The specimens were printed using 0° and 90° print orientation, with each layer 0.5 mm in height and 0.6 mm in width. The printed roads overlapped by 0.1 mm and the scan speed in x, y and z directions was 1200 mm/min. The samples printed using 0° print orientation were processed at 300, 305, 310 and 315 ℃ to study the improvement in tensile properties and to identify the print temperature that leads to the maximum retention of the tensile properties of the filaments.

5.3.6 Tensile Testing

Tensile testing was performed on the filaments and the samples generated by means of compression molding, and printing using an Instron Mechanical Tester (model: 4468). The crosshead speed and the load cell used was 1 mm/minute and 5kN, respectively. The filaments were tested using 15.0 cm long strands. The compression molded plaques were cut into 8.0 mm wide rectangular specimens in the fiber alignment direction for tensile testing.

5.3.7 Scanning Electron Microscopy

The sample preparation for studying the morphology of 67.0 wt.% HX3000/PPS filaments was carried out by fracturing the filaments along their length and transverse to the length in liquid nitrogen. The fractured surfaces were sputter coated with a 5 nm thick gold layer in a Cressington 208HR Sputterer. Following sample preparation, images were taken using a field-emission scanning election microscope (model: LEO (Zeiss) 1550) with an accelerating voltage of 5 kV.

5.4 Results and Discussions

5.4.1 Selection of Processing temperatures for generating HX3000/PPS filaments

The goal of this work is to reinforce PPS with a higher melting TLCP so that the resulting composite filaments can be postprocessed at temperatures between the melting temperatures of the two components. To attain this objective, the selection of a desired TLCP is crucial and is required to exhibit its melting temperature above that of PPS. Thus, HX3000, because of its melting temperature of 330 ℃ being greater than that of PPS (melting temperature: 280 ℃), is a suitable reinforcing candidate. To select processing conditions required for filament generation, rheological tests were carried out on PPS and HX3000. The first step is to identify temperatures that lead to a stable PPS melt. Figure 5-2 shows the results of the SAOS measurements carried out isothermally at 300, 310, 320, 330 and 340 ℃ on PPS, which shows a gradual drop in the complex viscosity at each temperature. Additionally, with an increase in the test temperature, the drop in complex viscosity becomes more severe. At 300 ℃, the complex viscosity drops by around 7% from 224 to 209 Pa*s whereas at 340 ℃ it drops by around 57% from 122 to 53 Pa*s.

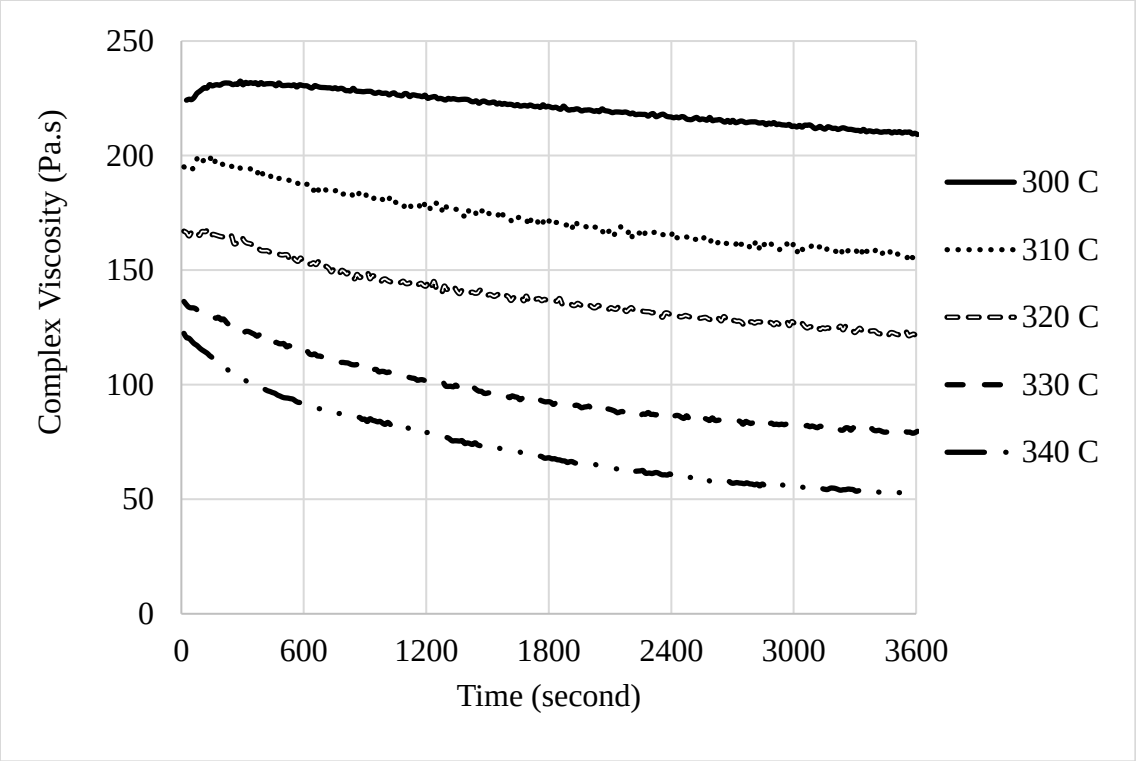

Figure 5-2: Small amplitude oscillatory tests in the isothermal mode carried out on PPS at 300, 310, 320, 330 and 340 ℃ in a nitrogen atmosphere.

Because the selection of the PPS processing temperature needs to be in accordance with HX3000 rheology, the discussion of HX3000 rheology will now follow. The processing temperatures of the TLCPs have been reported to be well above their melting temperatures due to the presence of higher melting crystallites [17, 18]. To determine the equilibration temperature of HX3000 for filament generation and for the rheological tests, shear step strain tests were carried out. Figure 5-3 shows the resulting relaxation modulus as a function of time for HX3000. The relaxation modulus curves in Figure 5-3 drop monotonically with time at 360 and 370 ℃, whereas at 340 and 350 ℃, there is an initial drop following which the property plateaus represented by the presence of tails. Done and coworkers [26] ascribed the tails in the relaxation modulus curve of TLCPs to the presence of solid structures. Based on the results of the shear step strain tests, 360

°C led to the removal of higher melting crystallites of HX3000. Therefore, 360 °C was chosen as the minimum equilibration temperature to remove residual crystallites during filament fabrication and in the rheological tests.

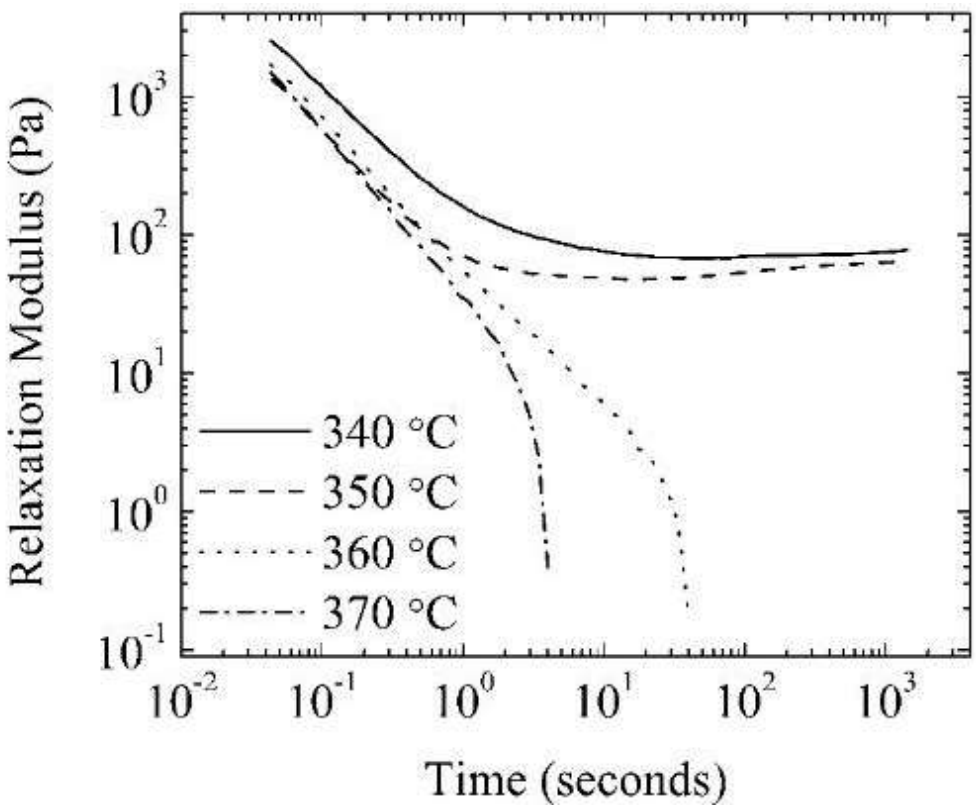

Figure 5-3: Shear step strain test results for HX3000 carried out at 340, 350, 360 and 370 °C.

Researchers have reported that the TLCPs exhibit supercooling behavior that allows for the existence of their molten state below their melting temperatures once higher melting crystallites are removed by heating [17, 27]. Because PPS does not exhibit a stable melt at elevated temperatures, the advantage of the supercooling behavior of HX3000 is taken to lower the processing temperature of HX3000 below its melting temperature. In previous studies, the extent of supercooling was identified using SAOS tests in the cooling mode [15, 25, 27-29]. Therefore,

HX3000 was subjected to SAOS tests in cooling mode after equilibrating at 360 °C, and the effect of cooling rates on the extent of supercooling was studied. Figure 5-4 shows that on cooling the HX3000 melt, its complex viscosity increases. This increase becomes more rapid as the temperature approaches lower values. Researchers have attributed this increase to the initiation of solidification [27]. From the plots in Figure 5-4, the cooling rate of 5 °C/min led to the solidification temperature of 293 °C, higher in comparison with other cooling rates that led to the solidification temperature of around 287 °C. Therefore, in all subsequent rheological tests, the cooling rate of 10 °C/min was used.

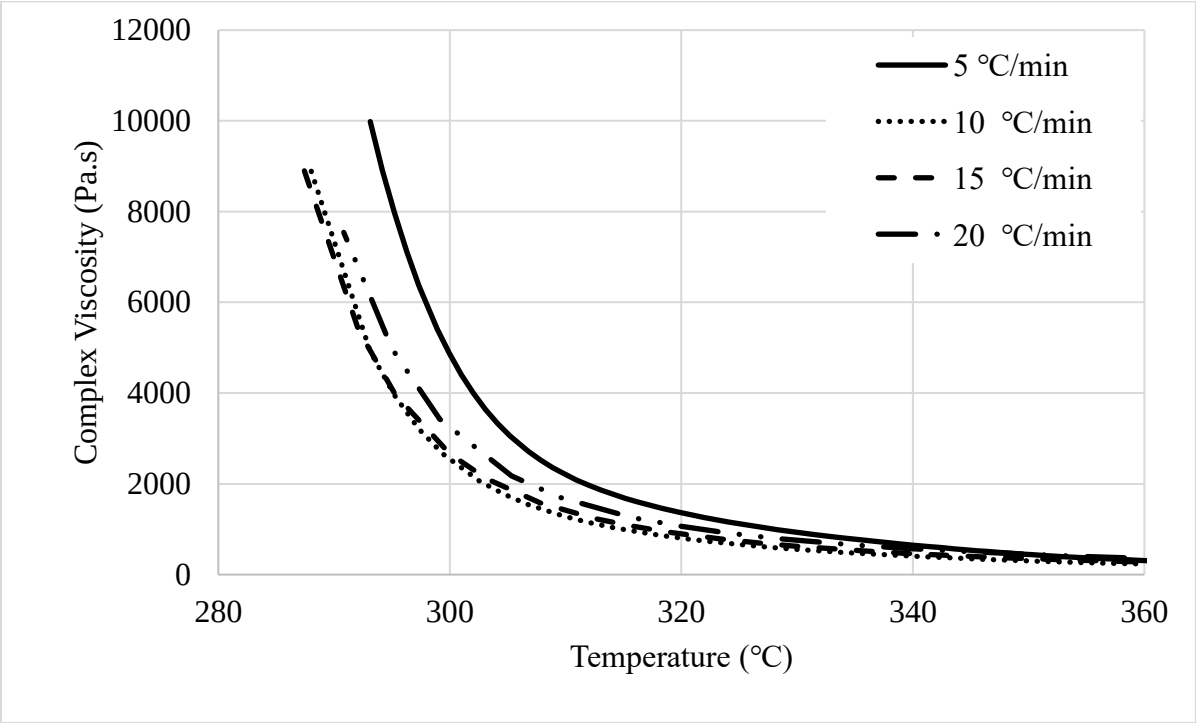

Figure 5-4: SAOS tests in cooling mode carried out on HX3000 after equilibrating at 360 °C, using cooling rates of 5, 10, 15 and 20 °C/min.

As previously discussed, HX3000 exhibits a molten state even below its melting temperature. However, the TLCPs in their supercooled state do not exhibit a stable melt at all temperatures as reported by Qian and coworkers [25]. To identify temperatures at which HX3000 exhibits a stable melt, SAOS tests under isothermal conditions were carried out at 290, 295, 300, 305 and 310 ℃ after cooling from 360 ℃ at 10 ℃/min. Figure 5-5 shows the resulting storage and loss moduli plotted as a function of time for each test temperature. Notably, at each temperature the storage modulus is lower than the loss modulus, signifying viscous behavior is dominant over the elastic behavior. The storage and loss moduli crossover in less than an hour at 290 and 295 ℃; whereas at 300 ℃ and above, the quantities do not crossover for at least an hour. Qian and coworkers [27] have attributed this crossover to the solidification of the TLCP melt. Therefore, to avoid solidification of HX3000 during processing, the temperature should be maintained above 300 ℃.

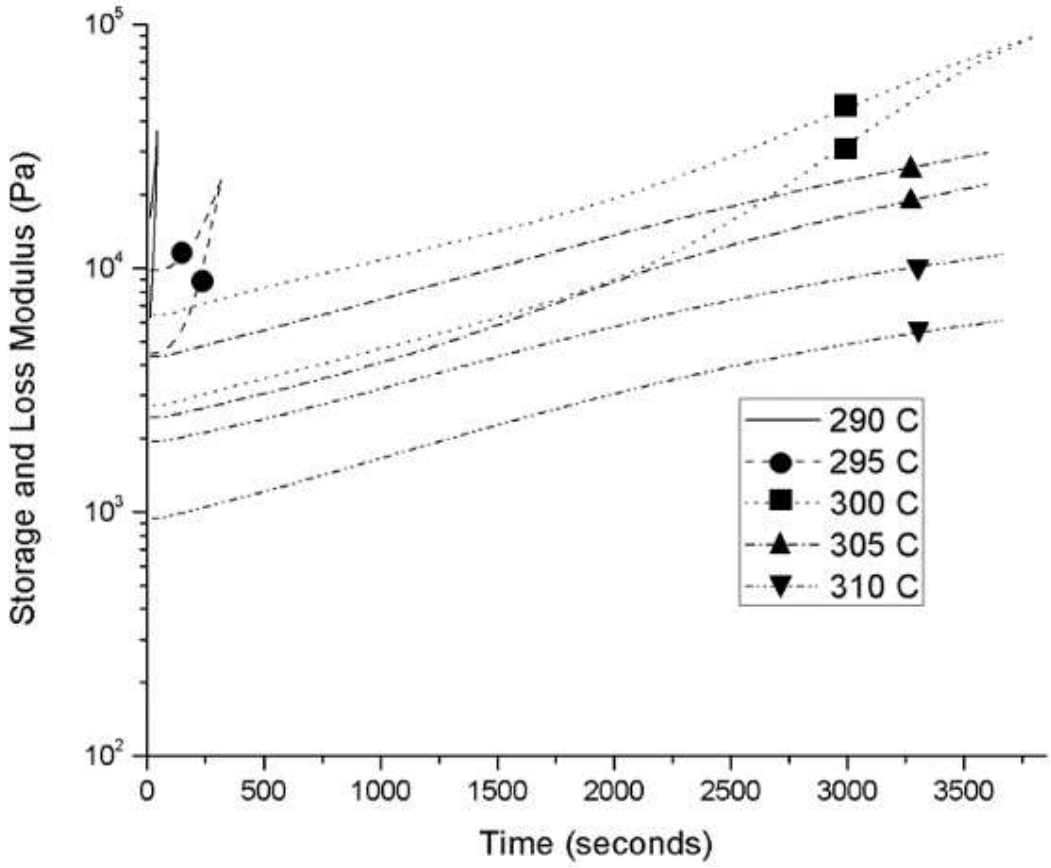

Figure 5-5: SAOS test carried out in isothermal mode at 290, 295, 300, 305 and 310 °C. The samples were equilibrated at 360 °C, followed by cooling at 10 °C/min to the test temperatures. The top curve at each temperature represents the loss modulus (G") and the bottom curve represents the storage modulus (G').

The HX3000 melt was also studied using shear step strain tests below its melting temperature to identify temperatures that lead to avoiding solid structures in the melt. Thus, HX3000 was cooled from its equilibration temperature to the test temperatures of 290, 300, 310 and 320 °C for conducting shear step strain tests. Figure 5-6 shows the resulting relaxation modulus as a function of time at each temperature. At 290 and 300 °C, the presence of tails can be observed,

signifying the presence of solid structures which may be due to the initiation of crystallization at these temperatures. Thus, processing the temperature needs to be above 300 °C to avoid premature nucleation and crystallization of the HX3000 melt.

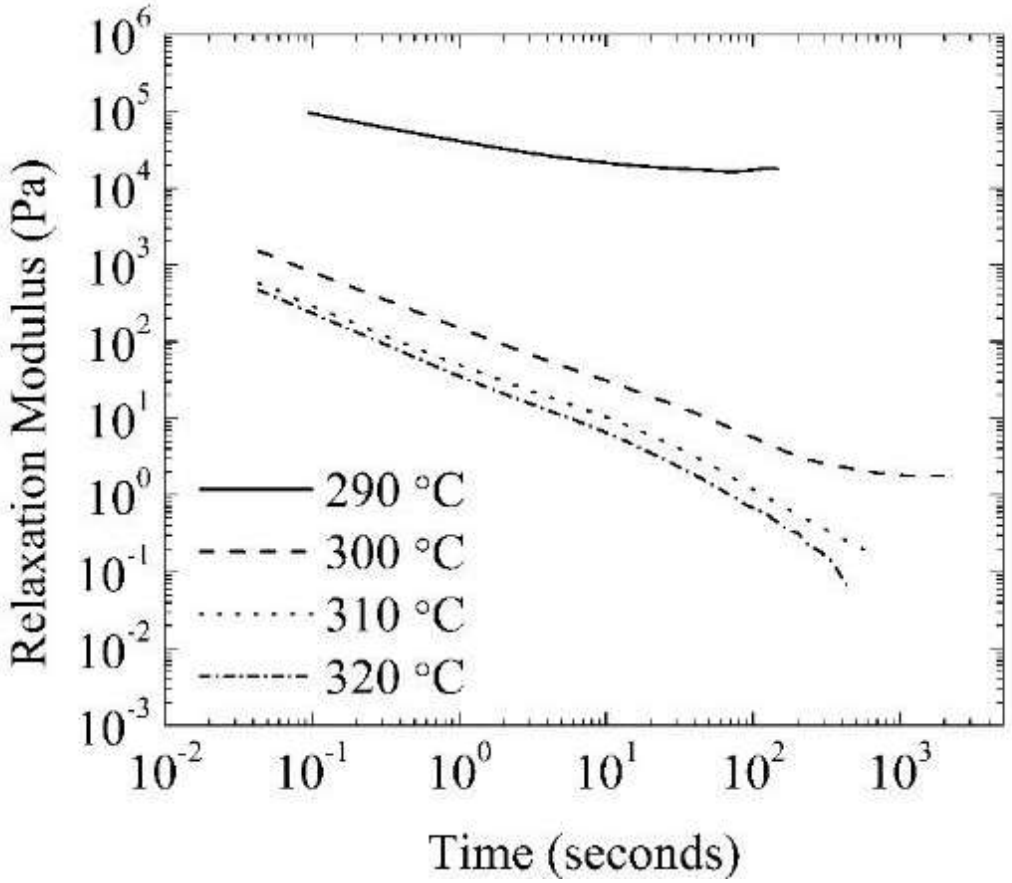

Figure 5-6: Shear step strain tests carried out on HX3000 at 290, 300, 310 and 320 °C. The samples were equilibrated at 360 °C, followed by cooling at 10 °C/min in nitrogen atmosphere.

Based on the rheology of PPS and HX3000, the processing temperatures selected for carrying out filament generation is shown by the schematic in Figure 5-7. The PPS processing temperature was selected to be 320 °C because it exhibits a relatively stable melt. From Figure 5-

2, the complex viscosity of PPS drops by 27% from 167 to 123 Pa*s in an hour, which is relatively a smaller percentage drop in comparison with the percentage drops at higher temperatures. The HX3000 processing temperature selected was 360 °C for equilibrating in the extruder, followed by decreasing the temperature to 320 °C before injecting HX3000 into PPS. This is to avoid exceeding temperatures above the temperature where PPS exhibits a stable melt and to avoid conditions that lead to the onset of solidification of HX3000. The temperature was dropped to 310 °C at the extrusion die to achieve the desired melt stability for drawing the extrudate.

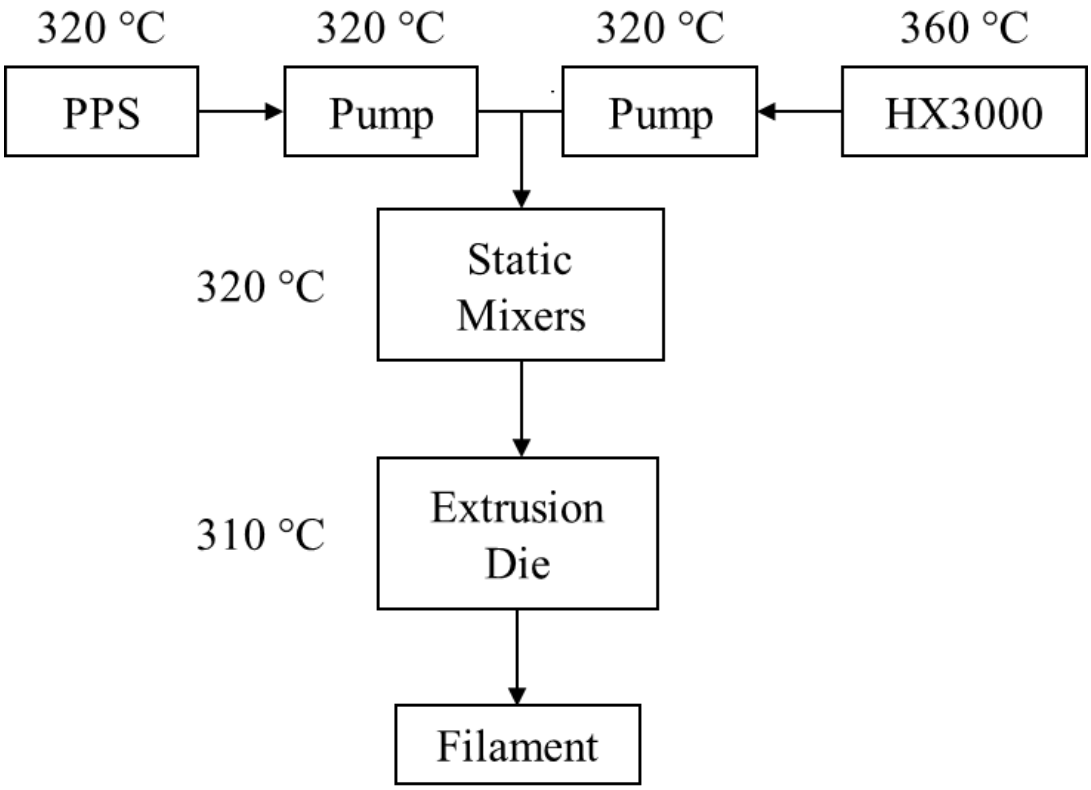

Figure 5-7: Temperature schematic used in the dual extrusion technology.

In summary, the selected processing temperature of PPS (320 °C) is below the melting temperature (330 °C) and processing temperature (360 °C) of HX3000. Therefore, processing both

components in a single extruder is not desirable. Hence, the temperature schematic represented in Figure 5-7 was used for filament generation in the dual extrusion technology that enables processing of the components by imposing separate thermal histories.

5.4.2 HX3000/PPS Filament Tensile Properties and Morphology

The composite filaments (67.0 wt.% HX3000/PPS) generated using the dual extrusion technology were subjected to tensile testing, which resulted in the tensile strength and modulus of 155.0±24.2 MPa and 40.4±7.5 GPa, respectively. The improvement in the tensile strength and modulus is around 2 and 12 times, respectively, in comparison to those of pure PPS, which exhibits a tensile strength and modulus of 80.0 MPa and 3.4 GPa, respectively (as reported by the supplier).

Table 2 shows the tensile properties reported in the literature for TLCP/PPS blends, which were generated by direct blending in a single extruder. The comparison shows that 67.0 wt.% HX3000/PPS filaments exhibit significantly improved tensile properties. This is due to the blending technology used to generate the filaments that allowed continuous injection of HX3000 into PPS. The fibrillation process in the dual extrusion technology is due to the continuous injection of 28 HX8000 streams formed by the injection nozzle followed by the striations caused by the static mixers. As the blend exits the die, the drawing process further decreases the fibril diameter, leading to high aspect ratio fibrils. Because the fibril aspect ratio and tensile properties are highly dependent on the draw ratios used during their processing, the use of higher draw ratios is desired. Krishnaswamy and coworkers [17] reported that the tensile properties plateau at draw ratios of around 100 for HX8000, which is composed of different same monomers as HX3000. As the draw ratio used for generating 67.0 wt.% HX3000/PPS filaments was only 22, the tensile properties of the filaments can potentially be improved even further using higher draw ratios.

Table 5-1: Tensile properties of TLCP/PPS composites, reported in literature.

Concentration (wt.% TLCP/PPS)		**Tensile Strength (MPa)**	**Tensile Modulus (GPa)**	**Reference**
30.0		~100.0	~6.0	[19]
50.0	uncompatibilized	96.0	5.6	[30]
	compatibilized	108.0	9.3	
90.0		158.0	8.3	[31]

The morphology of 67.0 wt.% HX3000/PPS filaments was studied to understand the effect of HX3000 fibril morphology on the printing performance and the tensile properties of the filaments. Figure 5-8a shows the cross section of the filaments along the filament length, which shows nearly continuous reinforcement, represented by fibrils that are highly aligned along the filament length and nearly uniformly distributed across the cross section. Moreover, the diameter of the fibrils is on the order of a micron. Figure 5-8b shows a single HX3000 fibril which is less than a micron in diameter, which is an order in magnitude lower than that of carbon and glass fiber [32]. The lower fibril diameter can potentially reduce the roughness of the printed surfaces.

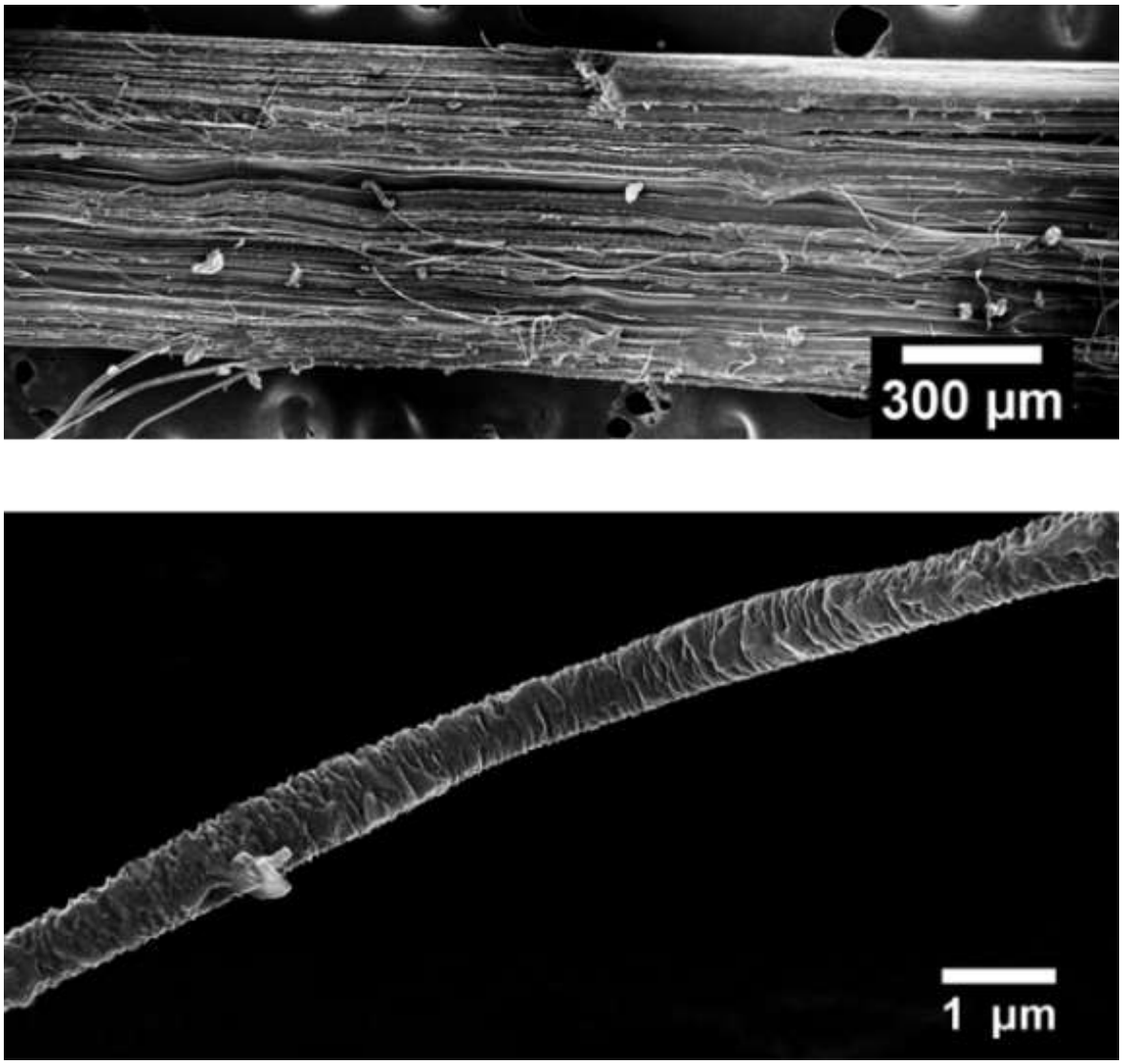

Figure 5-8: Cross section of 67.0 wt.% HX3000/PPS filament in the filament's length direction (top) and a single HX3000 fibril (bottom).

The filament morphology was also studied perpendicular to the filament length, which is shown in Figure 5-9. The image shows a uniform distribution of the fibrils and fibril pull-outs (represented by the holes). Although the distribution is uniform, gaps can be seen around the fibrils in the image, signifying poor matrix-fiber interaction. It is important to have a good interaction

between the matrix and the fibril to transfer the load from the matrix to the fibril when the composite is subjected to a load. This issue may be addressed by using compatibilizers to promote interactions between the matrix and the fibrils. Effort has been made in the past to improve PPS-TLCP interactions using compatibilizers to improve the tensile properties. Gopakumar and coworkers [30] compatibilized PPS-TLCP blends with dicarboxyl-terminated PPS in a co-rotating twin screw extruder and found that the tensile strength and modulus of 50.0 wt.% TLCP/PPS increased from 96.0 MPa and 5.6 GPa, respectively, to 108 MPa and 9.3 GPa, respectively. Therefore, an approach for improvement in the tensile properties exists by exploring the use of compatibilizers.

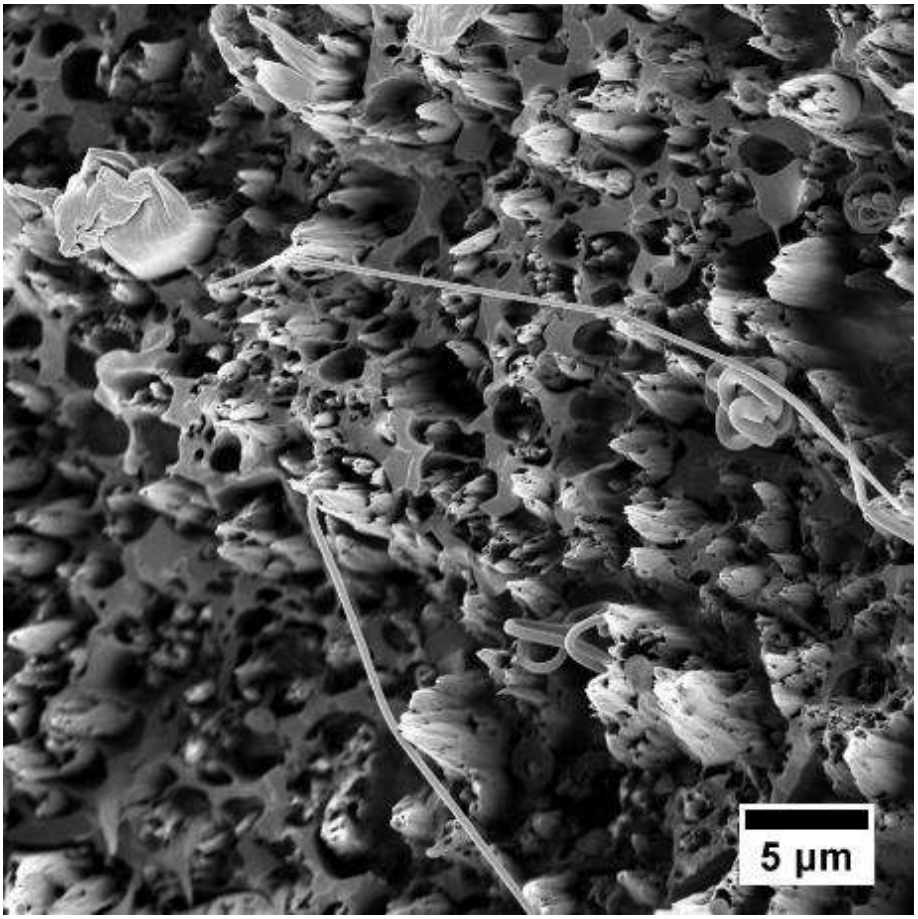

Figure 5-9: SEM image of the filament cross section perpendicular to the filament length.

5.4.3 Identification of the Postprocessing Temperature of HX3000/PPS Filaments

The composite filaments generated using the dual extrusion technology are intended for processing carbon and glass fiber reinforced composites. To keep the TLCP reinforcement in solid state during processing, the postprocessing temperatures should be below the melting temperature of HX3000 (330 °C). Therefore, compression molding of 67.0 wt.% HX3000/PPS was carried out at 300, 310 and 320 °C. The tensile strength and modulus that resulted from tensile testing in the fiber alignment direction at each temperature are shown in Figure 5-10. The maximum tensile strength and modulus were obtained at the lowest temperature and were found to be 92.7±12.5 MPa and 26.3±3.4 GPa, respectively. Compression molding pure PPS resulted in the tensile strength and modulus of 75.3±0.4 MPa and 3.5±0.1 GPa, respectively. Therefore, the lowest compression molding temperature led to the improvement in the tensile strength as well as modulus with respect to pure PPS. The improvement in tensile strength is lower than the tensile modulus, probably due to poor fiber wetting as explained earlier.

The tensile properties of the compression molded specimens decrease with increase in the postprocessing temperature, as shown in Figure 5-10. Researchers have associated the drop in the tensile properties on postprocessing the TLCP/matrix composites to the orientation relaxation and fiber breakage [16, 18]. Therefore, to minimize loss in the properties on postprocessing, the temperatures should be kept as low as possible. The lowest postprocessing temperature is limited by the melting temperature of the matrix polymer and the highest temperature is limited by the temperature that leads to minimum TLCP orientation relaxation.

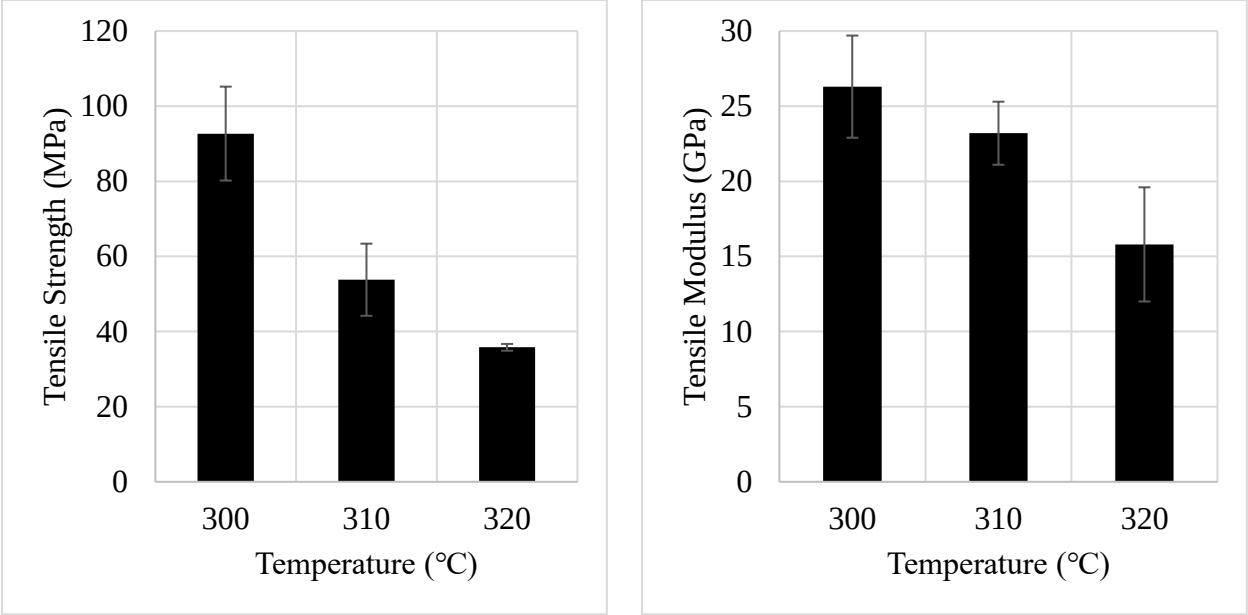

Figure 5-10: Tensile strength (left) and modulus (right) of unidirectionally compression molded specimens in the fiber alignment direction as a function of molding temperature.

5.4.4 Performance of HX3000/PPS Filaments in FFF

The performance of 67.0 wt.% HX3000/PPS filaments in FFF was assessed by printing specimens as shown in Figure 5-11. The tool paths chosen were to assess if the printer can take sharp turns on processing nearly continuously reinforced HX3000/PPS filaments. Figure 5-11 also shows the rectangular specimens that were successfully printed with 67.0 wt.% HX3000/PPS filaments using 0° and 180° print orientations. It was found that the continuous nature of the reinforcement did not prevent the printer from taking 180° turns. Contrarily, researchers have reported that the stiffness of continuous carbon fiber reinforcement does not allow sharp turns of the printers [21, 23, 33]. In addition, the use of continuous carbon fiber demands modifications of the printer to allow impregnation of the fibers in the printed parts [21-23, 33, 34]. Therefore, the tunable flexibility of the thermoplastic HX3000 fibrils enables printing HX3000/PPS filaments

like pure matrices such that the printer mobility is not restricted due to the reinforcement. This advantage avoids any printer modification as the fibers are embedded in the filament itself, and it is not required to separately impregnate the fiber bundles, unlike continuous carbon/glass/Kevlar fiber. This alleviates poor fiber-matrix adhesion as well, which otherwise is an issue when fibers are separately impregnated [23, 33]. The higher loading of TLCP-reinforcement was successfully printed with minimal nozzle clogging issues. The is due to high alignment of the fibrils along the length of the filaments. Contrarily, Tekinalp and coworkers [10] reported significant nozzle clogging issues on printing with 40.0 wt.% short carbon fiber/ABS filaments, probably due to the random fiber orientation and fiber bridging at the nozzle entrance. Moreover, the combined effect of highly aligned and small diameter of HX3000 fibrils led to smoother print surfaces, as shown in Figure 5-11.

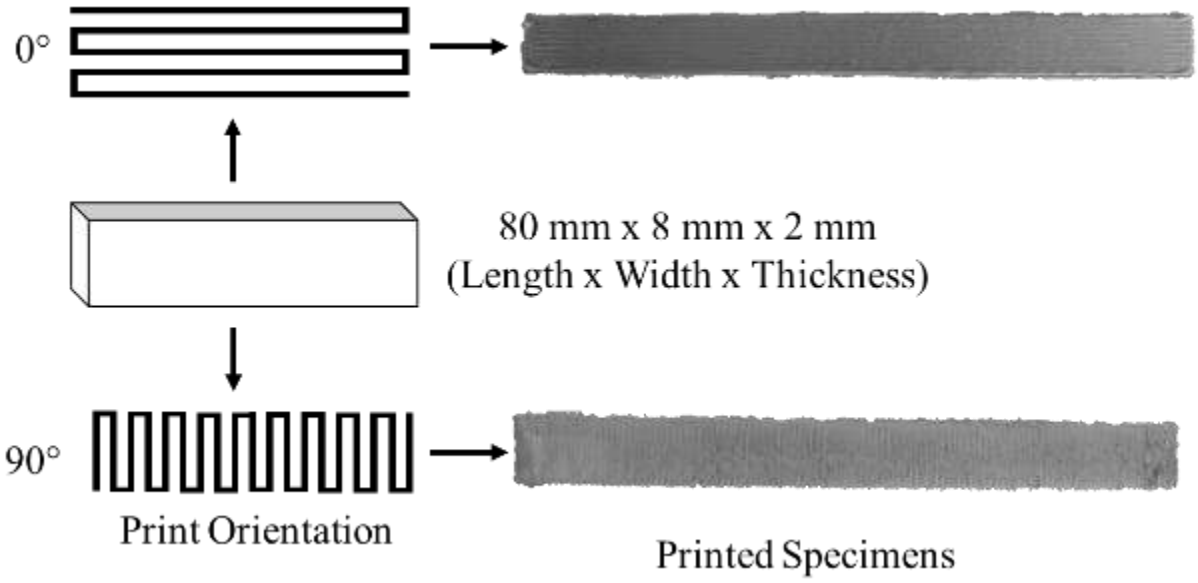

Figure 5-11: Parts printed using 67.0 wt.% HX3000/PPS using 0° and 90° print orientation.

Figure 5-12 shows the tensile properties of the specimens printed using 67.0 wt.% HX3000/PPS filaments. These properties shown in the figure are in the print direction, i.e. 0º print orientation. A significant improvement is noticeable at all print temperatures in comparison with the parts printed using pure PPS that exhibited the tensile strength and modulus of only 45.0±6.0 MPa and 3.5±0.6 GPa, respectively. As previously discussed, the tensile properties are maximum at the lowest print temperature, i.e. 300 °C. The maximum tensile strength and modulus obtained on using the print temperature of 300 °C are 108.5±19.4 MPa and 25.9±1.1 GPa, respectively. On comparing these properties with the maximum properties obtained on compression molding, the properties obtained on using FFF are higher. This may be due to a combined effect of misalignment of the strands during compression molding, longer residence time at elevated temperatures in compression molding that leads to orientation relaxation, and fiber breakage during strand consolidation. In addition, with an increase in the print temperature, a decrease in tensile properties is observed, which is believed to be primarily due to orientation relaxation of the fibrils.

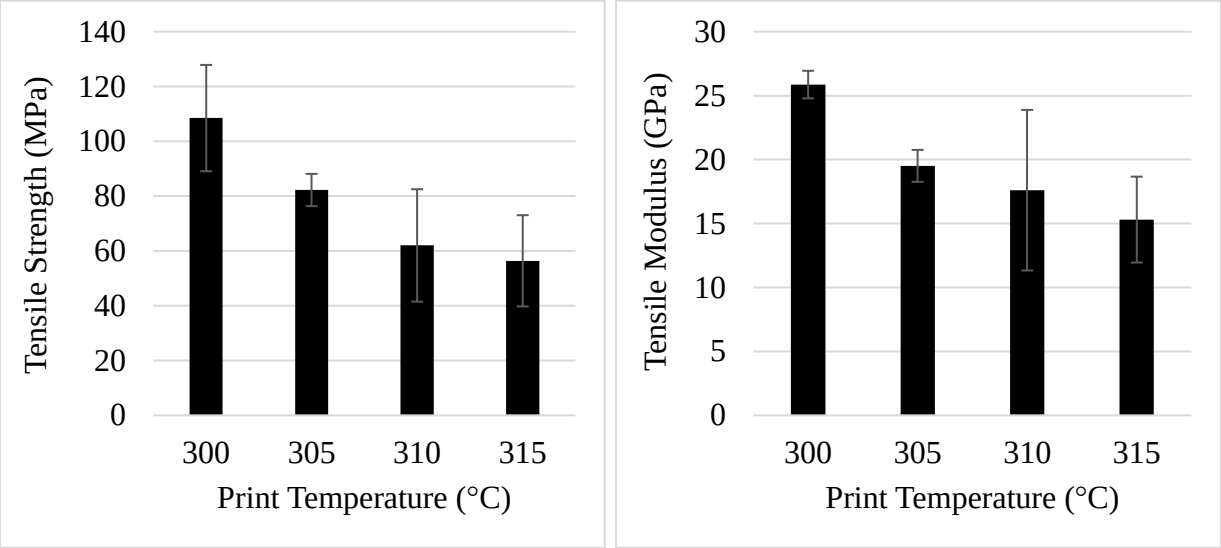

Figure 5-12: Tensile strength (left) and modulus (right) of the parts printed using 67.0 wt. HX3000/PPS filaments in the print direction at different print temperatures.

A comparison of the properties obtained on printing with 67.0 wt.% HX3000/PPS filaments with the reported use of PPS and its composites demonstrates significantly improved tensile properties. For example, Geng et al. [13] reported a maximum tensile strength and modulus of 57.1 MPa and 3.1 GPa, respectively. Similarly, Fitzharris and coworkers [35] reported a tensile strength and modulus of 61.1±3.3 MPa and 2.2±0.1 GPa, respectively, on printing with pure PPS. The reported use of the composites of PPS in LFAM also led to lower tensile properties in comparison with the unidirectionally printed 67.0 wt.% HX3000/PPS specimens. For example, Hassen et al. [5] reported that the use of 50.0 wt.% CF/PPS in LFAM for printing in-autoclave tools resulted in the tensile strength of only 74.0±1.6 MPa, which is only 68% of the tensile strength obtained on printing with 67.0 wt.% HX3000/PPS filaments.

In comparison with the tensile properties of short fiber printed composites, researchers have reported higher tensile properties on using continuously reinforced polymers [18, 21-23, 32, 34, 36, 37]. The continuous carbon/glass, or Kevlar fibers are processed using a commercially available modified printer that enables impregnation of the fibers during printing. Dickson et al. [21] reported tensile strength and modulus values of 212.0±5.0 MPa and 4.9±0.4 GPa, respectively, on printing with continuous carbon fiber/nylon 6. Similarly, Matsuzaki and coworkers [22] used continuous carbon fiber and PLA and reported a tensile strength and modulus of 185.2±24.6 MPa and 19.5±2.1 GPa, respectively. A comparison with commonly used matrices reinforced with short fiber demonstrates superior properties of parts printed with continuous fibers. For example, Tekinalp and coworkers [10] reported a maximum tensile strength and modulus of around 67.0 MPa and 14.0 GPa, respectively, on using 40.0 wt.% carbon fiber/ABS. Although the tensile strength of the parts printed with 67.0 wt.% HX3000/PPS are lower than those obtained using continuous fibers, the tensile modulus is higher than the reported values using continuous

fibers. Moreover, the tensile properties obtained on using HX3000/PPS filaments are higher than those of the short fiber reinforced printed specimens. Therefore, the use of HX3000 reinforced PPS is a viable solution for extending the application of FFF to printed parts that require superior properties.

5.5 Conclusions

The need for novel composites for use in FFF was addressed by reinforcing a high performance matrix, PPS, with a higher melting thermotropic liquid crystalline polymer, HX3000. Due to non-overlapping processing conditions, the temperatures selected using rheology led to a successful generation of 67.0 wt.% HX3000/PPS filaments using a dual extrusion technology. The filament tensile strength and modulus improved by 2 and 12 times to 155.0±24.2 MPa and 40.4±7.5 GPa, respectively, in comparison with pure PPS. The postprocessing temperatures determined using compression molding led to attaining the highest tensile properties in the print direction of the printed parts. Subsequently, the maximum tensile strength and modulus obtained following postprocessing at 300 °C were 108.5±19.4 MPa and 25.9±1.1 GPa, respectively. Additionally, on postprocessing the filaments in FFF, matrix-like printing performance was obtained as the printer mobility was not restricted due to a nearly continuous reinforcement. Therefore, printer modification was not required to enable, unlike on processing continuous carbon fiber in the printers [21-23, 33]. A comparison of the tensile properties of the printed parts showed significantly better performance than obtained on compression molding as FFF enabled taking maximum advantage of the aspect ratios and the high fibril orientation. Moreover, the tensile properties obtained were higher than the reported use of the short fiber reinforced composites. The tensile modulus on using 67.0 wt.% HX3000/PPS also resulted in higher tensile modulus values in comparison with the reported use of continuous fibers, whereas the tensile strength was lower.

In conclusion, HX3000 reinforced PPS led to printing stronger specimens without requiring any printer modifications.

References

[1] M.A. Waller, S.E. Fawcett, Click here for a data scientist: Big data, predictive analytics, and theory development in the era of a maker movement supply chain, Journal of Business Logistics 34(4) (2013) 249-252.

[2] R. d'Aveni, The 3-D printing revolution, Harvard Business Review 93(5) (2015) 40-48.

[3] I. Gibson, D.W. Rosen, B. Stucker, Additive manufacturing technologies: rapid prototyping to direct digital manufacturing, Springer Publishing Company, Incorporated2009.

[4] B. Lyons, Additive manufacturing in aerospace: Examples and research outlook, The Bridge 44(3) (2014).

[5] A.A. Hassen, J. Lindahl, X. Chen, B. Post, L. Love, V. Kunc, Additive manufacturing of composite tooling using high temperature thermoplastic materials, SAMPE Conference Proceedings, Long Beach, CA, May, 2016, pp. 23-26.

[6] V. Kunc, R.B. Dinwiddie, B.K. Post, L.J. Love, C. Duty, M. Matlack, R. Fahey Jr, A.A. Hassen, Investigation of In-autoclave Additive Manufacturing Composite Tooling.

[7] F. Ning, W. Cong, J. Qiu, J. Wei, S. Wang, Additive manufacturing of carbon fiber reinforced thermoplastic composites using fused deposition modeling, Composites Part B: Engineering 80 (2015) 369-378.

[8] V. Kishore, X. Chen, C. Ajinjeru, A.A. Hassen, J.M. Lindahl, J. Failla, V. Kunc, C.E. Duty, Additive manufacturing of high performance semicrystalline thermoplastics and their composites, Oak Ridge National Lab.(ORNL), Oak Ridge, TN (United States), 2016.

[9] M. Chapiro, Current achievements and future outlook for composites in 3D printing, Reinforced Plastics 60(6) (2016) 372-375.

[10] H.L. Tekinalp, V. Kunc, G.M. Velez-Garcia, C.E. Duty, L.J. Love, A.K. Naskar, C.A. Blue, S. Ozcan, Highly oriented carbon fiber–polymer composites via additive manufacturing, Composites Science and Technology 105 (2014) 144-150.

[11] V. Kishore, C. Ajinjeru, C.E. Duty, A.A. Hassen, J.M. Lindahl, P. Liu, V. Kunc, Rheological Characteristics of Fiber Reinforced Poly (ether ketone ketone)(PEKK) for Melt Extrusion Additive Manufacturing, Oak Ridge National Lab.(ORNL), Oak Ridge, TN (United States), 2017.

[12] R. Stewart, Lightweighting the automotive market, Reinforced plastics 53(2) (2009) 14-21.

[13] P. Geng, J. Zhao, W. Wu, Y. Wang, B. Wang, S. Wang, G. Li, Effect of Thermal Processing and Heat Treatment Condition on 3D Printing PPS Properties, Polymers 10(8) (2018) 875.

[14] A. Handlos, D. Baird, Processing and associated properties of in situ composites based on thermotropic liquid crystalline polymers and thermoplastics, Journal of Macromolecular Science, Part C: Polymer Reviews 35(2) (1995) 183-238.

[15] M. McLeod, D. Baird, The crystallization behavior of blends of thermotropic liquid crystalline polymers, Polymer 40(13) (1999) 3743-3752.

[16] M.A. McLeod, D.G. Baird, The influence of processing variables on the mechanical properties of injection molded pregenerated microcomposites, Composites Part B: Engineering 30(3) (1999) 297-308.

[17] R.K. Krishnaswamy, D.G. Baird, Wholly thermoplastic composites from woven preforms based on nylon-11 fibers reinforced in situ with a hydroquinone-based liquid crystalline polyester, Polymer composites 18(4) (1997) 526-538.

[18] R.W. Gray IV, D.G. Baird, J.H. Bøhn, Effects of processing conditions on short TLCP fiber reinforced FDM parts, 4(1) (1998) 14-25.

[19] M.T. Heino, J.V. Seppälä, Extruded blends of a thermotropic liquid crystalline polymer with polyethylene terephthalate, polypropylene, and polyphenylene sulfide, Journal of applied polymer science 44(12) (1992) 2185-2195.

[20] J. Seppälä, M. Heino, C. Kapanen, Injection-moulded blends of a thermotropic liquid crystalline polymer with polyethylene terephthalate, polypropylene, and polyphenylene sulfide, Journal of applied polymer science 44(6) (1992) 1051-1060.

[21] A.N. Dickson, J.N. Barry, K.A. McDonnell, D.P. Dowling, Fabrication of continuous carbon, glass and Kevlar fibre reinforced polymer composites using additive manufacturing, Additive Manufacturing 16 (2017) 146-152.

[22] R. Matsuzaki, M. Ueda, M. Namiki, T.-K. Jeong, H. Asahara, K. Horiguchi, T. Nakamura, A. Todoroki, Y. Hirano, Three-dimensional printing of continuous-fiber composites by in-nozzle impregnation, Scientific reports 6 (2016) 23058.

[23] F. Van Der Klift, Y. Koga, A. Todoroki, M. Ueda, Y. Hirano, R. Matsuzaki, 3D printing of continuous carbon fibre reinforced thermo-plastic (CFRTP) tensile test specimens, Open Journal of Composite Materials 6(01) (2015) 18.

[24] D.G. Baird, A. Sukhadia, Mixing process for generating in-situ reinforced thermoplastics, U.S. Patent, 5225488, 1991.

[25] C. Qian, G. Wan, C.E. Frazier, D.G. Baird, Isothermal crystallization of blends containing two thermotropic liquid crystalline polymers, Materials Today Communications 9 (2016) 16-21.

[26] D. Done, D.G. Baird, Transient flow of thermotropic liquid crystalline polymers in step strain experiments, Journal of Rheology 34(5) (1990) 749-762.

[27] C. Qian, D.G. Baird, The transient shear rheology of a thermotropic liquid crystalline polymer in the super-cooled state, Polymer 102 (2016) 63-72.

[28] M. McLeod, D. Baird, Modification of the processing window of a thermotropic liquid crystalline polymer by blending with another thermotropic liquid crystalline polymer, Journal of applied polymer science 73(11) (1999) 2209-2218.

[29] C. Qian, C. Mansfield, D. Baird, Extrusion Blow Molding of Polymeric Blends Based on Thermotropic Liquid Crystalline Polymer and High Density Polyethylene, International Polymer Processing 32(1) (2017) 112-120.

[30] T. Gopakumar, S. Ponrathnam, A. Lele, C. Rajan, A. Fradet, In situ compatibilisation of poly (phenylene sulphide)/wholly aromatic thermotropic liquid crystalline polymer blends by reactive extrusion: morphology, thermal and mechanical properties, Polymer 40(2) (1999) 357-364.

[31] P. Subramanian, A. Isayev, Blends of a thermotropic liquid-crystal polyester with poly (phenylene sulphide), Polymer 32(11) (1991) 1961-1969.

[32] S.-Y. Fu, B. Lauke, E. Mäder, C.-Y. Yue, X. Hu, Tensile properties of short-glass-fiber-and short-carbon-fiber-reinforced polypropylene composites, Composites Part A: Applied Science and Manufacturing 31(10) (2000) 1117-1125.

[33] N. Li, Y. Li, S. Liu, Rapid prototyping of continuous carbon fiber reinforced polylactic acid composites by 3D printing, Journal of Materials Processing Technology 238 (2016) 218-225.

[34] G.W. Melenka, B.K. Cheung, J.S. Schofield, M.R. Dawson, J.P. Carey, Evaluation and prediction of the tensile properties of continuous fiber-reinforced 3D printed structures, Composite Structures 153 (2016) 866-875.

[35] E.R. Fitzharris, I. Watt, D.W. Rosen, M.L. Shofner, Interlayer bonding improvement of material extrusion parts with polyphenylene sulfide using the Taguchi method, Additive Manufacturing 24 (2018) 287-297.

[36] P.J. Hine, H.R. Lusti, A.A. Gusev, Numerical simulation of the effects of volume fraction, aspect ratio and fibre length distribution on the elastic and thermoelastic properties of short fibre composites, Composites science and technology 62(10-11) (2002) 1445-1453.

[37] W. Zhong, F. Li, Z. Zhang, L. Song, Z. Li, Short fiber reinforced composites for fused deposition modeling, Materials Science and Engineering: A 301(2) (2001) 125-130.

6 Conclusions and Recommendations

Chapter 6: Conclusions and Recommendations

6.1 Conclusions

The following are the overall conclusions that stem from the work discussed in Chapter 3, Chapter 4 and Chapter 5.

Objective 1: Establish a method of selection of TLCP's and processing conditions for reinforcing acrylonitrile butadiene styrene (ABS) and polyphenylene sulfide (PPS) using the dual extrusion technology for use in Fused Filament Fabrication (FFF).

Conclusion: The work discussed in the Chapter 3 and Chapter 5 demonstrates a method of selection of thermotropic liquid crystalline polymers (TLCPs) and the processing temperatures for reinforcing lower melting matrices, ABS and PPS, with higher melting TLCPs. Small amplitude oscillatory shear tests (SAOS) carried out isothermally on the matrices determined the melt stability at different temperatures. To avoid exceeding temperatures at which the matrices do not exhibit a stable melt and to generate a nearly continuous TLCP-reinforcement, the blend temperatures were determined using rheology for use in the dual extrusion technology. SAOS tests in cooling mode and in isothermal conditions below the TLCP-melting temperature determined the extent of supercooling and the melt stability, respectively. The composite filaments generated contained nearly continuous TLCP fibrils that were an order in magnitude smaller in diameter than those of the traditionally used carbon and glass fiber.

Objective 2: Identify a procedure for the selection of the printing temperatures of the TLCP-reinforced filaments to retain their optimum tensile properties.

Conclusion: The filaments generated were reinforced using TLCPs of higher melting temperatures in comparison with the intended postprocessing temperatures of the filaments in order to process

them as a solid-filled composite, similar to carbon and glass fiber. Therefore, the postprocessing temperatures were determined using compression molding and a dynamic mechanical analysis (DMA) test. It was found that the tensile properties were retained to the maximum extent when the exposure temperature of the composites were the lowest. As the temperatures were increased, a drop in the tensile properties was reported, primarily due to orientation relaxation of the TLCPs and fiber breakage. Moreover, the use of the DMA test on pure TLCP for the identification of the postprocessing temperatures, discussed in Chapter 3, predicted the conditions that lead to a drop in the storage modulus. With an increase in the exposure time and temperature, a drop in the storage modulus was reported.

Objective 3: Using the conditions determined in Objective 2, determine the performance (printing characteristics and tensile properties) of the printed specimens using TLCP/ABS and TLCP/PPS filaments.

Conclusion: ABS and PPS filaments reinforced with TLCPs were successfully postprocessed in FFF to print basic rectangular specimens. A significant improvement in the tensile properties of the printed specimens in the print direction was reported in Chapter 4 and Chapter 5. The maximum tensile strength and modulus obtained on printing with 40.0 wt.% HX8000/ABS filaments was found to be 74.9±2.4 MPa and 16.5±0.8 GPa, respectively, at the print temperature of 260 ℃. Additionally, 67.0 wt.% HX3000/PPS resulted in the tensile strength and modulus of 108.5±19.4 MPa and 25.9±1.1 GPa, respectively, at the print temperature of 300 ℃. In both cases, the properties obtained were a maximum at temperatures lower than the melting temperatures of the respective TLCPs. As the print temperatures increased a drop in tensile properties were observed, which was speculated to be due to orientation relaxation of the TLCP phase. Moreover, the printer was able to take sharp turns despite having a nearly continuous reinforcement due to the flexibility

of the TLCP fibrils at elevated temperatures. On contrary, in Chapter 4, the use of continuous carbon fiber demonstrated the inability to print regions that required sharp turns due to fiber stiffness.

6.2 Recommendations

The following recommendations are recommended to direct future research in the development of thermotropic liquid crystalline polymer reinforced filaments for use in fused filament fabrication:

1. The draw ratios used for the generation of TLCP reinforced filaments were significantly lower due to equipment limitations. For examples, 40.0 wt.% HX8000/ABS filaments were generated using a draw ratio of only 35 and 67.0 wt.% HX3000/PPS filaments were generated using a draw ratio of only 22. The research carried out by the past researchers reported the dependence of the tensile properties on the draw ratio [1, 2]. Krisnaswamy et al. [1] reported that the tensile properties of HX8000 reach its maximum at a draw ratio of around 75. Therefore, the use of a take-up winder that is capable of imparting higher draw ratios during filament generation is highly encouraged.
2. The injection nozzle used to inject the TLCP stream into ABS and PPS had only 28 holes. To obtain increased number of fibrils in the composite filament, the use of a higher number of holes should be used. Moreover, a study of reduction in the diameter of the injection nozzle hole diameter should also be carried out to decrease the fibril diameter even further.
3. In Chapter 4, the properties of the printed specimens were lower at the lowest print temperatures. It was speculated that the fibrils are stiffer at lower temperatures that lead to fiber breakage due to a change in direction during material deposition. To minimize the

severity of the change in the angle during deposition, the use of 6-axis printers is highly encouraged to minimize fiber breakage.

4. The SEM images of the filaments performed on the cross section of the filaments (Figure 4-3 and Figure 5-9) indicate presence of gaps around the TLCP fibrils. This is due to the poor interaction of the matrix with the TLCP fibrils. To improve such interactions, compatibilizers may be chosen to improve the tensile properties of the filaments even further.
5. Lastly, the method of reinforcing filaments may be extended to include other commonly used matrices, such as PLA and PC. The method may also be extended to include high performance matrices, such as PEEK and PEKK. A detailed procedure for reinforcing the filaments is summarized in section 6.3.

6.3 Generalized Procedure for using TLCP-Reinforced Filaments in FFF

Chapters 3-5 detail the generation of filaments reinforced with TLCPs and their processing in FFF. The procedures have been demonstrated using an amorphous matrix (ABS) and a semicrystalline matrix (PPS). Based on these case studies, a generalized procedure is summarized below to reinforce any matrix for use in FFF:

1. Identify the degradation conditions for the matrix. A combination of thermogravimetric analysis and rheological tests can be used to obtain degradation temperatures.
2. Using DSC, determine the melting temperature of TLCPs.
3. Select the TLCPs that exhibit their melting temperatures well above the processing temperatures of the matrix polymer.

4. Conduct shear step strain tests on the chosen TLCPs to determine temperatures that remove all residual crystallites. The temperatures determined are the equilibration temperatures of TLCPs.
5. Conduct SAOS test in cooling mode by cooling the TLCPs from their equilibration temperatures, determined in step 4. By tracking storage and loss modulus, determine the solidification temperatures of the TLCPs.
6. Based on the temperatures determined in step 5, select the TLCP that exhibits its solidification temperature below to the degradation temperature of the matrix polymer.
7. Study the stability of the TLCP melt below its melting temperature to determine conditions that lead to a stable melt. This can be done by cooling the TLCP from its equilibration temperature to the test temperatures and conducting SAOS tests under isothermal conditions.
8. Choose conditions for filament generation using the tests discussed above. The temperatures are for use in dual extrusion technology. The TLCP is equilibrated in one extruder at its equilibration temperature, determined in step 4. The TLCP is then cooled to a temperature below its melting temperature, where the melt is stable, determined using step 7. The blend is maintained at temperatures where the matrix does not degrade and TLCP melt is stable.
9. After the filaments are generated, postprocessing temperatures are determined to process the filaments in FFF. The temperatures are determined using DMA method (discussed in chapter 3), and compression molding method (discussed in chapters 4 and 5). The criteria for the selection of temperature is to avoid melting the TLCP reinforcement, minimize orientation relaxation of the TLCP phase and induce fiber flexibility to allow the printer to take sharp turns during material deposition. The filaments may be printed at multiple temperatures

below the TLCP melting temperature to determine conditions that lead to avoiding fiber breakage during printing process.

References:

[1] R.K. Krishnaswamy, D.G. Baird, Wholly thermoplastic composites from woven preforms based on nylon-11 fibers reinforced in situ with a hydroquinone-based liquid crystalline polyester, Polymer composites 18(4) (1997) 526-538.

[2] A. Handlos, D. Baird, Processing and associated properties of in situ composites based on thermotropic liquid crystalline polymers and thermoplastics, Journal of Macromolecular Science, Part C: Polymer Reviews 35(2) (1995) 183-238.

[3] A.A. Hassen, J. Lindahl, X. Chen, B. Post, L. Love, V. Kunc, Additive manufacturing of composite tooling using high temperature thermoplastic materials, SAMPE Conference Proceedings, Long Beach, CA, May, 2016, pp. 23-26.

[4] V. Kunc, R.B. Dinwiddie, B.K. Post, L.J. Love, C. Duty, M. Matlack, R. Fahey Jr, A.A. Hassen, Investigation of In-autoclave Additive Manufacturing Composite Tooling.

Appendix A: Recyclable Composites Based on Polymers Reinforced with Thermotropic Liquid Crystalline Polymers

Mubashir Q. Ansari[1], Craig D. Mansfield[1], Tianran Chen[2], Donald G. Baird[1,2]

[1]Department of Chemical Engineering, Virginia Tech, Blacksburg, VA 24061-0211, USA

[2]Macromolecules Innovation Institute, Virginia Tech, Blacksburg, VA 24061-0201, USA

Abstract

In this work, wholly thermoplastic composites were generated using a dual extrusion technique for processing by means of various polymer processing technologies. These composites were generated by continuously injecting thermotropic liquid crystalline polymers (TLCP's) of higher melting point into matrix polymers of lower melting point. The use of the TLCP's allowed *in situ* fibril generation, thereby avoiding fiber breakage, very common when processing traditional fiber filled composites, e.g. carbon fiber reinforced composites. A wide range of thermoplastics were reinforced in this work, such as acrylonitrile butadiene styrene (ABS), polyphenylene sulfide (PPS) and a lower melting TLCP. On post processing the composites using injection molding, compression molding and Fused Filament Fabrication (FFF), a form of additive manufacturing (AM), a significant improvement in the mechanical properties was obtained. The composites generated are highly recyclable by either direct reprocessing after grinding or by a TLCP reclamation process developed earlier.

Background and Requirements

Growing pressure on the automotive industry to cut greenhouse gas emissions [1], improve recyclability of the composites [2], and achieve the ambitious goal of doubling fuel economy [3] requires that the solutions that are adopted be multipronged. Industry requires switching to

composites that are highly recyclable without compromising the mechanical properties. Moreover, with the introduction of novel processing methods such as additive manufacturing (AM), the composites need to be compatible with the AM processes for faster adoption of the AM technologies [4]. This is to harness the advantages of AM to achieve the goals of the automotive industry, mentioned earlier, faster than can be achieved by conventional processing technologies.

In the quest for light weighting, the automotive industry constantly relies on composites. Traditionally, composites are generated by reinforcing using solid fibers such as carbon and glass fiber. One major disadvantage of using these composites is poor recyclability. For example, in the work carried out by Kuram et al. [5], reprocessing of the glass-fiber reinforced composites by repeated injection molding until five processing cycles showed a decrement of 33.5 % in tensile strength and 23.5 % in flexural strength compared to the virgin blend. The processing technologies, such as injection molding and extrusion, are known for fiber breakage with each processing cycle. Improvement in recyclability can be achieved by switching to *in situ* composites. In these composites, polymeric fibrils are generated during the processing stage which avoids the fiber breakage problems in addition to allowing regeneration of the fibrils on subsequent recycling cycles. The utilization of polymeric reinforcement eliminates the drop in the aspect ratio of the fibrils, which on contrary is very common on using traditional fibers.

In this work, generation and reprocessing of *in situ* composites has been described. The matrix polymers were reinforced using TLCP's, composed of rod-like aromatic monomers, which under extensional flow kinematics lead to excellent one-dimensional mechanical properties [6]. In addition, the TLCP's are wholly thermoplastics and have lower density. Two recycling schemes are viable for TLCP composites: direct reprocessing after grinding and reclamation of the TLCP's from the composites. *In situ* composites based on TLCP-reinforced thermoplastics have the

advantage of regeneration of reinforced fibrils during melt processing steps under elongational flow. Sasaki et al. [7] used a twin-screw extruder to prepare polypropylene-TLCP strands and then pelletized and re-extruded until the 10th cycle. The results showed no loss in tensile strength with the reprocessing cycles. This illustrates the greater ability of TLCP's to endure multiple processing cycles than carbon or glass reinforced composites.

For TLCP composites with non-overlapping processing temperature, direct reprocess may not be feasible without significantly deteriorating properties of the composites. The reclamation process developed in our laboratory by Collier et al. [8] successfully realized the separation of the TLCP from the polypropylene matrix with 96.0 wt.% purity. On re-injection molding, composites showed no discernible difference in mechanical properties compared to the virgin blends. Reactive extrusion was incorporated in this process to degrade the polypropylene and enhance the phase separation. The extrudate was dissolved in a mineral oil bath for selective dissolution of the polypropylene. TLCP was filtered out of solution and reprocessed. The material cost of producing the reclaimed TLCP was found to be three times lower than the cost of pure TLCP. This process is potentially suitable for use in other TLCP-reinforced thermoplastics as well.

One major problem in using TLCP's is that the processing temperature of TLCP's is higher compared to most matrix polymers which may prevent blending in a single extruder [9]. This problem can be solved by utilizing super-cooling behavior of the TLCP's in technology developed in our lab, called dual extrusion technology [10]. The dual extrusion technology leads to nearly continuous injection of the TLCP in the matrix polymer, thereby generating nearly continuously reinforced composites. In this technology, discussed elsewhere in detail [11], the TLCP's and the matrix polymers are plasticated in two different extruders. TLCP is then injected into the matrix polymer using a multiport injection nozzle, following which the blend is passed through static

mixers which subdivides the TLCP stream into finer streams. The extrudate is drawn at high draw ratio and subsequently cooled in a water bath to lock down the fibril orientation. The selection of temperatures is determined using rheological tests discussed in detail elsewhere [9]. The generated filaments can then be post processed as solid filled systems by only melting the matrix polymer and keeping the reinforcing polymer solid. Different post-processing technologies, such as injection molding, compression molding and Fused Filament Fabrication have been utilized to process the TLCP reinforced composites generated using dual extrusion technology.

This paper will discuss two subtypes of the composites generated in our laboratory by using TLCP as a reinforcement in the dual extrusion technology. In the first type, thermoplastics such as acrylonitrile butadiene styrene (ABS), polyphenylene sulfide (PPS) and polypropylene (PP) were reinforced with the TLCP's. These composites will henceforth be termed as thermoplastic-TLCP *in situ* composites (TTICs). TLCP/ABS and TLCP/PPS composite strands generated using dual extrusion technology were post processed in fused filament fabrication (FFF), a form of additive manufacturing (AM). In FFF, polymeric filaments are used to fabricate objects layer upon layer [12]. The TLCP/PP strands generated using the dual extrusion technology were injection molded. The second subtype of the composites generated in our lab are called as two TLCP in-situ composites (TPICs). In TPICs, a lower melting TLCP is reinforced by a higher melting TLCP using the dual extrusion system. TPIC strands generated were injection molded.

Materials

ABS used in this work, MAGNUM 555, was generously supplied by Trinseo. The PPS used was generously supplied by Solvay and melts at 285 °C. The TLCP's used, HX3000 and HX8000, were supplied by DuPont and are believed to be synthesized from different ratios of terephthalic acid (TA), 4-hydroxybenzoic acid (HBA), hydroquinone (HQ) and hydroquinone derivatives (HQ-

derivatives). The melting temperatures of HX3000 and HX8000 are 280 and 330 °C, respectively, determined using dynamic scanning calorimetry. Vectra A950, henceforth referred to as Vectra A, was provided by Hoechst Celanese. Vectra A is a random copolyester based on 73% hydrobenzoic acid and 27% 2-hydroxy-6-napthoic acid. It has a glass transition temperature of 108°C and a melting point of 283°C [6]. Polypropylene used was the 4018 grade provided by Amoco.

Experimental

The dual extrusion system consisted of two Killion KL-100 single screw extruders with Maddock screws of 25.4 mm diameter and length-to-diameter ratio of 30. Two Zenith gear pumps (model number: 6135419-001 and flow/revolution: 1.725 cm^3/rev) were used to meter the reinforcing TLCP and the corresponding matrix polymer. A 28-hole injection nozzle was used to inject the TLCP phase into the matrix phase. The melt was then passed through a 4-element KOCH mixer and a 4-element Kinecs mixer. The die used had a diameter of 3 mm and length-to-diameter ratio of 20.

The key step in the fabrication of our wholly thermoplastic composites is the selection of TLCP's. The selected TLCP's should have a melting temperature above that of the matrix polymer to avoid melting the TLCP on reprocessing in various polymer processing technologies discussed earlier. In addition, the temperature selected for processing in FFF needs to be such that relaxation in orientation of the TLCP's is minimum to avoid loss in mechanical properties. Selected processing temperatures should also avoid degradation of the matrix polymers.

HX8000/ABS and HX3000/PPS were processed in the dual extrusion system using the temperatures shown in Figure 1. Detailed discussion of generation, morphology and postprocessing of HX8000/ABS and HX3000/PPS has been carried out elsewhere [13, 14, 15].

56 wt.% Vectra A/PP strands were generated using dual extrusion technology by plasticating Vectra A and PP at 325°C and 245°C, respectively. TPICs were generated by using HX8000 as matrix and HX3000 as reinforcement. HX8000 and HX3000 were plasticated at 320 and 360 °C, respectively, to generate 50.0 wt.% HX8000/HX3000 TPIC strands.

Postprocessing of the 40.0 wt.% HX8000/ABS and 67.0 wt.% HX3000/PPS strands were carried out by printing rectangular specimens (80mm x 8mm x 2mm) using a RoVa3D printer using the print parameters shown in Table I. Extrusion multiplier is the relation between the extrusion rate and scan speed. The nozzle diameter was chosen to avoid clogging of the nozzle. The specimens were printed without severing such that the roads were aligned parallel to each other along the length of the specimen.

56.0 wt.% HX3000/PP and 50.0 wt.% HX8000/HX3000 TPICs were injection molded using a BOY 35E machine. End-gated rectangular plaques were produced using both, 56.0 wt.% HX3000/PP and 50.0 wt.% HX8000/HX3000 pelletized strands. For HX3000/PP, zone temperatures used were 190, 250, 250 and 280 °C. The mold temperature was 60°C. For HX8000/HX3000 TPIC, zone temperatures were 300, 310, 310, and 310 °C. The mold temperatures were set to 210 °C. 56.0 wt.% HX3000/PP was also used to compression mold square plaques of dimension (76.2mm x 76.2mm x 2mm) by laying 76.2mm long strands parallel to each other and molding at 290, 300, 310 and 330 °C. Tensile testing strips were cut in the alignment direction to assess improvement in the mechanical properties.

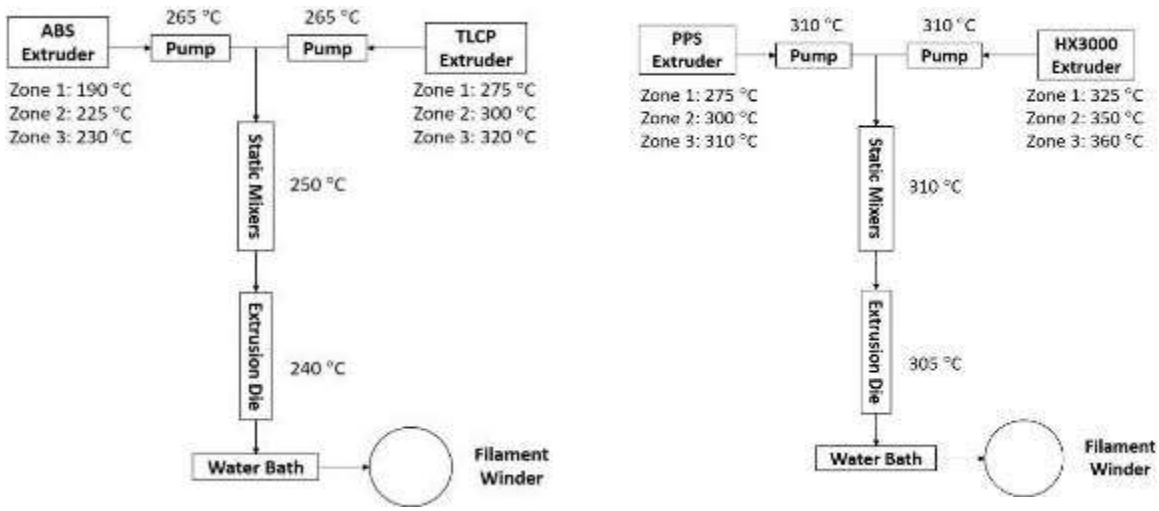

(a) (b)

Figure 1: Temperature schematic used to carry out to generate strands using dual extrusion technology consisting of (a) HX8000/ABS and (b) HX3000/PPS.

Table I: Print parameters used in FFF to print specimens.

Printing Parameters	**Settings**
Layer Width	0.65 mm
Layer Height	0.65 mm
Scan Speed (X, Y & Z)	1200 mm/min
Extrusion Multiplier	1
Nozzle Diameter	1 mm

Results

This section has been arranged to show improvement in tensile properties of the strands generated using dual extrusion technology. It also demonstrates processability of these composite strands using various processing technologies. The tensile properties of the post-processed parts have also been shown. Table II shows the tensile properties of the composite strands generated using dual extrusion technology. A significant improvement in the mechanical properties can be seen compared to those of the pure matrices shown in the table. The rectangular parts printed using 40.0% HX8000/ABS and 67.0 wt.% HX3000/PPS can be seen in Figure 2. Tensile properties of the 3d printed parts, printed using 40.0 wt.% HX8000/ABS and 67.0 wt.% HX3000/PPS composite filaments are shown in Figure 3 and Figure 4, respectively. Drastic improvement in the properties can be seen, which is very promising in FFF. All of these properties are in the alignment direction.

Table II: Tensile property of the composite strands generated using dual extrusion technology and that of the pure matrix strands generated using single screw extruder.

Strands	**Composition (Wt. %)**	**Tensile Strength (MPa)**	**Tensile Modulus (GPa)**
HX8000/ABS	40.0	169.2±4.0	39.9±3.7
HX3000/PPS	67.0	155.0±24.2	40.4±7.5
HX3000/PP	56.0	147.9±13.1	55.2±8.4
ABS	Pure	39.3±3.3	2.3±0.4
PPS (Processing Guide)	Pure	80.0	3.5
PP [6]	Pure	23.2±3.9	1.0±0.2

(a)

(b)

Figure 2: Rectangular specimens printed using (a) 40.0 wt.% HX8000/ABS and (b) 67.0 wt.% HX3000/PPS for tensile testing. All roads are aligned in the length direction

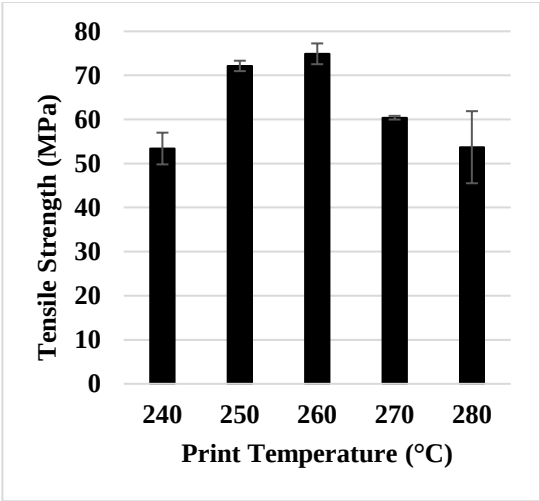

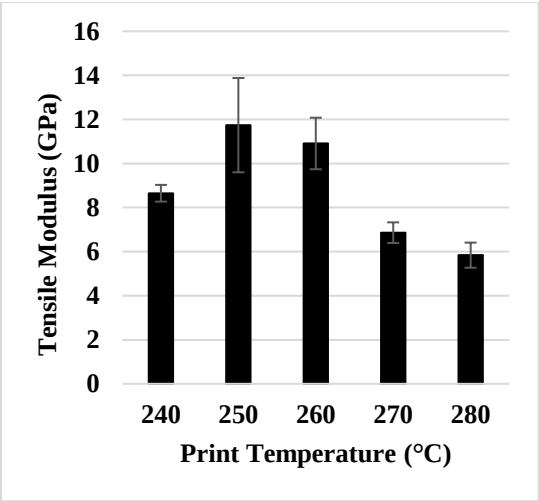

(a) (b)

Figure 3: Tensile (a) strength and (b) modulus of the rectangular specimens printed using 40.0 wt.% HX8000/ABS composite filaments.

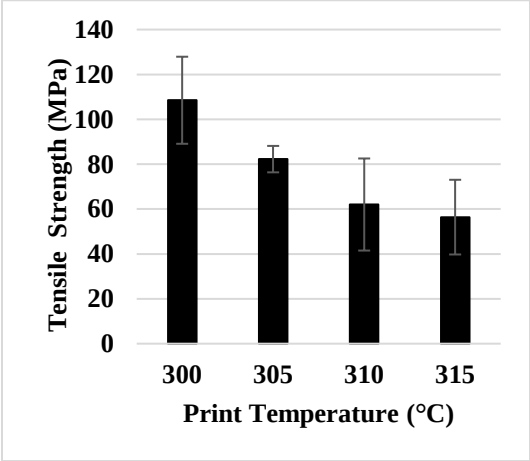

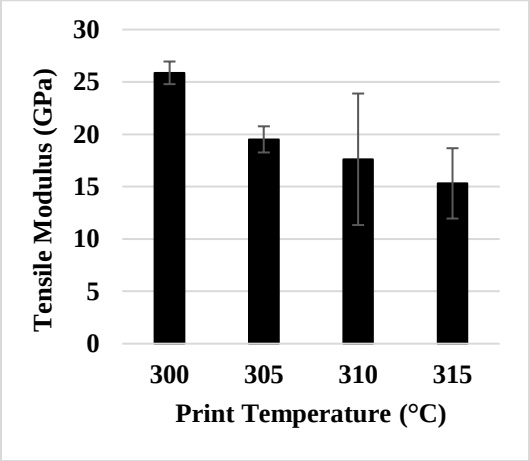

(a) (b)

Figure 4: Tensile (a) strength and (b) modulus of the rectangular specimens printed using 67.0 wt.% HX3000/PPS composite filaments.

Now follows the tensile properties obtained on post processing 56.0 wt.% HX3000/PP. Table III shows improvement in tensile properties on compression molding. On the other hand, injection molded plagues, molded using pelletized 56.0 wt.% HX3000/PP strands had tensile properties shown in Table IV in the flow and transverse direction. Tensile properties of the injection molded 50.0 wt.% HX3000/HX8000 TPIC end-gated plaques in the flow and transverse direction have been shown in Table V. End-gated plaques molded using 56.0 wt.% HX3000/PP and 50.0 wt.% HX3000/HX8000 TPIC pelletized strands are shown in Figure 5. The tensile properties of the postprocessed parts produced using wholly thermoplastic composites are similar to those reinforced using traditional fibers [16] and in some cases even better. Thus, these composites have potential to replace traditionally used composites.

Table III: Tensile properties of the compression molded 56.0 wt.% HX3000/PP, molded at 290, 300, 320 and 330 °C. All properties are in the alignment direction.

Molding Temperature (°C)	**Tensile Strength (MPa)**	**Tensile Modulus (GPa)**
290	129.3	39.7
300	127.7	30.5
320	129.8	28.6
330	142.2	26.8

Table IV: Tensile properties of the injection molded 56.0 wt.% HX3000/PP end-gated plaques in the flow and transverse directions.

Orientation	**Tensile Strength (MPa)**	**Tensile Modulus (GPa)**
Flow Direction	54.0±7.3	5.1±0.2
Transverse Direction	24.5±3.2	2.8±0.2

Table V: Tensile properties of the injection molded 50.0 wt.% HX3000/HX8000 TPIC end-gated plaques in the flow and transverse direction.

Orientation	**Tensile Strength (MPa)**	**Tensile Modulus (GPa)**
Flow Direction	68.4±9.4	4.1±1.0
Transverse Direction	36.0±6.9	2.2±0.4

(a) (b)

Figure 5: Injection molded end-gated plaques, molded using (a) 56.0 wt.% HX3000/PP and (b) 50.0 wt.% HX3000/HX8000 TPIC pelletized strands.

Summary and Next Steps

In summary, wholly thermoplastic strands composed of a thermotropic liquid crystalline polymer and a matrix polymer were successfully generated using dual extrusion technology. Our efforts not only reinforced commonly used thermoplastics such as acrylonitrile butadiene styrene (ABS) and polypropylene (PP) but also extended the work to reinforce high performance thermoplastics such as polyphenylene sulfide (PPS). Upon post processing the composite strands using compression molding, injection molding and FFF, significant improvement in the tensile properties were obtained. The properties were similar and, in some cases, superior to those of the traditional fiber composites.

Future efforts will be to extend the work carried out in the past in our laboratory to study the recyclability of TLCP/ABS and TLCP/PPS composites. In the past, work carried out in our laboratory was to develop a separation method to separate TLCP and PP. We will now focus on extending the work to separate other wholly thermoplastic composites as well. In addition, the

effect of direct reprocessing after grinding will also be studied.

Acknowledgements

Authors would like to acknowledge Dr. Michael Bortner and his student Cailean Pritchard for providing RoVa3D printer for printing. Both are in the department of chemical engineering at Virginia Tech. Also, we would like to acknowledge help from our material suppliers, DuPont for TLCP's, Solvay for PPS and Trinseo for ABS.

Bibliography

1. Yang, C., et al., Meeting an 80% reduction in greenhouse gas emissions from transportation by 2050: A case study in California. Transportation Research Part D: Transport and Environment, 2009. 14(3): p. 147-156.

2. Miller, L., et al., Challenges and alternatives to plastics recycling in the automotive sector. Materials, 2014. 7(8): p. 5883-5902.

3. Anderson, S.T., et al., Automobile fuel economy standards: Impacts, efficiency, and alternatives. Review of Environmental Economics and Policy, 2011. 5(1): p. 89-108.

4. Chapiro, M., Current achievements and future outlook for composites in 3D printing. Reinforced Plastics, 2016. 60(6): p. 372-375.

5. Kuram, E., B. Ozcelik, and F. Yilmaz, The influence of recycling number on the mechanical, chemical, thermal and rheological properties of poly (butylene terephthalate)/polycarbonate binary blend and glass-fibre-reinforced composite. Journal of Thermoplastic Composite Materials, 2016. 29(10): p. 1443-1457.

6. Gray IV, R.W., D.G. Baird, and J. Helge Bøhn, Effects of processing conditions on short TLCP fiber reinforced FDM parts. Rapid Prototyping Journal, 1998. 4(1): p. 14-25.

7. Keita SASAKI, T.T., Development of Liquid Crystalline Polyester Composite as Recyclable High-Strength Material. Japanese Journal of Polymer Science and Technology, 1993. 50(11): p. 855-862.

8. Collier, M.C. and D.G. Baird, Separation of a thermotropic liquid crystalline polymer from polypropylene composites. Polymer composites, 1999. 20(3): p. 423-435.

9. Ansari, M.Q., Mansfield, C.D., Baird, D.G., 2016, May. "A Process for Generating Composites of Acrylonitrile-Butadiene-Styrene Reinforced with a Thermotropic Liquid Crystalline Polymer for Use in Fused Filament Fabrication," ANTEC 2016 - Indianapolis, Indiana, USA May 23-25, 2016. [On-line].

10. Handlos, A. and D. Baird, Sheet extrusion of microcomposites based on thermotropic liquid crystalline polymers and polypropylene. Polymer composites, 1996. 17(1): p. 73-85.

11. Handlos, A. and D. Baird, Processing and associated properties of in situ composites based on thermotropic liquid crystalline polymers and thermoplastics. Journal of Macromolecular Science, Part C: Polymer Reviews, 1995. 35(2): p. 183-238.

12. Stucker, B., I. Gibson, and D. Rosen, Additive Manufacturing Technologies. Springer, 2010.

13. Ansari M.Q., Baird, D.G., 2018, May. "Assessing the Performance of Continuously Reinforced Acrylonitrile Butadiene Styrene with a Thermotropic Liquid Crystalline

Polymer in Fused Filament Fabrication," ANTEC 2018 - Orlando, Florida, USA May 7-10, 2018. [On-line].

14. Ansari, M.Q. and Baird, D.G. "Generation of High performance Polyphenylene Sulfide-Thermotropic Liquid Crystalline Polymer Composite Filaments for Use in Fused Filament Fabrication." 33rd International Conference of The Polymer Processing Society. 2017.

15. D.G. Baird, M.Q. Ansari, C.D. Mansfield, “Wholly Thermoplastic Composites for Use in Fused Filament Fabrication, a 3-D Printing Process”, US Patent Application 62/662,956, filed April 2018. Patent Pending.

16. Carlson, L., Thermoplastic Composite Materials: Composite Materials Series. 1991, Elsevier.

Appendix B: Effect of Fiber Aspect Ratio on the Bending Energy

In this section of the appendix, the reasons for 180º turns during printing of TLCP reinforced filaments will be further analyzed by treating the fibers as elastic rods. The energy required to bend a rod into an arc of radius 1/k requires bending energy calculated using the following equation:

$$E_b = \frac{\pi}{8} E k^2 r^4$$

where E_b represents modulus and r is the radius of the fiber. Therefore, to bend the fibers into 0.25 mm turning radius requires energy given in the table below:

Fiber	Diameter (µm)	Modulus (GPa)	Bending Energy (J)
HX8000	0.6	47	2.3×10^{-9}
Carbon Fiber	10	238	0.002

Comments:

1. The modulus used for HX8000 was the value obtained at the room temperature. Because the modulus of HX8000 fibrils are temperature dependent and therefore much lower that the room temperature value, the energy required will be even lower than shown in the table. On the other hand, the energy required to bend carbon and glass fiber will be independent of temperature.
2. Based on the morphology of the carbon fiber printed specimens, minimum turn radius of carbon fiber is 0.55 mm [1]. The turn radius of TLCP reinforced filaments range between 0.15-0.2 mm. For HX3000/PPS, the turn radius was 0.15 and for HX8000/ABS, the turn radius was 0.2 mm.

Reference:

1. N. Li et al., Journal of Materials Processing Technology 238 (2016) 218–22.